Slow Potentials of the Sensorimotor Cortex during Rhythmic Movements of the Ankle

Ryan J. McKindles
Marquette University

SLOW POTENTIALS OF THE SENSORIMOTOR CORTEX DURING RHYTHMIC MOVEMENTS OF THE ANKLE

by

Ryan J. McKindles, B.S.

A Dissertation submitted to the Faculty of the Graduate School,
Marquette University,
in Partial Fulfillment of the Requirements for
the Degree of Doctor of Philosophy

Milwaukee, Wisconsin

December 2013

ABSTRACT
SLOW POTENTIALS OF THE SENSORIMOTOR CORTEX
DURING RHYTHMIC MOVEMENTS OF THE ANKLE

Ryan J. McKindles, B.S.

Marquette University, 2013

The objective of this dissertation was to more fully understand the role of the human brain in the production of lower extremity rhythmic movements. Throughout the last century, evidence from animal models has demonstrated that spinal reflexes and networks alone are sufficient to propagate ambulation. However, observations after neural trauma, such as a spinal cord injury, demonstrate that humans require supraspinal drive to facilitate locomotion. To investigate the unique nature of lower extremity rhythmic movements, electroencephalography was used to record neural signals from the sensorimotor cortex during three cyclic ankle movement experiments. First, we characterized the differences in slow movement-related cortical potentials during rhythmic and discrete movements. During the experiment, motion analysis and electromyography were used characterize lower leg kinematics and muscle activation patterns. Second, a custom robotic device was built to assist in passive and active ankle movements. These movement conditions were used to examine the sensory and motor cortical contributions to rhythmic ankle movement. Lastly, we explored the differences in sensory and motor contributions to bilateral, rhythmic ankle movements. Experimental results from all three studies suggest that the brain is continuously involved in rhythmic movements of the lower extremities. We observed temporal characteristics of the cortical slow potentials that were time-locked to the movement. The amplitude of these potentials, localized over the sensorimotor cortex, revealed a reduction in neural activity during rhythmic movements when compared to discrete movements. Moreover, unilateral ankle movements produced unique sensory potentials that tracked the position of the movement and motor potentials that were only present during active dorsiflexion. In addition, the spatiotemporal patterns of slow potentials during bilateral ankle movements suggest similar cortical mechanisms for both unilateral and bilateral movement. Lastly, beta frequency modulations were correlated to the movement-related slow potentials within medial sensorimotor cortex, which may indicate they are of similar cortical origin. From these results, we concluded that the brain is continuously involved in the production of lower extremity rhythmic movements, and that the sensory and motor cortices provide unique contributions to both unilateral and bilateral movement.

ACKNOWLEDGMENTS

Ryan J. McKindles, B.S.

My most sincere gratitude goes to Dr. Brian D. Schmit for his mentorship, support, and guidance throughout my doctoral dissertation. I admire your enthusiasm for scientific investigation and ardent search for the Truth, which have been an inspiration to your students and colleagues alike. Thank you for such an *Outstanding* experience! To Dr. Michael R. Neuman, who introduced me to research, design, and innovation, thank you for recognizing and nurturing my tenaciously inquisitive mind. I am here today because your guidance and commitment to education, for which I am truly grateful. Thank you to the members of my dissertation committee: Dr. Scott Beardsley, Dr. Allison Hyngstrom, Dr. Kristina Ropella, and Dr. Sheila Schindler-Ivens. Your continued advice and council have been invaluable, and it has been a pleasure getting to know each of you. My parents, Maureen & Joseph McKindles, and my siblings, Adam, Derek, and Jessica McKindles, I love you all. Your patience, compassion, and love are a solid foundation on which I can always rely. To my family and friends throughout the world, I have appreciated all your kindness and encouragement throughout these past years. In addition, I would like to thank all the members of the Integrative Neural Engineering & Rehabilitation Laboratory, especially Eric Walker and Tanya Onushko. Thank you to the Department of Biomedical Engineering, the College of Engineering, and Marquette University for the educational opportunity, funding, and support. I especially want to acknowledge and thank Mrs. Brigid Lagerman, Mrs. Patricia Smith, and Mrs. Mary Wesley. I have immensely valued all of your support and your dedication to our department.

TABLE OF CONTENTS

LIST OF FIGURES

CHAPTER 1: INTRODUCTION & BACKGROUND

1.1 THESIS STATEMENT

An analysis of movement-related slow potentials of the sensorimotor cortex provides evidence that the brain plays an essential role in the perpetuation of lower extremity rhythmic movements in humans.

1.2 LOWER EXTREMITY RHYTHMIC MOVEMENTS

1.2.1 Motivation

Since the early experiments by Sir Charles S. Sherrington and T. Graham Brown there has been controversy over the roles of spinal reflexes (Sherrington, 1908) and central pattern generation (Brown, 1911) in the control of rhythmic movements of the lower extremities. Through separate mechanisms, both men provided scientific evidence that rhythmic stepping motions could be elicited on a treadmill without descending supraspinal drive in decerebrate cat preparations. From his experiments, Sherrington believed that reflexes were the primary driver that perpetuated lower extremity rhythmic movements. Whereas, Brown demonstrated that after deafferentation, stimulation the spinal cord could produce similar rhythmic stepping movements. Brown believed there were intrinsic pattern generators in the spinal cord that alone could facilitate locomotion. For extensive reviews on the spinal level control of locomotion, please see Grillner (1975) and Hultborn & Nielsen (2007).

Several decades later, scientists attempted to transfer these theories to humans by training patients who had suffered spinal cord injuries (SCI) to walk on a treadmill with

bodyweight support. However, even with support and training, SCI patients were unable to produce significant muscle activity to elicit independent stepping movements (Dietz et al., 1995). Therefore, it has been suggested that afferent sensory feedback and spinal networks are alone not sufficient to perpetuate lower extremity rhythmic movements in man. It has been hypothesized that through evolution humans have developed a greater dependency on supraspinal structures to compensate for bipedal locomotion (Nielsen, 2003). The hypothesis of bipedal compensation and the unique nature of human locomotion motivate the research in this dissertation with the goal of understanding more fully the role of the cerebral cortex in the perpetuation of lower extremity movements.

1.2.2 Neural Control of Rhythmic Movements

Three individual components of the nervous system that play a role in the lower extremity control of rhythmic movements are peripheral afferent feedback, spinal networks, and supraspinal structures. During movement, afferent feedback from muscle spindles and Golgi tendon organs relay position, velocity, and force information to the central nervous system (For a review, please see Windhorst (Windhorst, 2007)). Specifically, muscle spindles are most sensitive to the position and velocity properties of muscle stretching and send monosynaptic projections to motor neurons, via Ia afferent sensory fibers, to autoregulate muscles. This is known as the monosynaptic stretch reflex (Liddell & Sherrington, 1924). Golgi tendon organs, however, are located in the musculotendinous junction and are primarily sensitive to the force of muscle tension. Proprioceptive information to the ipsilateral, dorsal horn of spinal cord is relayed through type Ib afferent fibers.

Spinal networks integrate sensory information from the periphery, other spinal segments, and descending supraspinal drive onto the motor system's final pathway: the motor neuron. The spinal cord is organized from rostral to caudal into the cervical, thoracic, lumbar, and sacral regions. Within each region, there are several spinal segments from which sensory and motor neurons project to specific groups of muscles, or myotomes. Sensory inputs to the spinal cord also create polysynaptic connections, where minimally there is one interneuron between the sensory afferents and motor neurons. Interneurons create networks that have been shown to facilitate muscle coordination, inhibit antagonist muscles (Windhorst, 1996), or even create rhythmic movement patterns (Jankowska et al , 1967). In lesser mammals, spinal centers that are able to produce rhythmic muscle patterns are known as central pattern generators (CPGs). Though there is evidence of CPGs in humans, the specific location(s) is not well understood (For a review, please see MacKay-Lyons (2002)). Moreover, it has been suggested that the neural mechanisms required for rhythmic movement may be distributed across multiple spinal segments or even into the subcortical and cortical areas of the brain (Ivanenko, Poppele, & Lacquaniti, 2009).

Supraspinal structures, such as the brainstem, cerebellum, and sensorimotor cortices, are active during rhythmic movements of the lower extremities (Gwin et al., 2011; Jain et al., 2013; Mehta et al., 2012; Raethjen et al., 2008; Schneider et al., 2013; Wagner et al., 2012). During movement, proprioceptive afferent information from the muscles is relayed through the brainstem and thalamus to the sensory cortex. Here, projections are sent to supplementary sensory areas and to the motor cortex. The motor cortex integrates information from the sensory and premotor cortices to produce the

appropriate efferent motor command. Moreover, modulations in both the afferent somatosensory evoked potentials (SEPs) (Altenmüller et al, 1995; Duysens et al., 1995) and in the efferent motor evoked potentials (MEPs) (Schubert, 1997) during walking demonstrate that sensory and motor pathways are continuously active during rhythmic lower extremity movement. However, these measures are indirectly linked to the underlying physiology. The work in this dissertation is further motivated by developing a method that allows for interpretation of natural cortical signals to understand their relationship to the perpetuation of rhythmic lower extremity movements.

1.3 ELECTROENCEPHALOGRAPHY

1.3.1 Recording Electrical Potentials from the Brain

Electroencephalography (EEG) is the noninvasive recording of the electrical potentials associated with neural activity from the brain. First used for human recordings by Hans Burger (1929), EEG is one of three technologies used primarily for recording electrical potentials from the cerebral cortex. The other recording devices are electrocorticography (ECoG) (Jasper & Penfield, 1949), also known as intracranial EEG, and cortical electrode arrays (Maynard et al., 1997). Though the implantation of these other devices requires invasive surgery, they are able to record comparatively high quality signals from the brain. Conversely, EEG electrodes are placed on the surface of the scalp; consequently, the cortical signals are highly attenuated by the electrical impedance of the pia matter, arachnoid membrane, dura matter, skull, periosteum, and skin before it reaches the electrode surface (Cooper et al., 1965). For that reason, a typical ECoG signal recording has a significantly better signal-to-noise ratio than an EEG

recordings (Ball et al., 2009). However, EEG is advantageous for studying the brain because it is low cost, noninvasive, and reusable. In comparison to other neural imaging modalities, such as fMRI,PET, and MEG, the high temporal recording resolution and portability of EEG can be advantageous. Most EEG devices can sample signals from 100 to 20,000 Hz. Though high sampling rates are beneficial for some research projects, the tradeoffs are large data file sizes and reduced post-processing speed.

1.3.2 EEG Electrodes

A typical EEG device is comprised of an array of 8 to 512 electrodes that sample the electric field present at the scalp surface. EEG electrodes are traditionally round in shape (approx. 0.5 to 1.5 cm diameter) and made from conductive materials, such as tin, gold, silver-chloride, or sintered silver/silver-chloride (Teplan, 2002). However, some new dry electrode caps have multiple finger like projects to reach through the hair to the scale surface and some use conductive polymers instead of metal in their electrode designs (Lin, Liao, et al., 2011). Whatever the electrode type, each design must meet any special requirements of the recording environment, such as high strength magnetic fields in an MRI or movement induced noise during walking.

EEG electrodes are categorized as either passive or active. A passive EEG electrode records electrical potentials from the scalp surface and transferred via wires or cables to an amplifying and recording system. In contrast, active electrode systems implement operational amplifiers (op amps) between the electrodes and the main amplification stage. Either, the op amps are used to amplify the EEG signal immediately after recording to increase the signal amplitude to be larger than external noise that could

be introduced by cable movement or electrical line noise from nearby lighting (Teplan, 2002). Otherwise, the op amps can be used as a bridge to better match the low impedance EEG signals to the high impedance inputs of the main amplifiers. Because the op amps require power at the electrode site, they are not compatible with certain recordings environments, such as the high magnetic field in an MRI machine.

1.3.3 Closing the Impedance Gap

Electrolytic gels and pastes are used to reduce the high impedance gap caused by the irregular shape and consistency of the scalp surface and the material properties of the electrodes. Lowering this impedance gap reduces the effects of capacitively coupled noise and signal attenuation. This process is known as impedance matching and is the electrical equivalent of the acoustical measurement technique used in ultrasound (Bushberg et al., 2002). Traditionally, scalp preparation was performed before an EEG experiment to clean and abrade the skin surface, which removes any oils and increases surface area to further reduce the electrical impedance. However, with the development of high impedance amplifiers and better digital filtering techniques, high quality EEG signals can be recorded without the use of skin abrasion (Ferree et al., 2001). This is beneficial because there is less risk of infection or bleeding during the preparation process. As previously mentioned, dry electrode systems do not require gel. These systems are designed for quick application and use both metal and electroconductive polymers for their electrode design. However, because of their high impedance interface, these electrodes are prone to low-frequency noise, which is often analog filtered or otherwise removed before recording. The placement of EEG electrodes on the scalp

surface can be accomplished manually or, with new higher density electrode system, electrodes are placed in an elastic cap for easy setup. In both methods, electrodes are placed in predetermined locations over the cortical surface.

1.3.4 Electrode Placement (10-20 System)

The current standard for EEG electrode placement that is most widely used in both clinical and research settings is the International 10-20 system. This system was proposed at the first EEG congress by H.H. Jasper to standardize the placement of EEG electrodes (Jasper, HH, 1958). Since then, the International Federation of Clinical Neurophysiology (IFCN) has kept standards and recommendations on the practice of EEG recording, including the 10-20 system (Klem 1999). The 10-20 system is named for the measurements used to find the correct electrode locations. Measuring the total distance in the sagittal plane from the nasion to inion, the first electrode is placed at 10% of that distance and subsequent electrodes at 20% intervals with the last electrode at 10% above the inion. Similarly, electrodes are placed based on measurements in the frontal plane between the left and right prearticular points. Both measurements pass through the vertex. The electrodes are named alphanumerically with the odd numbers over the left hemisphere, the even numbers over the right hemisphere, and increasing in value as they move laterally from the midline. Along the midline, the number is substituted with the letter z. The letters roughly indicate the different regions of the brain over which the electrodes are placed. For example, F2 is over the frontal lobe just to the right of the midline, and CPz is located near the border of the central and parietal areas over the midline.

1.3.5 Referencing

As is true with any electrical recording, signal properties are always relative to a reference. In the case of monopolar recordings, EEG signals are measured as the voltage difference between each electrode location and a separate reference electrode also placed on the surface of the skin. Moreover, both electrodes and the reference are originally referenced to ground voltage value that is used to hold the signal within the range of the amplifier. Therefore, the final voltage value sampled at any time point is the difference between each electrode (including the reference) and a ground voltage, then the difference between each electrode and the reference. This effect of the ground voltage is eliminated by the second difference measure. Please see Ferree et al. (2001) for additional details. Therefore, what is most important is the placement of the reference electrode. Since there are no electrically quiet areas on the skin surface, the placement of this electrode has been controversial. Some of the most common locations have been the ear lobe, linked ear lobes, over the midline and in front of the vertex, and the nose. Additionally, other types of referenceless procedures have been suggested, including the common average reference (Bertrand et al., 1985; Goldman, 1950) and a reference at infinity (Yao, 2001). The common average reference, which has become one of the most popular referenceless recording procedures, allows the reference electrode to be placed anywhere during the experiment. Then during post processing, the mean signal of all the elctrodes is removed from each individual electrode signal. However, as with any referencing procedure there are caveats and caution should be taken when choosing the correct procedure (Desmedt et al., 1990; Dien, 1998). Another type of EEG recording is the bipolar recording. In this type of recording, the signals that are observed are the

differences between pairs of electrodes, typically adjacent to each other, which demonstrate local differences in cortical potentials, and are used for specific clinical and research purposes.

1.4 CLINICAL AND RESEARCH USE OF EEG

Electroencephalography is a prominent neural recording device in both clinical and research settings. Clinically, EEG has been the dominate technology for the detection and diagnosis of many sleep and seizure disorders for many years. During sleep studies, temporal waveforms and the rate of neural oscillation in specific electrodes indicates when a patient enters or exits different stages of sleep. Irregularities in the order or duration of specific sleep stages are used to diagnose neural disorders. The clinical use of EEG for seizure disorders, such as epilepsy, has been developed with advanced mathematics to detect and track the progression of epileptic activity (Guerrero-Mosquera et al., 2012). More recently, the field of neurofeedback has bridged the gap from research to the clinical setting. This field focuses on the self-regulation of neural signals by presenting visual or auditory feedback to the patient (Holtmann et al., 2011; Lofthouse et al., 2012).

There is a more extensive use of EEG for research purposes in neuroscience, neuropsychology, biomedical engineering, and many other fields. The noninvasive nature of EEG has made it advantageous when studying neurophysiology in humans. Neuroscientists have used EEG to understand basic neurophysiology of the brain with evoked potentials. Neuropsychology uses EEG to measure changes in the cerebral cortex to learn about cognitive function and changes within different diseased populations, such

as Alzheimer's disease (Leiser, 2011) and autism (Van Hecke et al., 2013). More recently, a new field has emerged that uses brain signals recorded with EEG to interact with electronics. This field has been termed brain machine interfacing (BMI) or brain computer interfacing (BCI), both of which are part of broader field known as human machine interfaces (HMI) (Nicolas-Alonso & Gomez-Gil, 2012). Research into BMI devices has helped fuel the research in some of the basic physiology of how the brain controls movements, as many of the devices being developed are to control prosthetic upper limbs (Jackson et al., 2006) and lower extremity exoskeletons (Contreras-Vidal et al., 2012). Because of this, more interest has been put on how the brain is used to control movement and what signals can we extract from EEG to use as controls for such BMI devices. However, as with many new fields, there are a number of ethical questions that need to be considered (Clausen, 2011).

1.5 ELECTRICAL POTENTIALS OF THE CEREBRAL CORTEX

1.5.1 Physiological Origin of EEG

Electroencephalography records electrical field potentials produced by neuronal populations in the brain. Since the field potential produced by a single neuron is small and there is significant skull attenuation, EEG signals recorded at the scalp surface represent the field potentials of populations of neurons with synchronized firing. Moreover, these populations must be aligned in parallel so that the electrical fields of individual neurons do not cancel. Advantageously, columns of pyramidal cells in the cerebral cortex are aligned parallel with each other and perpendicular to the cortical surface. When a population of these cortical neurons is excited, the electrical field

produced along the axis (toward the cortical surface) is enhanced and can be recorded with EEG at the scalp surface. Conversely, the portion of the field that is perpendicular to the axis of the neuron is cancelled by the fields of nearby neurons. Even with a large population of neurons, the amplitude of the electrical potentials produced quickly dissipates with increasing distance from the scalp surface. Therefore, recording of neuronal signals from the scalp surface, such as EEG, are often thought be primarily of cortical origin. Moreover, since EEG measures the electrical component of an electromagnetic signal, the cortical sources that align perpendicular to the scalp surface give the largest field potentials. For reviews, please see Lopes (2010) and Niedermeyer (1999). This is opposite for MEG, as the electric and magnetic potentials are perpendicular to each other (Salmelin & Baillet, 2009). Oscillations of these neuronal populations are commonly known as brain waves.

1.5.2 EEG Frequency Spectrum

One way in which EEG signals are categorized is by the number of times it oscillates per second or its frequency. Generally, there are five defined categories in the frequency domain known as EEG frequency bands. These bands include the delta (0 – 4 Hz), theta (4 – 8 Hz), alpha (8 – 12 Hz), beta (12 – 30 Hz), and gamma (> 30 Hz) bands. The size of the frequency ranges, bounds, and even naming conventions vary slightly between different fields of EEG study. For example, alpha rhythms recorded over the sensorimotor cortex during movement are also known as mu rhythms (Lopes, 2010). Each frequency band has been shown to be important over different parts of the cortex for different activities. For example, the delta band is often associated with sleep (Lopes,

2010) and movement-related slow potentials and modulations of beta band power have been shown over the sensorimotor cortex during movements (Kilavik et al., 2013). The characteristic frequency spectrum of a resting state EEG signal is $\frac{1}{f^n}$, where n is approximately 1 to 2. This relationship is known as the power law and it describes the relationship between the amplitude of the neural signal and its frequency. Though still under debate, it is hypothesized that this scaling is due to the low-pass frequency filtering attributes of dendrites (Buzsáki et al., 2012).

1.5.3 Evoked and Induced Potentials

Two general categories of brain signals used to study the brain are known as evoked and induced potentials. Evoked potentials (EPs) or Event Related Potentials (ERPs) are so named because the signals are time-locked to a specific event. Events are usually sensory (visual, auditory, somatosensory, etc.) in origin, such as flash of light, an audible tone, electric stimulation, or movement perturbation. This technique used with temporal averaging of the signals is an indirect measure of cortical processing. The stimuli are repeated dozens or hundreds of time to improve the signal-to-noise ratio of the averaged signal, which will provide a better signal estimate. Induced responses to a stimulus, however, are not time locked to a stimulus. Therefore, temporal averaging of such responses yields no or little discernible signal. For example, if a neural signal is oscillating at 25 Hz and an event occurs that causes the amplitude of that 25 Hz oscillation to decrease or increase, temporal averaging of that signal with noise and other factors will be near zero. In order to capture the modulation of that signal, the signal can be rectified and smoothed to produce the amplitude modulation profile. This,

consequently, can be time-locked to a stimulus event and then can be detected and used for analysis.

1.5.4 Movement-related Cortical Potentials

Two types of movement-related brain potentials are slow cortical potentials and amplitude modulations in beta power. The most studied slow cortical potential is the bereitschaftspotential (BP), or readiness potential (Colebatch, 2007; Shibasaki & Hallett, 2006). This movement-related brain potential (MRBP) is associated with premotor areas and the preparation to execute movement. Interestingly it can be detected 1.5 seconds before the movement occurs, which has caused some controversy and discussions about the state of free will (Libit, 1999). Amplitude modulations of beta power have also been associated with movement. Preceding and during movement, the beta power reduces in amplitude. This is known as an event-related desynchronization (ERD), and it is hypothesized that this reduction in power is associated with an increase in neural activity that disrupts the resting oscillations of the cortex. After movement, a rebound in the beta power amplitude overshoots the resting state level. This is referred to as an event-related resynchronization (ERS). The BP, ERD, ERS, and various other movement-related cortical potentials have been used as probes to study how the sensorimotor cortex controls movements in neurologically intact people, people with neural injuries (Gourab & Schmit, 2010; Müller-Putz et al., 2007), and in brain computer interfaces (Pfurtscheller et al., 2003).

1.6 EEG ARTIFACTS AND SIGNAL PROCESSING

1.6.1 EEG Artifacts

There a number of well-known artifacts present in most EEG recordings. These include ocular, movement, slow drift, and electrical artifacts. Ocular artifacts reflect the EMG activity of the eye muscles during movement and blinks. Movement-related artifacts are often induced by quick movements of the head that physically move the electrodes, thus changing the impedance between the electrode and the scalp. Since the voltage (V) recorded is proportional to this impedance (Z) (i.e. V=IZ), changes in impedance will change the recorded voltage even if the current remains the same. Slow drifting potentials can cause problems when recording very low frequency or DC potentials. These artifacts are typically the result of sweat on the scalp surface that slowly changes the impedance. Finally, external electrical noise can induce noise into the EEG data. The most common electrical artifact is the 60 Hz line noise from lights.

1.6.2 Artifact Removal

EEG artifact removal requires the appropriate selection and ordering of specific signal processing steps. For every dataset the goal of EEG signal processing is to = remove artifacts and reveal as much of the underlying neural signal as possible. Temporal filtering is one of the most basic types of EEG artifact removal. This technique can be implemented with both analog electronics during recording and with digital filtering techniques afterwards. For large repetitive artifacts, such as eye blinks, templating can be used to remove the blink artifact while preserving some of the cortical

signal. If an experiment includes a response time-locked to known points, such as an evoked potential, underlying cortical responses can be accentuated by temporally averaging many repetitions of the task. Finally, blind source separation techniques, such as principle component analysis (PCA) and independent component analysis (ICA) can be useful to remove distinct artifacts that are mixed with cortical EEG signals.

1.6.3 Independent Component Analysis

Independent component analysis (ICA) is classified as a Blind Source Separation (BSS) method for decomposing data into statistically independent components (Stone, 2004). For an ICA decomposition of EEG signals, recorded data from each electrode location are assumed to represent linear mixtures of underlying neural sources. Assuming there is at least the same number of electrodes as sources of neural activity and that the sources are independent, the first step of the ICA analysis *whitens* the data to remove any correlations between the individual electrodes. After whitening, the statistical properties of the mixed signals (e.g. variance, kurtosis) are used to extract a square weighting matrix the size of the number of original linearly independent electrodes. Though there are a number of methods to determine this matrix and the statistical independence of the components, two such methods include minimizing gaussianity or mutual information (Infomax). This weighting matrix is then used to convert EEG signals in electrode space into ICA component space. For artifact removal, ICA components that have distinct artifact characteristics are removed and the remaining components can be projected back to electrode space, now artifact free, for further

analysis. Similarly, the ICA components themselves can be used for continued analysis, as they represent the unmixed and localized neural activity.

1.7 SPECIFIC AIMS

1.7.1 Aim 1: Identify the sensorimotor cortical contribution of rhythmic and discrete movements of the ankle.

The purpose of this study was to ascertain the extent to which the sensorimotor cortex plays a role in the perpetuation of unilateral, rhythmic and discrete movements of the ankle. Electroencephalography was used to measure neural activity in ten young, healthy subjects while they performed rhythmic and discrete ankle movements at approximately 0.7 Hz. We hypothesized that if the cortex was continuously involved in rhythmic movements, movement-related slow potentials would be similar to those observed during discrete movements. However, during rhythmic movements, pre- and post-potentials would be absent.

1.7.2 Aim 2: Differentiate the sensory and motor cortical contributions to rhythmic movements of the ankle.

In this study, we aimed to decouple the unique involvement of the individual sensory and motor cortices in the propagation of rhythmic ankle movements. Ten young, healthy subjects performed unilateral, rhythmic ankle movements in a custom robotic device. The robot was used to constrain the position, range, and frequency of ankle movement to increase consistency between trials and subjects. The protocol included combinations of three factors: volition, attention, and movement frequency. Sensory and motor contributions to the cortical signal were identified with passive and active

movements, respectively. We hypothesized that movement-related slow potentials over the sensory cortex would be continuous during rhythmic movements. However, the motor related potential would be associated with the muscle activity.

1.7.3 Aim 3: Determine the sensory and motor cortical contributions to bilateral, rhythmic movements of the ankle.

The goal of this experiment was to determine the role of the sensory and motor cortices in the propagation of rhythmic, bilateral ankle movements. Similar to the previous experiment, electroencephalography was recorded during active and passive rhythmic ankle movements in a custom robotic device. The protocol for this experiment included four bilateral and two unilateral movement conditions. During bilateral movement conditions, the left ankle lagged the right by 0^{o}, 90^{o}, 180^{o}, and 270^{o}. We hypothesized that bilateral and unilateral movements require the same neural generators to perpetuate rhythmic movements. However, the close spatial locations of the generators produced destructive and constructive interference of the generated electrical fields.

CHAPTER 2: MOVEMENT-RELATED SLOW POTENTIALS OF THE SENSORIMOTOR CORTEX DURING RHYTHMIC AND DISCRETE ANKLE MOVEMENTS

2.1 INTRODUCTION

In humans, the cerebral cortex appears to be continuously involved in the production of rhythmic movements of the lower extremities. In comparison, non-human mammalian control of rhythmic leg movements, such as walking, swimming, and scratching is often described in terms of spinal reflexes and networks, such as central pattern generators (CPGs) (Fore a review, please see Frigon, 2012). However, these spinal networks in humans are not sufficient to produce consistent rhythmic movements when supraspinal drive is disrupted, as evidenced by gait impairments after spinal cord injury (SCI) (Dobkin et al., 2007) or stroke (Buurke et al., 2008). Therefore, it has been hypothesized that through evolution, the role of cortical structures in the production of lower extremity rhythmic movements has been emphasized to compensate for the less stable, bipedal nature of human locomotion (Nielsen, 2003). Recent studies have supported this concept, demonstrating that the human sensorimotor cortex is actively involved in producing lower extremity movement during stepping (Wieser et al., 2010), walking (Gwin et al., 2011; Petersen et al., 2012; Wagner et al., 2012), and pedaling (Jain et al., 2012; Mehta et al., 2009). Though these studies demonstrate cortical involvement and modulation of neural signaling, further knowledge of the fundamental aspects that underlay the cortical contribution to rhythmic movements is important to our understanding of movement deficits following neural injury.

Both kinematics and neural control mechanisms differentiate rhythmic and discrete movements; however, the variation and complexity of these movement types

have made definitions difficult to elucidate. A proposed kinematic taxonomy by Hogan and Sternad (2007) defines a discrete movement as a movement bounded by two postures, where a posture is a period of no movement. In contrast, the continuality, or absence of defined postures, generally defines rhythmic movements. Rhythmic movements are differentiated into specific sub-types that range from simple cyclic movements to more complex repetitive patterns. Neurologically, discrete movements require cortical involvement attributed to planning, execution, and termination of the individual movements (Kalaska, 2009; Sabes, 2000). However, the role of the sensorimotor cortex is less defined for the perpetuation of rhythmic movements, especially in the lower extremity.

One method of measuring the cortical contribution to rhythmic and discrete movements is electroencephalography (EEG); specifically, spatiotemporal characteristics of movement-related slow potentials might provide insight into cortical control. In contrast to other movement-related brain potentials (e.g. beta desynchronization), slow potential oscillations are time-locked to the movement profile (Grünewald-Zuberbier et al., 1980), and have been shown to be related to kinematic (Mayville et al., 2005) features of movement. Similar to other brain potentials, these slow potentials are thought to be cortical in origin because of their large signal amplitude recorded by surface EEG. However, the specific mechanisms underlying slow potentials are still largely unknown (see Birbaumer et al. (1990) for some theoretical explanations). In discrete movements there are various types of pre-potentials (e.g. Bereitschaftspotential), potentials during movement (e.g. movement monitoring potentials), and post-potentials; all of which depend on the kinematics or kinetics of the movement and various cognitive factors (e.g.

attention) (Deecke et al., 1984). To the best of our knowledge, the characteristics of slow potentials during rhythmic movements of the lower extremity have not been studied.

In the current study, we recorded EEG from young, healthy adults performing discrete and rhythmic ankle movements. We hypothesized that temporal profiles of movement-related slow potentials over the medial sensorimotor cortex would be similar for both rhythmic and discrete movements, but discrete movements would have additional pre- and post-potentials related to initiation and termination of movement. This would support the theory that rhythmic movements require a subset of the neural mechanisms observed during discrete movements (Schaal et al., 2004).

2.2 METHODS

2.2.1 Study Participants

Ten young adults (5 male and 5 female) with an age range of 20 to 32 years old participated in this study. All subjects were in good health and reported no history of neurological disease or injury. Prior to participation, each subject provided written, informed consent. All procedures were approved by the Institutional Review Board at Marquette University, in accordance with the Declaration of Helsinki (World Medical Association, 2008).

2.2.2 Experimental Protocol

Subjects sat upright at the end of a therapy table (Electro Medical, Marietta, GA) with their backs supported. Their lower legs were free hanging at approximately 90^{o} of knee flexion and their ankles at a relaxed neutral position (Figure 2-1).

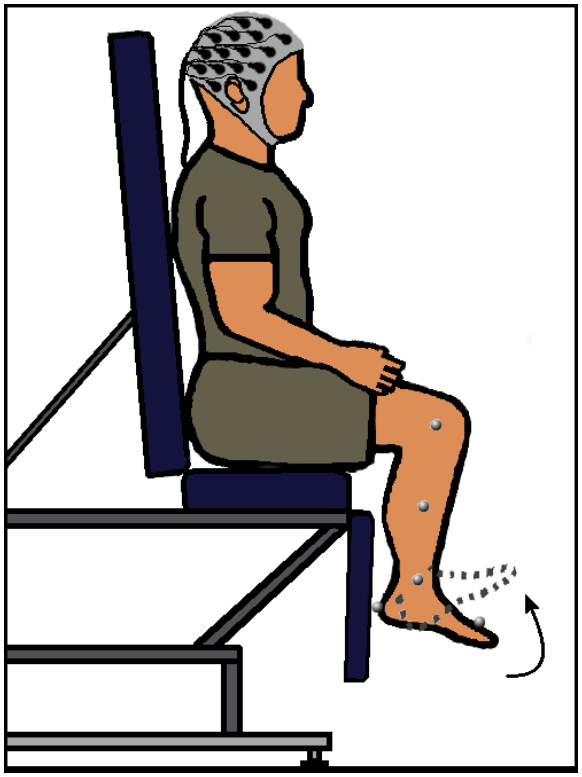

Figure 2-1: Experimental Setup. Subjects sat on a therapy table with their lower legs free hanging. Kinematic markers placed on the lower leg recorded right ankle movements. A 64-channel active electrode EEG cap recorded neural signals throughout each movement trial.

The experimental protocol consisted of rhythmic, discrete, and ballistic movement conditions with two, five-minute trials each. During all trials, subjects moved their right ankle in a cyclic pattern starting from a relaxed position up to a comfortable dorsiflexion and back down. For rhythmic movement trials, subjects continuously repeated this pattern at approximately 0.7 Hz. Conversely, discrete movement trials included a self-paced rest period between each movement of approximately 1 to 2 seconds. During ballistic trials, subjects concentrated on the screen, and a green circle appeared for 100 ms that served as an external visual cue to make a brisk dorsiflexion movement with a randomized intertrial rest period of 7 to 9 seconds.

To ensure kinematic consistency throughout the rhythmic and discrete trials, subjects matched their ankle movement with a virtual slider that moved up and down at a frequency of 0.7 Hz on a large screen, approximately two meters in front of them. In order to reduce the influence of eye movement artifacts in the EEG signal, the slider was visible in a pattern of 5 seconds *on* and 30 seconds *off*, during which subjects fixated on a cross on the screen. Data recorded during the *on* periods were excluded from the final analysis.

2.2.3 Physiological Measurements

During the experimental trials, a 64-channel active electrode actiCAP (Brain Products, Germany) continuously recorded EEG data. The electrode positions of this cap conformed to the international 10-20 coordinate system with a reference at FCz and a ground at AFz (See Appendix A). Experimenters placed the EEG cap on the subject's head so that the Cz electrode was at the vertex, in line with the prearticular points of each ear in the frontal plane and with the nasion and inion in the sagittal plane. Each electrode site was hydrated using a syringe, blunted needle, and SuperVisc gel (Brain Products, Germany) in order to reduce the electrical impedance to a level below 10 kOhms between the electrode and the scalp surface. Throughout the experimental session, EEG signals were amplified, sampled at 2000 Hz, and filtered from DC to 500 Hz using a Synamps^2 system (Neuroscan, Charlotte, NC), and recorded using the Neuroscan software, Scan 4.5.

Motion analysis and electromyography (EMG) were measured to characterize lower leg kinematics and muscle activation patterns throughout movement trials. Vicon

MX3+ motion capture cameras (Oxford, UK) were used to identify the position of five reflective markers that were placed on the lateral side of the right knee, tibia, and ankle, along with markers placed over the midheel and second digit of the foot (Figure 2-1). Additionally, wireless Trigno^{TM} EMG sensors (Delsys, Boston, MA) measured muscle activation patterns of the right tibialis anterior (TA), medial gastrocnemius (MG), and soleus (SOL). Vicon software sampled and recorded both the marker positions and EMG signals at 100 and 2000 Hz, respectively. Finally, custom LabVIEW (National Instruments, Austin, TX) code produced the intermittent virtual movement slider, visual cues, and generated digital pulses recorded in both Vicon and Neuroscan to synchronize the timing of the movement and EEG data offline.

2.2.4 Data Processing

EEG Artifact Removal

Initial processing steps removed noise and artifacts from the EEG signals using custom MATLAB scripts (2011a, The MathWorks, Natick, MA) and EEGLAB functions (version 12.0.0.0b) (Delorme & Makeig, 2004). First, corrections applied to the raw data removed any DC offset and drift (third-order polynomial) using Scan 4.3 software (Neuroscan, Charlotte, NC). Next, EEG data were referenced to a common average that included the reference electrode. Then low frequency and power line noise were removed using a band-pass, FFT square filter from 0.2 to 100 Hz and notch-filter from 59 to 61 Hz, respectively. Finally, an Adaptive Mixture Independent Component Analysis (AMICA) (Palmer et al., 2008) was implemented to decompose signals for each trial into 64 individual components, and then artifact components were identified for removal

using the ADJUST plugin (Mognon et al., 2010) to EEGLAB. We found these processing steps suitable to remove the eye blink and other artifacts, yet conservative enough to maintain the movement-related slow potential amplitude. Remaining components were back projected to the original EEG channel space for further analysis.

Electromyography Processing

Temporal processing of EMG data determined the max muscle activation during individual movement trials. EMG amplitude was defined as the max value of the root mean squared (RMS) muscle activation. To calculate the RMS EMG, first, band-pass filtering of the raw EMG data eliminated extraneous signal noise below 30 and above 200 Hz (zero-phase, 4^{th}-order, Butterworth). Signals were then squared and smoothed using a 50 ms sliding window with 25 ms padding of the first and last temporal values to retain the original signal length. Finally, a square root transform was applied to the signals.

Cycle Definition

Characteristics of the temporal ankle angle profile identified the initiation and termination of individual movement cycles. The angle between the three-dimensional vectors created by the heel to toe and ankle to knee markers defined the ankle angle at each point in time (See Appendix B). After calculation of ankle angle, temporal angle profiles were upsampled from 100 Hz to 2000 Hz using linear interpolation to match the sampling rate of the recorded EEG. Ankle angle data were then band-pass filtered (fourth-order, zero-phase, Butterworth) from 0.1 to 1.5 Hz to extract the main kinematic

movement pattern. Finally, the data were inverted so that local maxima corresponded to peak dorsiflexion.

For rhythmic trials, a cycle start point was identified as a position of relaxation (local minima), and a corresponding stop point was defined as the point before the subsequent start point. For discrete and ballistic trials, start and stop points were calculated as one *full width at half max* (FWHM) distance before and after each maximum dorsiflexion (local maxima), respectively. The difference between each max dorsiflexion and the previous baseline value defined the amplitude values for the FWHM calculation, where baseline values were the midpoint between the current and previous max dorsiflexion point (See Appendix C). Start and stop point pairs, during rhythmic and discrete movements, that overlapped the five-second visual cueing periods were removed from further analysis.

Temporal Processing

Temporal averaging extracted movement-related slow potentials and muscle activation patterns time-locked to the movement cycles. The EEG and EMG data of each trial were epoched into cycles from half a movement cycle before (-Half) each start point to half a movement cycle after (+Half) each end point. For rhythmic movements, this range was defined from the previous to the subsequent max dorsiflexion point. For discrete and ballistic movements, these points were defined as two FWHM before and after max dorsiflexion (See Appendix C). Individual cycles were eliminated from further processing if the movement time or amplitude exceeded three standard deviations from their respective means. Due to the variability in length, cycles were resampled to 2000

points and time warped to align the -Half, start, max dorsiflexion, stop, and +Half points (See Appendix D). Position data, EEG, and EMG for the remaining movement cycles were averaged. Due to consistency of amplitude and signal morphology, individual subject data were not normalized before creating grand average plots.

Source Localization

Cortical localization algorithms were used to determine the spatial distribution of current sources with the highest probability of producing the recorded EEG signals. For all subjects, sources were modeled using the default anatomical template of the cortex derived from the MNI/Colin27 brain in Brainstorm software (Tadel et al., 2011). The standard actiCAP electrode locations were fit to the scalp surface so that the Cz electrode was at the vertex. The center electrode row in the sagittal plane (i.e. Fz, Cz, Pz) was situated on the midline between the nasion and inion and the center row in the frontal plane (i.e. C3, Cz, C4) with the prearticular points of the ears. Since EEG is susceptible to geometrical approximations of the head, Brainstorm used boundary element modeling (BEM) to estimate the forward model (OpenMEEG) (Gramfort et al., 2010; Kybic et al., 2005), and the inverse model was estimated by the depth-weighted minimum L2 norm estimator of cortical current density (Hämäläinen & Ilmoniemi, 1994). Individual cortical projections were then averaged across cycles within each subject. To maintain signal amplitude for group comparison between conditions, single subject projections were not normalized before creating grand average plots.

Power Spectral Analysis

Two separate analyses of the EEG frequency spectrum were used to compare rhythmic, discrete, and ballistic movement types. Data were filtered and artifact components from ICA decomposition were removed as previously described. The first analysis examined changes in low delta frequency power (0.2 to 1 Hz), which used data from only one of the five-minute trials for each movement condition. Within each trial, only the data during the *off* periods of visual cueing were used for the rhythmic and discrete trials. The frequency spectrums were calculated for each EEG channel using Welch's method for estimating power spectral density (PSD). Parameters for this estimate included data segmentation of 8192 points (4.096 seconds) with 50% overlap, and each segment was windowed with a Hamming window of the same length. To ensure there were an equal number of segments (averages) per condition, times series for each condition were truncated to the shortest length of the three conditions. For example, if the rhythmic condition had a time series of 5.1 minutes, the discrete 5.0 minutes, and ballistic 4.9 minutes, all EEG time series were truncated to 4.9 minutes.

The second analysis examined power differences during the movement at frequencies above 1 Hz and excluded resting periods during discrete and ballistic conditions. For all conditions, cycles were epoched from the start to end of each movement and concatenated to remove rest periods. Data were subsequently high-pass filtered at 1 Hz (Butterworth, 8^{th}-order, zero-phase) to remove low frequency content induced by concatenation. As described previously, the data were then truncated to the shortest length of the three conditions and the PSD estimated for each EEG channel.

Subsequently, for both analyzes, total power for EEG frequency bands at each electrode location were calculated. Power bands were split into the low delta (0.2 to 1 Hz), high delta (1 to 4 Hz), theta (4 to 8 Hz), alpha (8 to 12 Hz), beta (12 to 30 Hz), and gamma (30 to 50 Hz) and the total power per band was calculated using the trapezoidal method for discrete integration.

Finally, for each frequency band, power differences at each electrode were calculated as the percent difference in power during the rhythmic movement task, using the discrete movement task as the baseline measurement. Significant electrodes were identified using Student's t-tests (Student, 1908) to compare the subject distribution of percent change values to zero. Multiple comparisons were corrected for using the false discovery rate (FDR) method (Benjamini & Hochberg, 1995) with an initial α value of 0.05.

2.3 RESULTS

The aim of this study was to describe the activity of the sensorimotor cortex during rhythmic and discrete ankle movements. For comparison, ankle kinematics were maintained between these trial types, and paired Student's t-tests confirmed no significant differences between the number of averaged cycles ($p = 0.17$) or mean cycle lengths ($p = 0.44$). Moreover, peak dorsiflexion during discrete movements was on average only 3^{o} greater than rhythmic movements. Additionally, the percent difference between conditions showed no correlation between EEG amplitude and TA EMG max amplitude ($p = 0.11$) or area ($p = 0.17$). Therefore, we based the comparisons of EEG potentials on similar movements, with the dominant difference being the rhythmic or discrete nature of

the task. Conversely, kinematic profiles and muscle activity during the ballistic trials were not controlled, as is the nature of this movement type.

Temporal averaging of EEG revealed slow potentials time-locked to each of the three movement conditions (Figure 2-2). The amplitudes of these movement-related slow potentials were largest over the medial sensorimotor cortex, confirmed by distributed source localization (Figure 2-3). Discrete and ballistic movement trials produced a large underlying potentiation at the movement frequency (0.7 Hz) that is referred to hereafter as the movement frequency component or MFC_1.

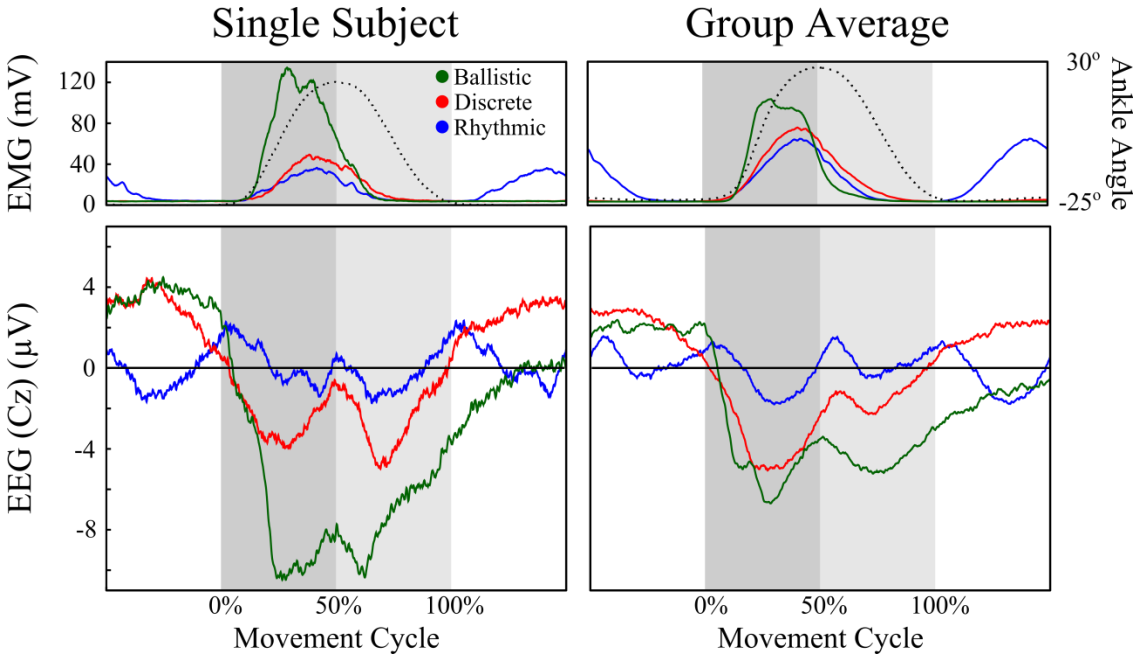

Figure 2-2: Slow Potentials during Rhythmic, Discrete, and Ballistic Movements. Temporal averages of the EEG response (bottom) for a single representative subject (Sub 1) (left) and the group average (right) over the medial sensorimotor cortex (Cz electrode) during ballistic (green), discrete (red) and rhythmic (blue) ankle movements. Root mean square (RMS) EMG of the TA muscle is color matched to the movement type (top). Position of the ankle is denoted with a dotted black line, which is most positive at peak ankle dorsiflexion. All movements are normalized in time to percent of the movement cycle. The dorsiflexion period is indicated by the dark gray background, the relaxation period with a light gray background, and half a cycle preceding and following the movement is displayed with a white background.

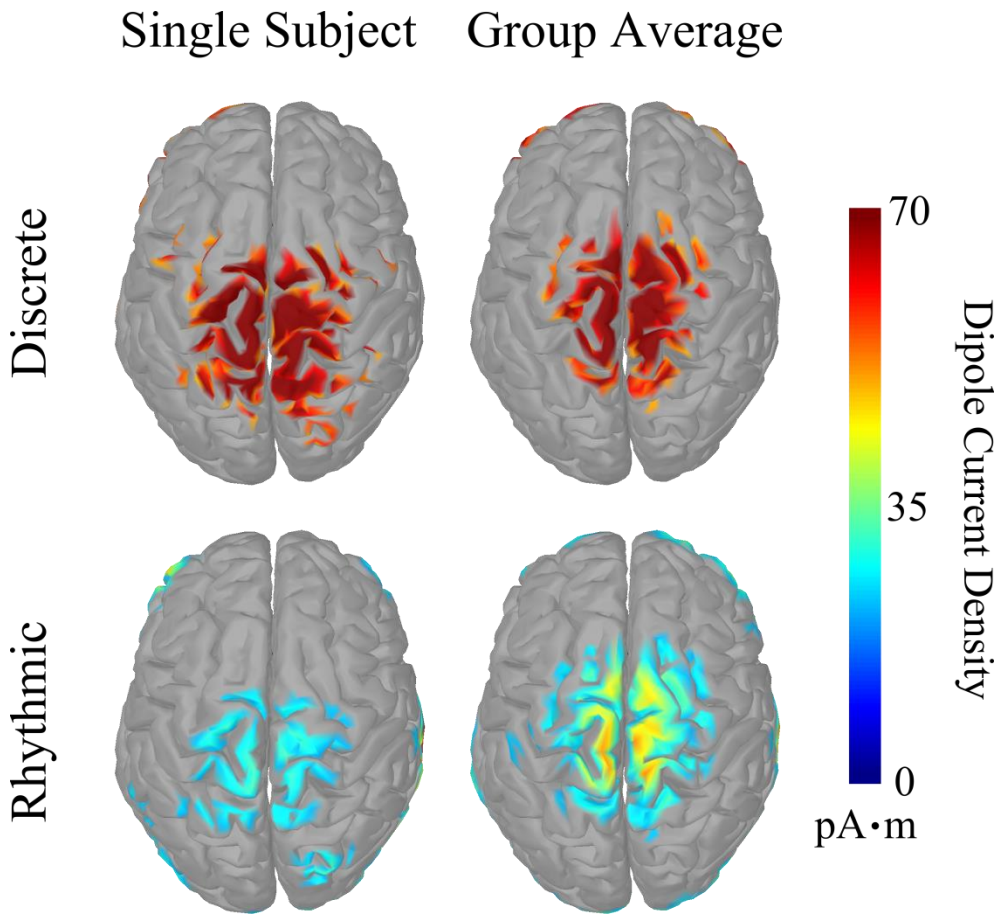

Figure 2-3: Spatial localization of Movement-related Slow Potentials. Cortical sources spatially localized to the medial sensorimotor cortex for both the rhythmic and discrete movement conditions. Plots represent the dipole current density of the time-averaged signal over a movement cycle. The movement cycle for both a single representative subject (Sub 1) (left) and the group average (right). For visual display, lower dipole current density thresholds were set at 50 pA·m for the discrete trials (top) and 20 pA·m for rhythmic trials (bottom) to highlight the local maxima.

This component of the slow potential was comprised of positive pre- and post-movement potentials and deflected negatively during the movement. Though masked by a harmonic frequency, the timing of the negative peak MFC_1 was approximated to be within 25% to 50% of the movement cycle. This potential was absent or significantly reduced in the rhythmic movement trials, as shown by a significant decrease in amplitude

during dorsiflexion ($F(1.3, 11.6) = 30.7$, $p < 0.0001$, Greenhouse-Geisser Correction) (Figure 2-4).

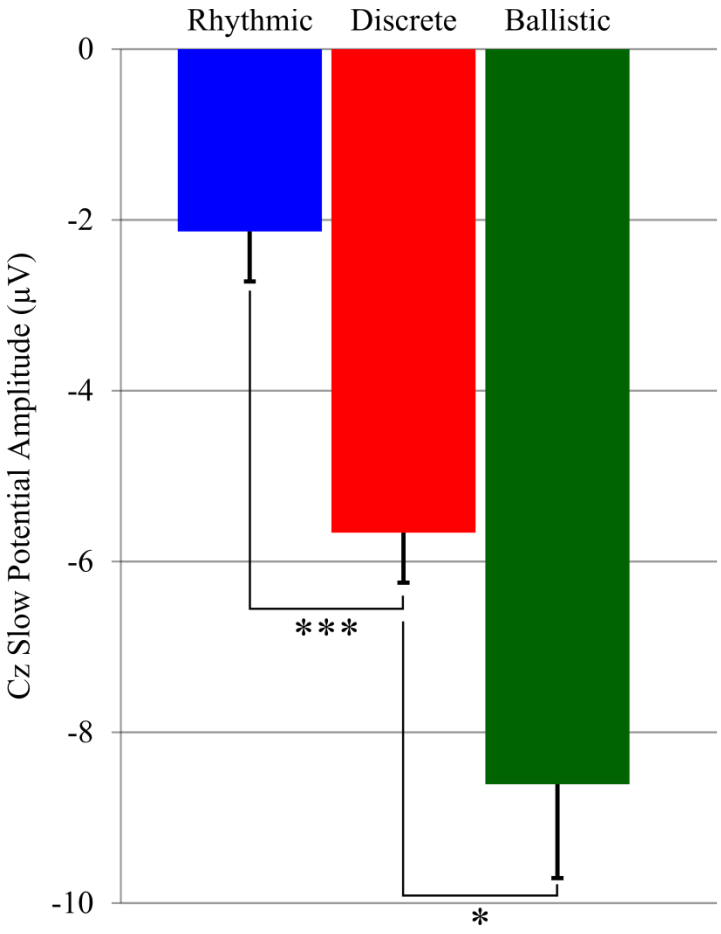

Figure 2-4: Local Negativity during Dorsiflexion. This figure displays the average local minimum value of the EEG slow potential over the medial sensorimotor cortex (Cz electrode) during the dorsiflexion phase of movement in Figure 2-2. Significance levels are denoted as * ($p < 0.05$) and *** ($p < 0.0005$). Error bars denote the standard deviation across subjects.

Additionally, a secondary component (MFC_2) at twice the movement frequency (1.4 Hz) was evident in the averaged trials. This component modulated similarly between all movement conditions and with approximately the same amplitude between the three conditions (Figure 2-5). Negative potentials were present during the transition phases of the movement, with a positive deflection observed during the period of TA

muscle relaxation. The similarity of this potential between the conditions was accentuated by high-pass filtering of the EEG signal at 1.0 Hz, above the movement frequency (0.7 Hz), to remove the slow, movement-frequency fluctuation.

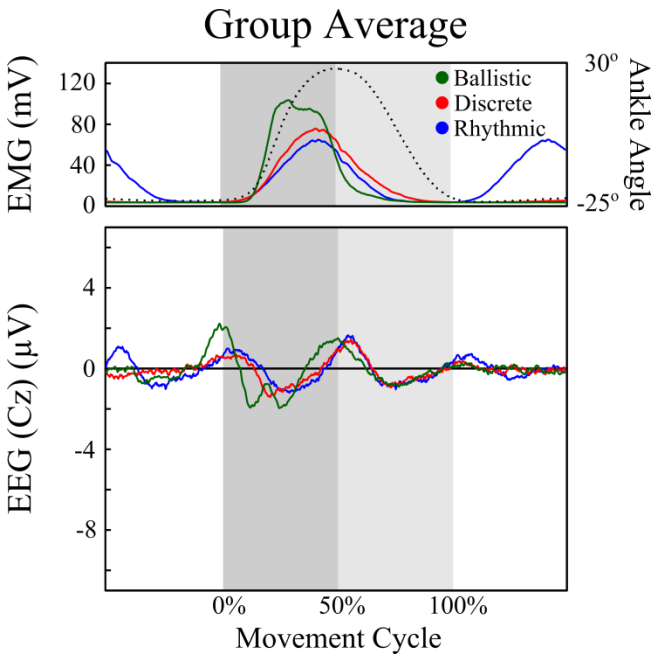

Figure 2-5: Second Harmonic of the Fundamental Movement Frequency. Group average of the EEG slow potentials during each movement type over the medial sensorimotor cortex (Cz electrode) high-pass filtered at 1.0 Hz. Filtering the slow potential responses above the movement frequency (0.7 Hz) demonstrates the similarity of the second harmonic signal, MFC_2, between the rhythmic and discrete trials.

Comparison of power between rhythmic and discrete movements revealed a localized reduction in delta frequency power for rhythmic movements (Figure 2-6). Differences in delta frequency power exhibited a greater reduction in low delta power (0.2-1 Hz) than high delta power (1-4 Hz). This was consistent across subjects with an average decrease in low and high delta power of 46% and 16%, respectively. This localized reduction in EEG power was observed over the medial sensorimotor cortex

(approximately the Cz electrode), and it dissipated from that point outward. No other significantly different electrodes were noted in any other frequency band.

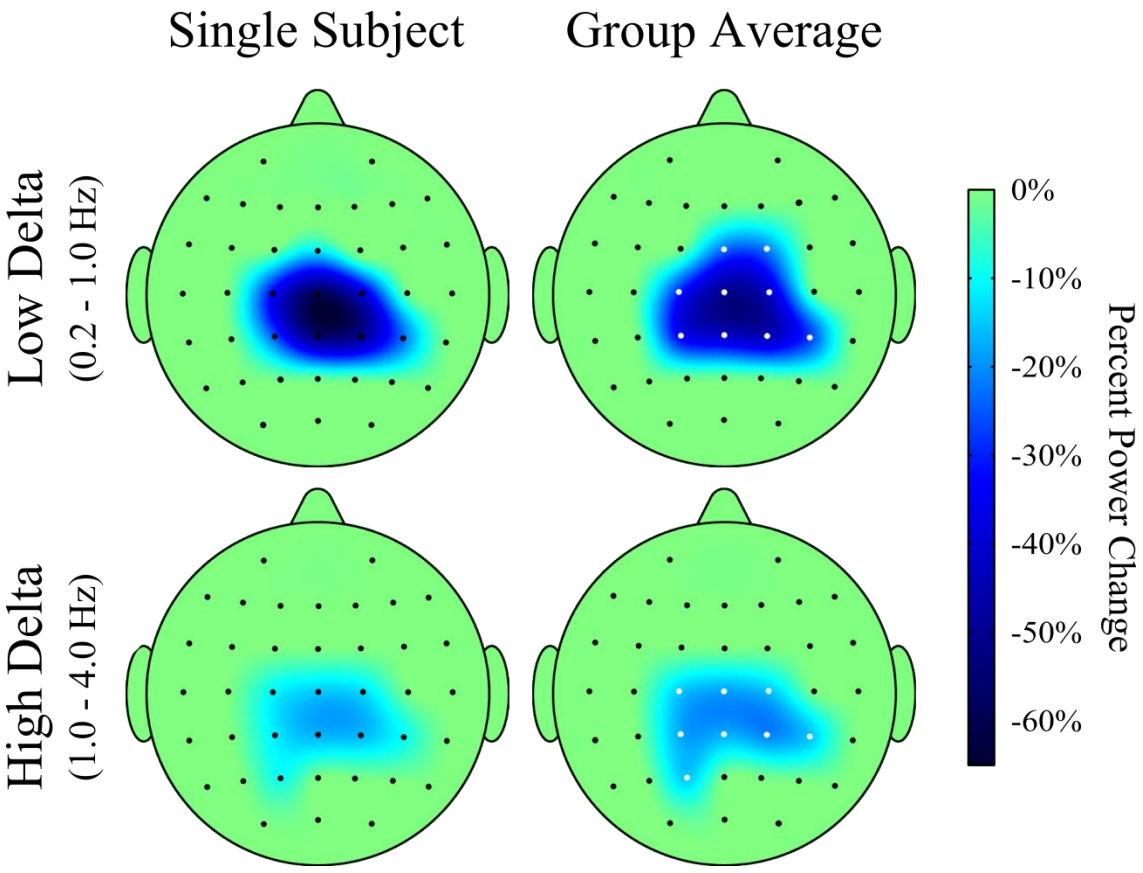

Figure 2-6: Percent Signal Change of Delta Frequency Power. 2-D surface maps of low delta (0.2 to 1 Hz) and high delta (1 Hz to 4 Hz) frequency bands expressed in percent power change for rhythmic relative to discrete movement trials. A localized negativity in the medial sensorimotor cortex was apparent in both a single representative subject (Sub 1) (left) and the group average (right). These maps (both single subject and group average) display only the percent change in power for the statistically significant electrodes (white in the group average). Peripheral electrodes were removed for display and were not significant.

2.4 DISCUSSION

Results from this study demonstrated that the cerebral cortex is continuously involved in lower extremity rhythmic movements. In all movement conditions, slow potentials recorded over the medial sensorimotor cortex established continuous neural activity time-locked to the movement. Though slow potentials related to rhythmic and discrete movements were similar, an attenuation of the fundamental movement frequency component, MFC_1, was a unique feature of rhythmic movements. Therefore, we believe that the control mechanisms of rhythmic movements are a subset of those associated with discrete movements.

Cortical slow potentials during rhythmic movements produce spatiotemporal characteristics similar to discrete movements. In this study, slow potentials of all movement types spatially localized to the medial sensorimotor cortex with comparable temporal profiles. These results are supported by previous reports of similar slow potential profiles that are observed during discrete wrist (Grünewald-Zuberbier & Grünewald, 1978) and finger (Mayville et al., 2005) movements. During movement, we described these slow potentials in terms of two unique components, MFC_1 and MFC_2. The first of these components was the fundamental movement frequency potential, MFC_1, as it oscillated once per movement cycle. This component produced perimovement positivities and a max negativity during the dorsiflexion phase of movement. The second component, MFC_2, was a harmonic of MFC_1, at twice the movement frequency. This component was most prominent during movement and characterized by negativities during transition phases of movement and positivity near

peak dorsiflexion. Though both the MFC_1 and MFC_2 components exist in rhythmic and discrete movements, their relative proportions appear to be different.

The amplitude of the fundamental movement frequency component differentiates rhythmic and discrete movements. Visually, the perimovement potentials and larger negativity apparent in the temporal traces of discrete movements are absent or highly attenuated in rhythmic movements (Figure 2-2). This is supported by the localized attenuation of low delta power over the medial sensorimotor cortex (Figure 2-6). In contrast, the MFC_2 component is similar between rhythmic and discrete slow potentials (Figure 2-5). Movement-evoked magnetic fields also reveal similar components during discrete finger movements at different rates (Mayville et al., 2005). As the rate of movement increases, the MFC_1 potential decreases in amplitude, but the amplitude of the MFC_2 remains constant. Therefore, the MFC_1 is likely associated with the initiation and termination of individual discrete movements, as they differentiate the movement conditions. Additionally, the MFC_2 is likely associated with the movement kinematics or muscle activation, which is consistent between both conditions.

The attenuation of the MFC_1 component coupled with the similar MFC_2 component supports the hypothesis that rhythmic movements are a subset of discrete movements. Therefore, the components of rhythmic movements may be contained or shared by the larger set of discrete components. Observed in this study, discrete movements share the MFC_2 component with rhythmic movements, but additionally have the MFC_1 component, most probably due to initiation and termination of movement. Though this study focuses on the temporal aspects of the neural processing, this same idea has been shown spatially using fMRI in the upper extremity (Schaal et al., 2004).

Together, these data suggest a high cortical influence on rhythmic movements that is similar temporally and spatially to discrete movements and the theory that discrete movements are aborted rhythmic movements. These results contradict the idea that rhythmic movements are a concatenation of discrete movements, since the added temporal traces would not equal the rhythmic signal. While it is possible that separate neural processes control rhythmic and discrete movements, the high degree of overlap suggests otherwise.

All together, these results suggest continuous involvement of the sensorimotor cortex in the production of lower extremity rhythmic movements. Moreover, the control mechanisms of lower extremity rhythmic and discrete movements appear similar, though discrete movements require additional cortical activity to initiate and terminate each individual movement. However, due to the poor spatial resolution of EEG recordings, it is still unknown whether the observed movement-related slow potentials represent motor, sensory, or mixed cortical activity. Future experimentation will use passive and active movements to explore the cortical origins of these potentials.

CHAPTER 3: UNIQUE MOVEMENT-RELATED SLOW POTENTIALS OF THE SENSORY AND MOTOR CORTICES DURING RHYTHMIC MOVEMENTS OF THE ANKLE

3.1 INTRODUCTION

The individual roles of the human sensory and motor cortices in the perpetuation of rhythmic movements of the lower extremities are still unknown. In lesser mammals, spinal reflexes and networks are alone sufficient to elicit lower extremity rhythmic movements (For a review, please see Frigon, 2012). However, the disruption of the supraspinal drive to the spinal cord results in greater impairments to human locomotion (Dietz et al., 1995). In a previous experiment, we observed movement-related slow potentials of human sensorimotor cortex are time-locked to both rhythmic and discrete movements, as evidenced by the spatiotemporal characteristics of movement-related slow cortical potentials (Chapter 2). However, the individual contributions of the sensory and motor cortices to the slow potentials were difficult to differentiate because of the contemporaneous afferent and efferent cortical activities.

One method used to decouple the individual sensory and motor cortical contributions to movement is the comparison of neural responses elicited by active and passive movements (Guzzetta et al., 2007; Mehta et al., 2012; Mima et al., 1999; Onishi et al., 2013). Here, neural imaging has been used in conjunction with a predetermined single- or multi-joint kinematic pattern held constant for all movement trials. During active trials, subjects produce volitional movements that elicit neural activity associated with both the motor drive to the muscles and the sensory feedback to the brain. Conversely, subjects are moved through the same kinematic pattern during passive trials, which primarily emphasizes the sensory component of the movement. Finally, the

difference in neural activities observed during the active and passive conditions describes the motor or volitional component of the movement.

Multiple studies have used active and passive movements together with various imaging modalities to study the sensory and motor contributions to rhythmic movements of the lower extremities. Positron emission tomography (PET) (Christensen et al., 2000) and functional magnetic resonance imaging (fMRI) (Mehta et al., 2012) during pedaling indicate similar areas of activation in the medial sensorimotor cortex and cerebellum during active and passive movements. These imaging modalities have better spatial compared to temporal resolution that provides precise localization of the movement-related neural activity in the brain. However, imaging modalities such as PET and fMRI have poor temporal resolution required to observe the underlying cortical dynamics.

These temporal profiles of neural activity during rhythmic leg movements have been documented using electroencephalography (EEG) and magnetoencephalography (MEG). For example, modulations in alpha and beta power time-locked to the movement cycle during pedaling (Swedler, 2012) and walking (Gwin et al., 2011; Wagner et al., 2012), and repetitive patterns of movement-related slow potentials during stepping (Wieser et al., 2010) and pedaling (Jain et al., 2012). However, EEG and MEG have poor spatial resolution and can only give general areas of cortical excitation. Together, however, these studies demonstrate distinct localization of lower extremity movements and modulations of cortical activity during movement cycles. Though, the movement types in these studies are complex and require multiple joint and muscle coordination and sometimes balance, so cortical responses are likely as complex as the tasks themselves.

In order to examine the individual roles of the sensory and motor cortices in the perpetuation of rhythmic movements, we chose to use a simplified unilateral, cyclic ankle movement task. Movement-related slow potentials and changes in neural power were recorded with EEG, and we examined the changes in cortical contributions to factors of volition, attention, and frequency of ankle movement. We hypothesized that unique sensory and motor slow potentials could be identified during rhythmic ankle movements.

3.2 METHODS

3.2.1 Study Participants

Ten young adults (five male and five female) ranging in age from 20 to 32 years old participated in this study. Subjects were all in good health and reported no history of neurological or orthopedic injury or disease that would inhibit normal ankle movement. We informed all subjects of the experimental procedures, and they provided written consent to participate in this study. The procedures and consent documentation were approved by the Institutional Review Board at Marquette University and were in accordance with the Declaration of Helsinki (World Medical Association, 2008).

3.2.2 Robotic Ankle Device

Throughout the experimental session, subjects sat upright on a therapy table (Electro Medical, Marietta, GA) with their right knee at approximately 25 degrees of flexion and their right foot in a custom robotic device (Figure 3-1). The ankle robot contained a servomotor (Kollmorgen, Radford, VA), an inline torque load cell (S. Himmelstein and Company, Hoffman Estates, IL), and a custom ankle brace.

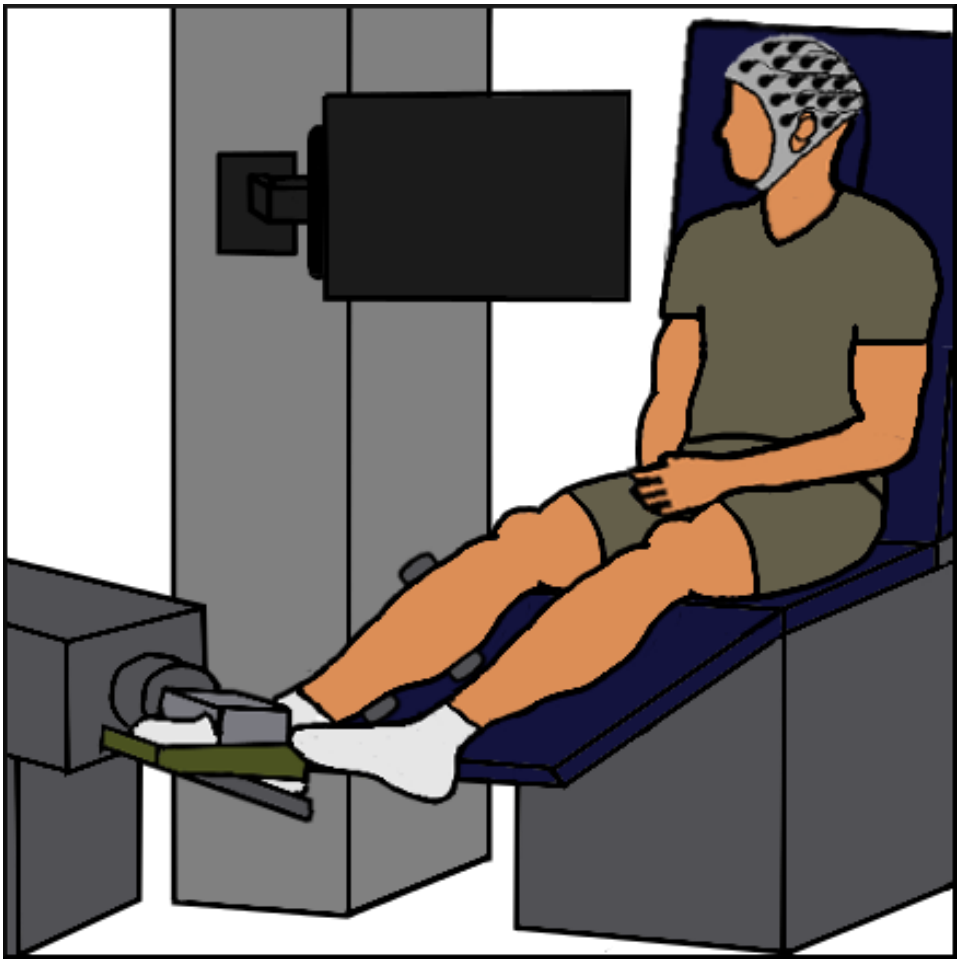

Figure 3-1: Experimental Setup. Subjects sat comfortably on a therapy table with their right foot in a robot device and a computer monitor in front of them. A barrier was placed on the bottom and left side of the monitor to remove any visual feedback of the leg or robot movement. During all experimental conditions, EEG, lower leg EMG, ankle torque, and ankle position were recorded.

Experimenters aligned the brace so that the center of rotation of the motor and sagittal plane rotation of the ankle were on the same axis. Rotation of the ankle robot was velocity controlled by custom LabVIEW code (National Instruments, Austin, TX), and the information from a digital position encoder attached to the robot allowed for online corrections of the velocity profile to prevent angular drift. Finally, to ensure the safety of all experimental subjects, mechanical, electrical, and software stops ensured ankle movement only within a comfortable range of motion. As an additional safety measure,

subjects held an emergency stop button to use at any time throughout the experimental session.

3.2.3 Experimental Protocol

Prior to the main protocol, subjects performed maximum voluntary contractions (MVCs) during cyclic ankle movements at 0.7, 1.0, and 1.3 Hz. While performing MVCs, subjects assisted the robot with maximal force during only the dorsiflexion phase of four consecutive movement cycles. Additionally, subjects remained relaxed during four passive movement cycles that measured the resting baseline electromyography (EMG) at each of the three movement frequencies. The MVC EMG values for the right tibialis anterior (TA), medial gastrocnemius (MG), and soleus (SOL) muscles were defined as the difference between the maximum amplitude of the root mean squared (RMS) EMG and mean resting baseline values.

The main protocol for this experiment consisted of 12 unilateral movement trials of the right ankle. During each trial, the robotic device, described previously, rotated the ankle 200 times in a cyclic pattern between 0 and 35 degrees of plantar flexion. Trials included the combinations of three factors: Volition (active and passive conditions), Attention (focused and distracted conditions), and Movement Frequency (0.7, 1.0, and 1.3 Hz). During the active condition, subjects assisted the robotic device during only the dorsiflexion phase of movement, and the experimenter gave verbal feedback to keep the muscle activation produced for each cycle between 10% and 30% of their speed-specific, TA MVC EMG value. Conversely, subjects completely relaxed during the passive trials. During the focused trials, subjects were instructed to fixate on a monitor in front of them

and to mentally stay focused on the ankle movements. The experimenter gave a verbal instruction to "please stay focused" intermittently throughout each trial. During the distracted trials, subjects watched a TV show on the same monitor. Additionally, a barrier was placed within the subject's line of vision, extending from the bottom and left side of the monitor toward the subject to remove any visual feedback of right ankle movement (Figure 3-1). Finally, each experimental session concluded with a slow passive movement and inertial trial for offline torque calibration (Steldt & Schmit, 2004).

3.2.4 Physiological Measurements

During all trials, an active electrode actiCAP (Brain Products, Germany) recorded EEG from 64 scalp locations. The cap placement procedure and electrode locations were similar to those reported in the second chapter of this dissertation. Briefly, electrodes aligned to the international 10-20 system were hydrated to impedances below 20 kOhms using SuperVisc Gel (Brain Products, Germany). Analog EEG signals were further amplified, filtered from 0.3 to 200 Hz with a Synamps^2 system (Neuroscan, Charlotte, NC), and sampled at 1000 Hz in Scan 4.5. EMG signals were collected from the tibialis anterior (TA), medial gastrocnemius (MG), and soleus (SOL) muscles with the Trigno wireless EMG system (Delsys, Boston, MA). Additionally, sagittal plane ankle torque and angular position were measured using an inline torque load cell and a digital encoder (US Digital, Vancouver, WA), respectively, both mounted on the custom robotic device. Analog signals of position, torque, and EMG were anti-alias filtered below 500 Hz using custom hardware, sampled at 1000 Hz by a data acquisition system (PCI-06071E, National Instruments, Austin, TX) and recorded using custom LabVIEW software.

Lastly, analog square waves were used as triggers to indicate each cycle and were recorded in both LabVIEW and Neuroscan software to synchronize data offline.

3.2.5 Data Processing

EEG Artifact Removal

Preprocessing was performed in a similar manner as described in the second chapter of this dissertation. In summary, artifacts were removed from EEG data using custom MATLAB scripts (The MathWorks, Natick, MA) and functions from EEGLAB (12.0.0.0b) (Delorme & Makeig, 2004). EEG data were re-referenced to a common average that retained the reference (FCz) electrode. To remove low frequency drift, signals were filtered from 0.5 to 100 Hz using an FFT square filter. Additionally, line noise was removed using a 4^{th} order, zero-phase, Butterworth notch filter from 59 to 61 Hz. Signals from each trial were independently decomposed using an Adaptive Mixture Independent Component Analysis (AMICA) (Palmer et al., 2008) and components were identified for removal using the ADJUST plugin to EEGLAB (Mognon et al., 2010).

Additional Analog Signals Preprocessing

Custom MATLAB code was written for initial processing steps of the analog position, torque, and EMG signals. Motor position and torque signals were converted from voltage to degrees and newton meters, respectively, using linear calibration coefficients empirically derived previous to the experiment, and low-pass filtered at 5 Hz (Butterworth, zero-phase, 4^{th} order). Additionally, torque signals were adjusted to account for the inherent torque of the ankle brace (Steldt & Schmit, 2004). EMG

recordings were band-pass filtered from 30 to 200 Hz (Butterworth, zero-phase, 4^{th} order) and, the RMS values were calculated using a 50 ms sliding window with 25 ms padding of the first and last points to their respective ends to preserve signal length.

Temporal Processing

Neural activity time-locked to each movement trial was extracted by means of temporal cycle averaging. EEG, EMG, and position data were epoched into single cycles starting at peak dorsiflexion. Cycles with excess noise in the EEG signal were statistically identified and eliminated from further analysis by the *pop_autorej* function in EEGLAB with maximum epoch rejection rate of 5% and initial probability threshold of three standard deviations. Epoched data were averaged across cycles to produce estimated mean signals of the EEG, EMG, and position. Finally, EEG and EMG amplitude values for each electrode were defined as the difference between the maximum and minimum values over the average cycle.

Source Localization

Localization of the cortical source distribution was approximated for each trial in Brainstorm software (Tadel et al., 2011) on a default cortical template derived from the MNI/Colin27 brain. Electrode locations were registered to the scalp surface so that the Cz electrode was over the vertex, the midline electrodes (e.g. Fz, Cz, Pz) were in line with the sagittal plane between the nasion and inion, and the central lobe electrodes (e.g. C3, Cz, C4) were situated between the prearticular points of the ears. In Brainstorm, a boundary element model (BEM) approximation of the forward model was calculated

using the OpenMEEG (Gramfort et al., 2010; Kybic et al., 2005) plugin, and the inverse model was estimated by the min L2 norm estimator of cortical current density (Hämäläinen & Ilmoniemi, 1994). Individual source localization maps were then averaged across cycles for each trial. Finally, grand average maps were produced by averaging the current density maps of the ten subjects. Spatial localization plots in all figures are the time-averaged localization across the whole movement cycle or the average current density across movement cycle for each point on the cortex.

Power Spectral Analysis

Neural power in each of the traditional EEG bands (i.e. delta, theta, alpha, beta, and gamma) was calculated for each electrode within each trial (electrode/trial pair) using Welch's method for power spectral density (PSD) estimation. After filtering and artifact removal, as previously described, remaining cycles for each electrode/trial pair were concatenated in time. Since the trial time was shortest for the 1.3 Hz conditions, approximately 2 minutes (123.4 s, 123,040 points) of data was used for each trial. Trial data were then divided into 2048-point (2.048 s) segments with 50% overlap, which resulted in approximately 120 segments, and each segment was filtered using a Hamming window of the same length. The PSD of the electrode/trial pair was estimated by calculating individual spectrums for each segment with a frequency resolution of ~0.49 Hz and averaging across segments. Spectral averages were then split into delta (0.5 to 4 Hz), theta (4 to 8 Hz), alpha (8 to 12 Hz), beta (12 to 30 Hz), and gamma (30 to 50 Hz) bands, and the total power per band was calculated using the trapezoidal method for discrete integration.

Analysis of Variance for EEG Amplitudes and Band Power

Conditional differences in mean EEG amplitude and individual band power were calculated independently using repeated measures Analysis of Variance (ANOVA). For each electrode, the repeated measures ANOVA included a dependent variable of slow potential peak-to-peak amplitude or power in one of five bands (delta, theta, alpha, beta, or gamma) and three independent factors of Attention, Volition, and Movement Frequency. The assumption of sphericity was adjusted for by finding the average of the Greenhouse-Geisser and Huynd-Feldt corrections (Stevens, 2009), and a significance value was set at $\alpha = 0.05$. Type I error was constrained by only considering significant clusters of two or more adjoining electrodes. See Appendix A for a map of electrode locations. Spatial plots were created to map the percent signal change at each electrode location of the within-factor conditions and normalized (multiplied) by the partial eta squared value, a measure of intrasubject effect size (variance explained) by each factor or interaction. Baseline conditions for the Attention, Volition, and Movement Frequency factors were the distracted, passive, and 0.7 Hz conditions, respectively.

Analysis of Variance EMG Amplitudes

Consistency of EMG amplitude within Attention and Movement Frequency conditions was calculated using a repeated measures ANOVA. The set of peak RMS EMG values for the TA muscle was the dependent variable in this analysis. A two-way, repeated measures ANOVA was used to calculate the likelihood that EMG amplitudes were different between levels of the Attention and Movement Frequency conditions.

This analysis was run on only the active movement trials. The assumption of sphericity was again adjusted for by finding the average of the Greenhouse-Geisser and Huynd-Feldt corrections (Stevens, 2009), and a significance value was set at $\alpha = 0.05$.

Beta Power Modulation and Slow Potential Correlation

The cross correlation of the beta power modulation and movement-related slow potential temporal profiles was calculated to reveal any temporal relationship between the two phenomena. After initial artifact removal, EEG signals at each electrode location were band-pass filtered from 12 to 30 Hz (Butterworth, 6^{th} order, zero-phase), RMS transformed, epoched into cycles, and averaged for each movement condition. The cycle amplitude of the beta modulation was calculated as the difference between the maximum and minimum value of the averaged response across a cycle. The maximum correlation value between the beta power modulation and movement-related slow potential responses was calculated at each electrode location. A three-factor, repeated measures ANOVA was run to determine if the effects of Volition, Attention, and Movement Frequency had an effect on the amplitude measure of the beta power modulations.

3.3 RESULTS

The primary aim of this study was to improve understanding of the role of sensory and motor cortices in the control of lower extremity rhythmic movements. Our analysis focused on characteristics of movement-related slow potentials as a probe to identify the cortical activity elicited by different levels of Volition, Attention, and Movement Frequency. Additionally, we used source localization to determine the areas of cortical

activation produced by these slow potentials and examined factor-specific changes of the EEG power spectrum. Lastly, we explored the temporal relationship between the beta power modulations and movement-related slow potentials.

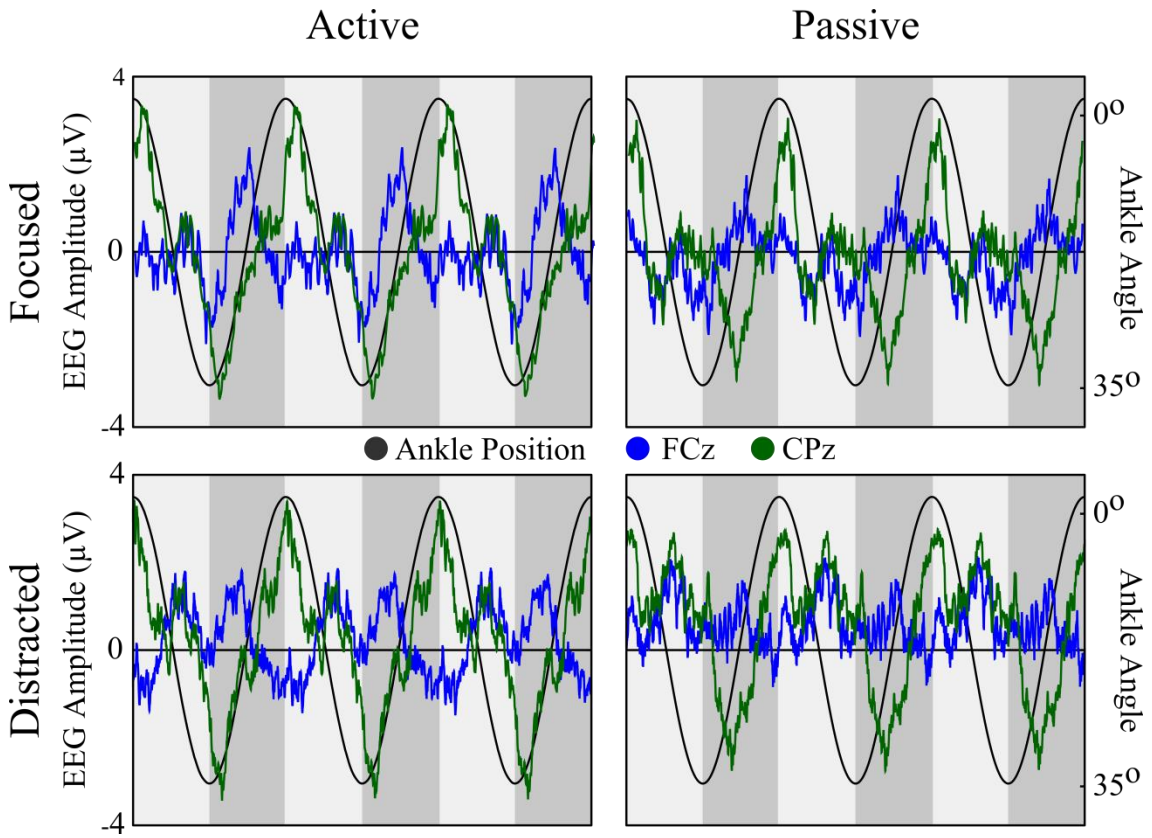

Figure 3-2: Slow Potentials of the Medial Sensorimotor Cortex (Sub 2). Slow potentials observed over the motor (FCz) and sensory (CPz) cortices during rhythmic ankle movement. Each plot displays three cycles (gray) of Volition/Attention combination at 0.7 Hz movement frequency. Background shading indicates each dorsiflexion (dark) and plantar flexion (light) phase of each cycle. During active dorsiflexion, there is a distinct potential in the FCz electrode (blue) that is absent during passive movement. Additionally, the CPz electrode (green) shows a reduction in peak-to-peak amplitude, but appears to retain a similar temporal profile during passive movements.

3.3.1 Temporal Slow Potential Profiles and Spatial Localization

Temporal averaging of EEG revealed two unique slow potentials time-locked to the ankle movement cycle for all experimental conditions. The first potential appeared to track, but slightly lag, the position of the ankle during the movement. This potential was prominent during the active condition in the more posterior electrode along the midline, CPz (Figure 3-2). The second characteristic potential appeared during the dorsiflexion phase of the active condition, and was more prominent in the more frontal electrode over the midline, FCz. During passive movements, these potentials were similar or smaller in amplitude compared to the active condition at 0.7 Hz. Group averages for all movement conditions demonstrated similar results as the representative subject (Figure 3-3). Moreover, these slow potentials consistently localized to the medial sensorimotor cortex (Figure 3-4) and this was similar across all subjects (Figure 3-5). The group average more clearly shows that during active movements both the sensory and motor cortices appear active. However, only the sensory cortex appears active during passive movements.

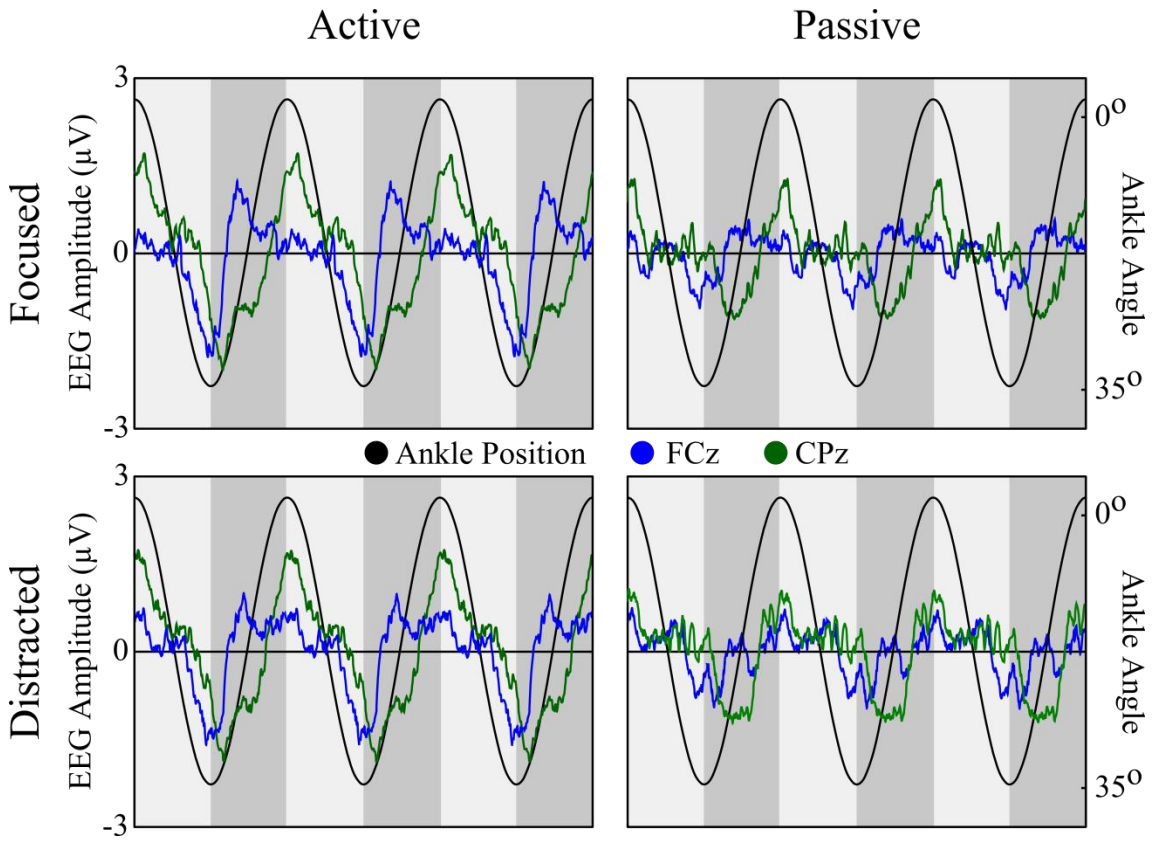

Figure 3-3: Group Average Slow Potentials of the Medial Sensorimotor Cortex. Group representation of slow potentials over the medial sensorimotor cortex during continuous movement of the ankle, similar to Figure 3-2.

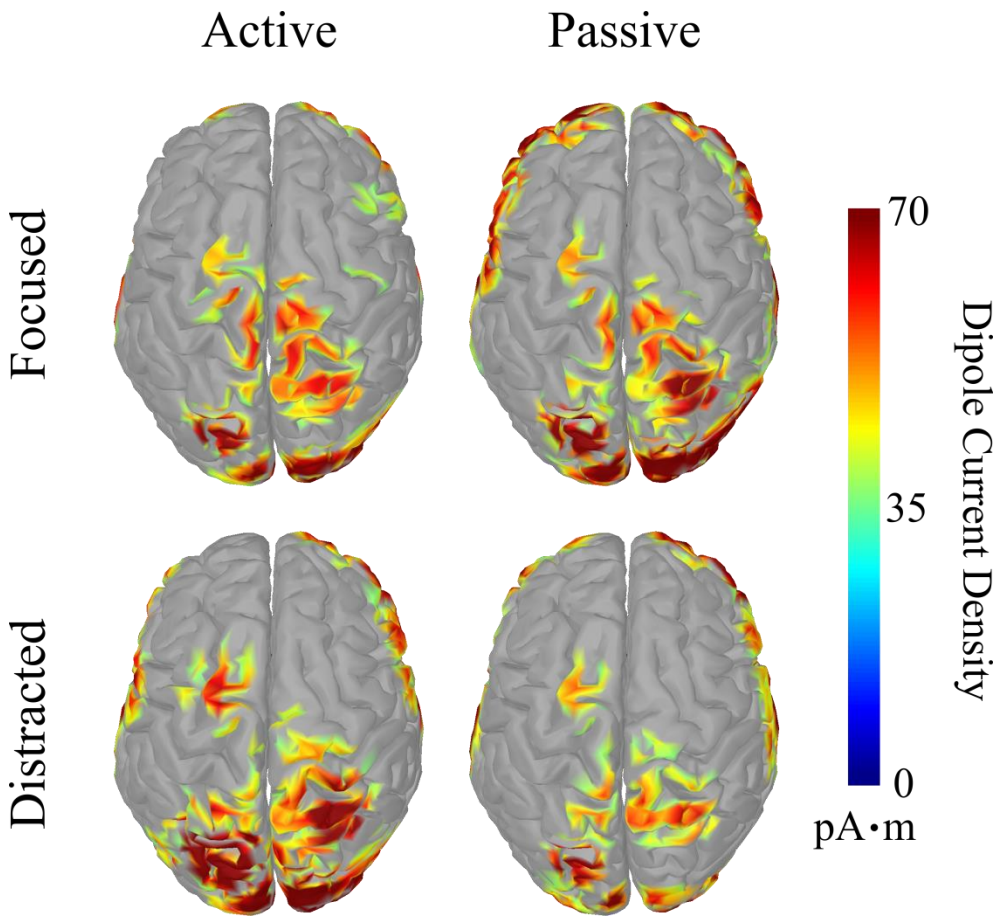

Figure 3-4: Slow Potential Localization for a Single Subject (Sub 2). Single subject representation of the time-averaged, source localization for the slow potentials during rhythmic ankle movement. Each plot represents one of the four Volition/Attention combinations at a Movement Frequency of 0.7 Hz. For visualization, only values above a threshold of 35 pA·m were displayed for all conditions.

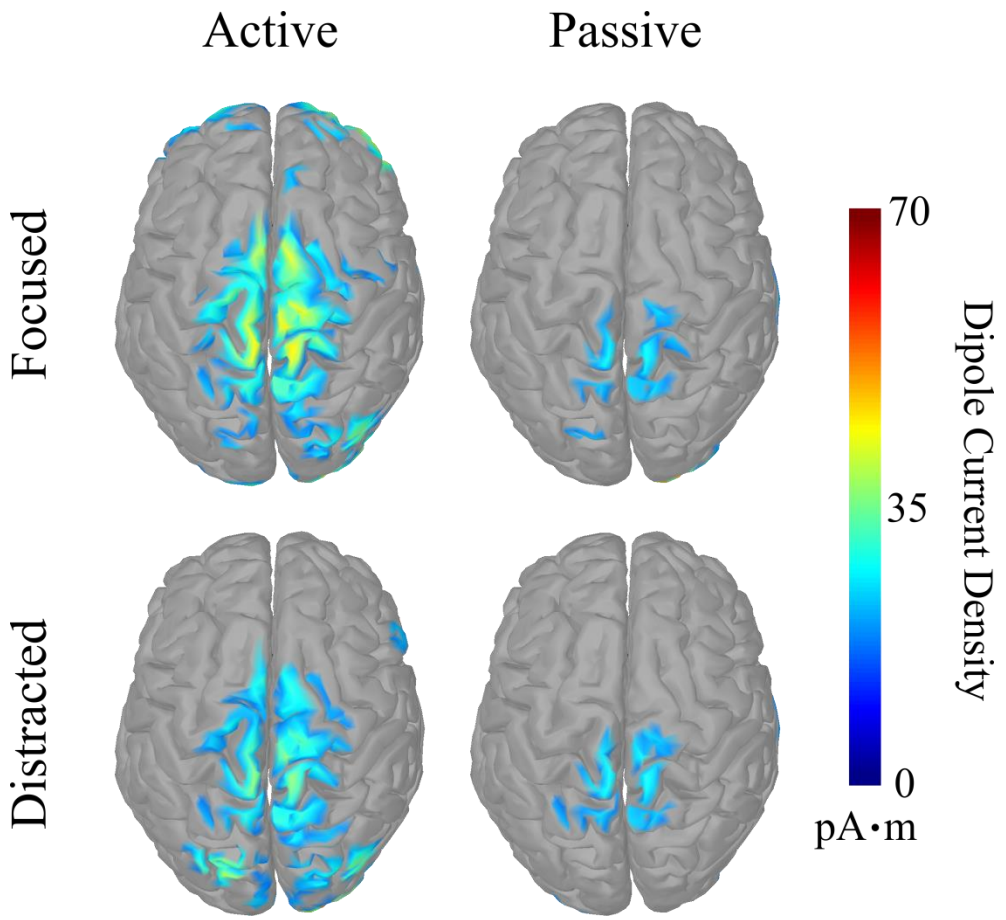

Figure 3-5: Group Average Slow Potential Cortical Localization. Group average plots of the slow potential localization in the medial sensorimotor cortex for each the four Volition/Attention task combinations at a Movement Frequency of 0.7 Hz. These plots represent the time-averaged dipole current density over a movement cycle. Similar localization maps were also observed at the 1.0 Hz and 1.3 Hz movement frequencies. For visualization, only values above a threshold of 14 pA·m were displayed for all conditions.

Because of the medial source localization near the vertex, the FCz and CPz electrodes (See Appendix A) were chosen to describe the motor and sensory cortical activity, respectively. This decision was based on the following knowledge of anatomy and physics. First, the ankle area of the sensorimotor cortex is known to be deep in the longitudinal fissure, under the midline electrodes near the vertex. Second, signals from a deep origin produce weaker, but more diffuse, electrical potentials at the scalp surface,

because electric fields broaden and dissipate as the distance from their center increases. Therefore, it is believed that all the electrodes along the midline are of mixed origin (sensory and motor), but in different proportions. This suggests that the FCz electrode has the largest proportion of motor to sensory activity as it is frontal to the primary motor cortex and further from the sensory cortex. Similarly, the CPz electrode would have the largest proportion of sensory to motor activity, as it is posterior to the primary sensory cortex.

3.3.2 Attention

Effects of Attention were evident in both changes of slow potential amplitude and theta power. Specifically, there were reductions in theta power bilaterally over the temporal and occipital lobes, during the focused compared to the distracted conditions (Figure 3-6a). During only the active conditions, there were greater slow potential amplitudes during the focused conditions along the frontal midline that dissipated over the right frontal lobe (Figure 3-6b). This was also observed in the temporal traces of the FCz slow potentials (Figure 3-3), and was more apparent in the single subject representation (Figure 3-2).

3.3.3 Movement Frequency

Movement Frequency had opposite effects on the amplitude of medial anterior (motor cortex) and posterior (sensory cortex) electrodes. Slow potential amplitudes during both active and passive movements were proportional to the frequency of movement in the more frontal electrode, FCz, along the midline with a significant linear

contrast, p = 0.036 (Figure 3-7a). For FCz, a significant linear contrast suggests that as the movement frequency was increased, there was a linear increase in the slow potential amplitude during both the active and passive movements. This was in contrast to the slow potential amplitudes in the more posterior electrode, CPz, along the midline and adjacent contralateral electrodes. Slow potentials in CPz were inversely proportional to the frequency of movement during the active condition (Figure 3-7b).

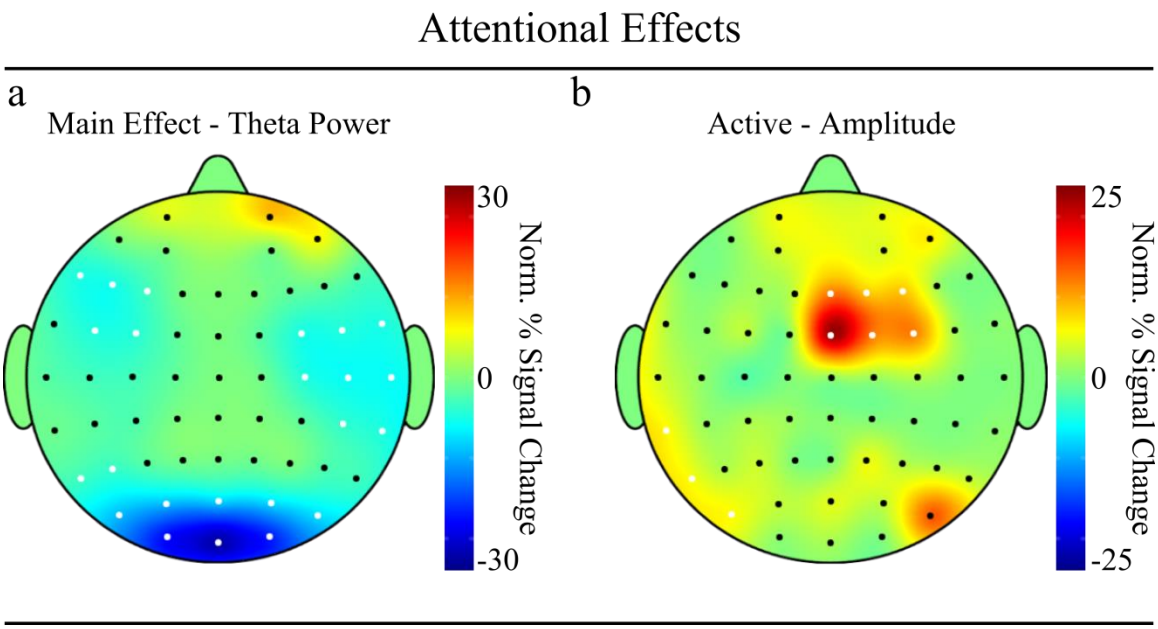

Figure 3-6: Effects of Attention on Slow Potential Amplitudes and Theta Power. Theta power is reduced over large areas of temporal and occipital lobes during the focused task (a). During active movements, there is an increase in slow potential amplitudes over the right frontal lobe including the FCz electrode (b). Amplitude is measured in percent signal change from lowest (0.7 Hz) to highest (1.3 Hz) frequency with the slowest frequency as the baseline and is normalized (multiplied) by the effect size of the factor for each electrode. White electrodes indicate significance ($\alpha = 0.05$, cluster ≥ 2).

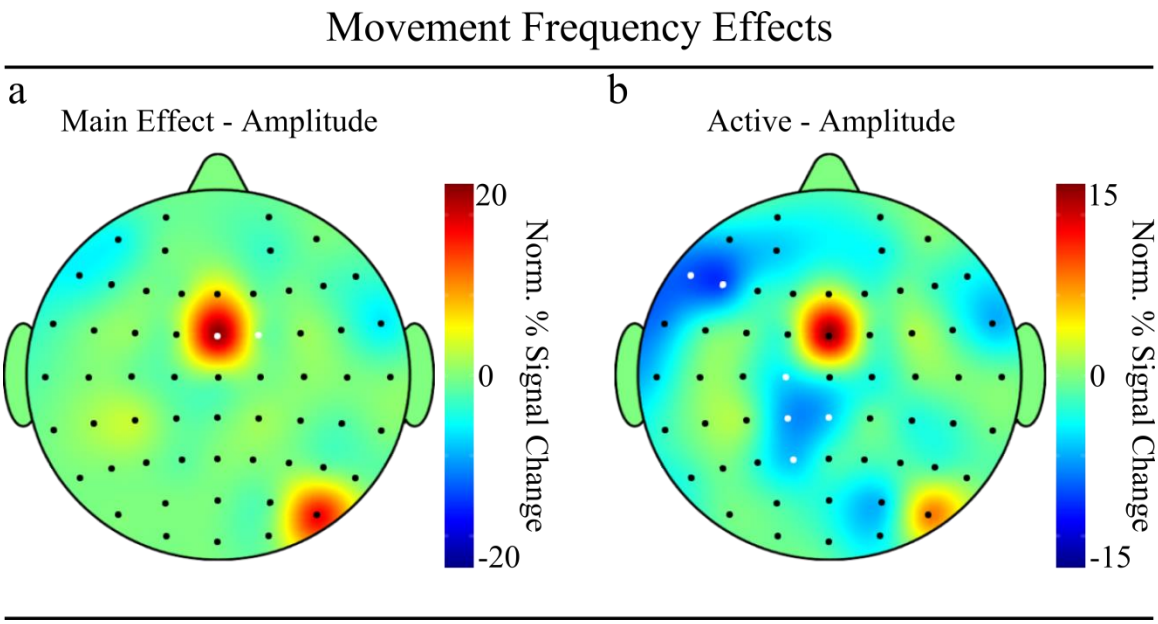

Figure 3-7: Effects of Movement Frequency on Slow Potential Amplitudes. Left: Main effect of the FCz electrode slow potential amplitude is proportional with the movement frequency. Right: During active movements, amplitude of the slow potential is inversely proportional with the movement frequency for contralateral areas over the medial sensory cortex. Amplitude is measured in percent signal change with the slowest movement frequency (0.7 Hz) as the baseline and is normalized (multiplied) by the effect size of the factor for each electrode. White electrodes indicate significance ($\alpha = 0.05$, cluster ≥ 2).

3.3.4 Volition

Signal power the alpha and the beta bands were attenuated during the active condition in comparison to the passive condition. Significant decreases in alpha and beta power occurred over the lateral area of contralateral sensorimotor cortex (Figure 3-8). Moreover, there was a significant decrease in Beta power over the lateral ipsilateral sensorimotor cortex, but to a lesser extent than the contralateral side. No significant change over the midline was observed.

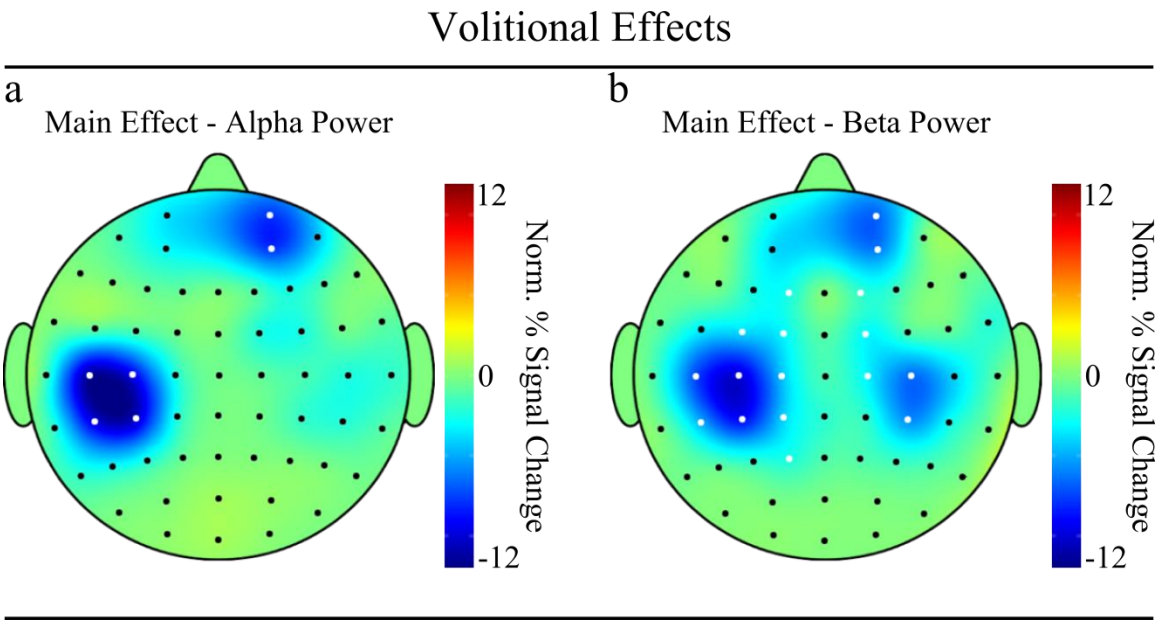

Figure 3-8: Effects of Volition on Alpha and Beta Power. Alpha power (left) and beta power (right) decreased during active movements over contralateral (left hemisphere) areas of the sensorimotor cortex. Additionally, beta power (right) decreased in a symmetrical location over the ipsilateral (right hemisphere) sensorimotor cortex, but to a lesser degree. No significant change in alpha or beta power was observed over the midline. Amplitude is reported in percent signal change with passive movement as the baseline and is normalized (multiplied) by the effect size of the factor for each electrode. White electrodes indicate significance ($\alpha = 0.05$, cluster ≥ 2).

3.3.5 Electromyography Attention & Movement Frequency

The EMG amplitudes were found to differ between each of the Attention and Movement Frequency conditions. Results of the repeated measures ANOVA demonstrated that during focused trials, the EMG was higher when compared to distracted trials ($F(1,9) = 5.74$, $p = 0.04$). Moreover, as the frequency of movement was increased, there was a proportional increase in the EMG amplitude ($F(2,18) = 6.28$, $p = 0.01$). There were no significant differences in EMG amplitudes during passive trials.

3.3.6 Beta Power Modulation and Correlation with Slow Potentials

Results of the repeated measures ANOVA revealed a significant increase in beta power modulation amplitude for the factors of Attention ($F(1,8) = 5.37$, $p = 0.049$) and Volition ($F(1,8) = 5.70$, $p = 0.044$) over the medial motor cortex. Though not significant, there was a similar trend in the amplitude increase of the beta power modulations proportional to the Movement Frequency (Figure 3-9). Moreover, there was a diffuse and significant decrease in power in over half of the electrodes at higher movement frequencies, including CPz and Cz.

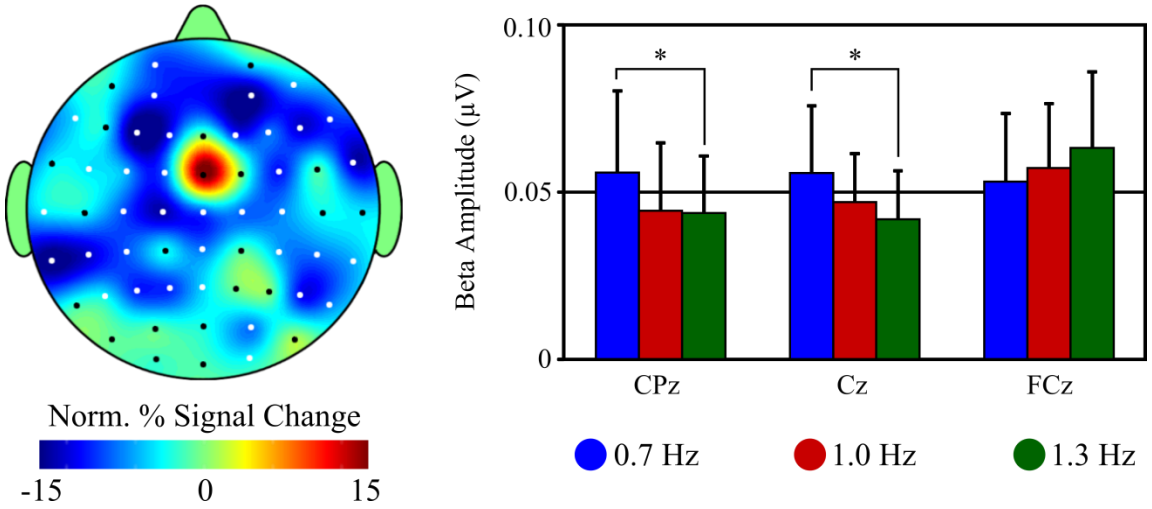

Figure 3-9: Effect of Movement Frequency on Beta Frequency Modulation Amplitude. Left: Significant decreases in amplitude for the beta power modulation over much of the cortex, except the medial motor cortex at increased movement frequencies. Amplitude is measured in percent signal change with the slowest movement frequency (0.7 Hz) as the baseline and is normalized (multiplied) by the effect size of the factor for each electrode. White electrodes indicate significance ($\alpha = 0.05$, cluster ≥ 2). Right: Amplitude of beta frequency modulation at 0.7, 1.0, and 1.3 Hz for the CPz, Cz, and FCz electrodes.

Beta power modulations and movement-related slow potentials correlated most highly over the medial sensorimotor cortex, specifically over the CPz and Cz electrodes

and decreased outwardly. This localization is depicted in Figure 3-10 at 0.7 Hz with the temporal profile recorded over the CPz electrode. We also observed that on average the slow potentials lagged the beta power modulations, but the timing was variable. However, the localization and temporal lag were consistent across all movement frequencies.

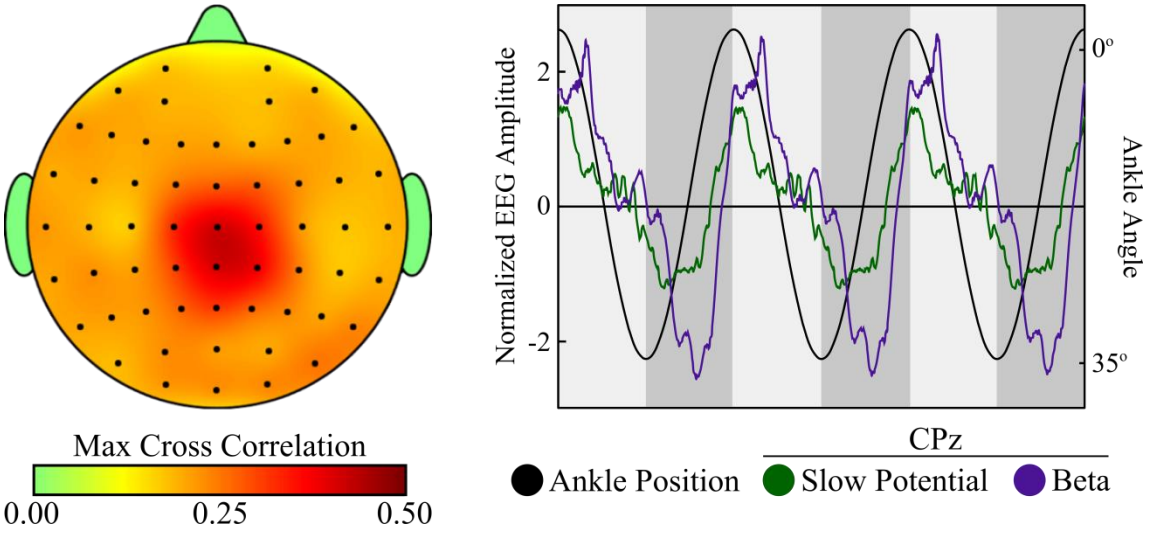

Figure 3-10: Correlation of Beta Frequency Modulations and Slow Potentials. Left: Grand average of the max cross correlation values of beta frequency modulations and slow potentials at each electrode location at 0.7 Hz. Right: Grand average temporal traces at 0.7 Hz of the slow potentials (green) and beta frequency modulations (x200) (violet) recorded over the CPz electrode. The ankle movement move profile is denoted in black. The background colors denote dorsiflexion (dark gray) and planter flexion (light gray).

3.4 DISCUSSION

Results from this study provided additional evidence in humans that both the sensory and motor cortices are involved in rhythmic movements of the lower extremities. Distinctive temporal patterns of movement-related slow potentials provide evidence that both cortices are active and unique in their contribution to movement control.

Additionally, the factors of Attention and Movement Frequency had effects localized to the medial motor and/or sensory areas of the cortex, though these results could be related to changes in EMG amplitude. Finally, beta modulations, which are commonly associated with motor tasks (Kilavik et al., 2013), had a temporal correlation with movement-related slow potentials.

Concurrent changes in movement-related slow potentials and EMG amplitudes gave insight into the relationship of the cortical and muscle activity during volitional tasks. During the active condition, the amplitudes of slow potentials over the motor cortex and EMG were both proportional to the movement frequency. Similar increases in neural activity in the medial areas of the motor cortex have been shown in both fMRI (Mehta et al., 2012) and PET (Christensen et al., 2000). Interestingly, the opposite effect was recorded over the sensory cortex. That is to say, as the EMG and motor cortical activity increased, the sensory cortical activity decreased. This is consistent with the theory of sensory gating (Jones et al., 1989),where the motor cortex 'gates' or attenuate the afferent sensory signal to the cortex when producing a volitional command.

During passive movements, however, the EMG and EEG slow potentials amplitudes were not proportional to each other. As expected, during passive movements, the amplitudes of the movement-related slow potentials of the sensory cortex were similar, indeterminate of the attentional state or movement frequency. This was in accord with the EMG amplitudes for all conditions which were near zero and never significantly different from each other. Similarly, the motor cortex showed no change with attention during passive movements. However, the motor cortex did show an increase during passive movements with increasing frequency. That is to say, as we increased the

frequency of the passive ankle movement, there was no change in EMG activation or in sensory cortical activity; however, there was an increase in slow potential amplitude recorded. It is interesting to note that the slow potential amplitude was larger as the EMG became more continuous. In the lowest frequency movement, the EMG was discrete in nature with times of no activation (Figure 3-3). However, the 1.0 Hz and 1.3 Hz movements had increasingly less time between each EMG contraction. The continuous EMG contraction that never goes back to rest could be one reason for the increased motor activity. In addition, though the amplitudes at these higher frequencies of the motor cortex between the active and passive conditions were not significantly different, the temporal morphology was different. Specifically, FCz peaked earlier during active movements compared to passive ones. The passive movement slow potentials of the motor cortex appeared to peak at a similar time with the sensory signals. We believe that the earlier peak in the slow potential amplitude is similar to the peak seen at the 0.7 Hz condition, but is masked by the passive component.

Increased attention reduced theta power over temporal and occipital lobes. The changes in theta power recorded over the bilateral, temporal cortices and over the occipital cortex are likely results of auditory and visual stimulation, respectively, that the subjects received while watching the television show. It is hypothesized this decrease was due to desynchronization of normal rhythmic oscillations of theta rhythms in these areas of the cortex during the focused conditions.

Additionally, there was a reduction in alpha and beta power during the active conditions over the lateral sensorimotor cortex. The largest percent change was observed over the ipsilateral cortex in the alpha band. The beta band decrease was symmetric over

lateral areas of the sensorimotor cortex. However, it was more negative over the contralateral side. This response has been observed previously during bilateral pedaling (Jain et al., 2013) and unilateral and bilateral wrist movement (Formaggio et al., 2013). Interestingly, this same response here during unilateral, lower extremity movements was also bilateral and lateral in location, which is not what would be expected. Possibly this is a result of subcortical activations that are projected to the lateral cortex and is inherent to all rhythmic motor tasks.

Movement-related beta power modulations appear to act similarly to the recorded slow potentials. The amplitude responses of the beta modulations increased during focused (Lin et al., 2011), active, and higher movement frequency trials over the medial motor cortex. Additionally, the beta modulations decreased in amplitude over the sensory cortex with increasing movement frequency. A similar responses was seen during finger tapping (Joundi et al., 2013). Moreover, the beta modulations and slow potential had the highest correlation over the medial sensory cortex (Figure 3-10).

In this study, we have shown that movement-related slow potentials are unique for motor and sensory cortices during lower extremity rhythmic movements. It appears that the medial sensory cortex modulates with the position of the ankle, and the motor cortex is linked to the continuity and temporal profile of muscle activation. Moreover, unilateral lower extremity movements activate bilateral beta desychronization that is greater during passive than active movements. Lastly, the amplitude of beta power modulations was affected similarly to the amplitudes of movement-related slow potentials for different conditions of Attention, Volition, and Movement Frequency. Moreover, beta frequency modulations were most highly correlated with movement-

related slow potentials over the medial sensory cortex. In order to use these potentials in the future for more functional tasks, such as pedaling or walking, we will need to explore how bilateral cortical generators for each foot/leg interact.

CHAPTER 4: MOVEMENT-RELATED SLOW POTENTIALS OF THE SENSORIMOTOR CORTEX DURING BILATERAL, RHYTHMIC MOVEMENT OF THE ANKLES

4.1 INTRODUCTION

There is still considerable debate over the role of the sensorimotor cortex in the control of bilateral, rhythmic movements of the lower extremities. Studies of animal locomotion demonstrate that supraspinal structures, such as the sensorimotor cortex, are not required to produce rhythmic movements of the lower extremities (Grillner, 1975). However, in humans severe deficits in locomotor capability after a neural injury, such as a spinal cord injury, demonstrate that the brain is vital in the production of lower extremity rhythmic movements (Dobkin et al., 2007). During walking, there is indirect evidence of afferent modulations with the use of somatosensory evoked potential (SEPs) (Altenmüller et al., 1995; Duysens et al., 1995) and changes in the excitability of efferent motor pathways, using transcranial magnetic stimulation (TMS) (Schubert et al., 1997) . These studies suggest that perpetuation of rhythmic movements of the lower extremities may at least partially require sensorimotor cortical contribution.

The role of the brain in rhythmic movements has been studied with functional magnetic resonance imaging (fMRI), which has demonstrated neural activity in both the primary sensory and motor cortices during rhythmic wrist (Schaal et al., 2004) and ankle (Kapreli et al., 2006) movements, foot tapping (Mehta et al, 2009). Similar activation is observed during bilateral multijoint movements, such as pedaling (Mehta et al., 2009). Additionally, cortical activity time-locked to the gait cycle has been recorded during walking using electroencephalography (EEG) (Gwin, 2011) and near-infrared spectroscopy (NIRS) (Miyai et al., 2001). Together, the combined spatiotemporal

profiles of neural activity suggest that the brain plays an essential role in lower extremity rhythmic movements. However, coupling of simultaneous afferent and efferent cortical activity during natural movements makes it difficult to discern the motor and sensory contributions to the recorded signals.

Therefore, various studies have explored the motor and sensory contributions to rhythmic movements of the lower extremities by the use of active and passive movements. Results from these studies, however, have been contradictory. Areas of the brain that are active during both passive and active movements (i.e. S1, M1, SMA, cerebellum) have been shown to elicit similar or slightly greater intensity of neural activity in areas of the medial sensorimotor cortex or cerebellum during active pedaling (Christensen et al., 2000; Mehta et al., 2012) and ankle plantar flexion (Ciccarelli et al., 2005). This suggests an increase in neural activity during active movements. In contrast, temporal patterns of electroencephalography (EEG) during active pedaling elicited reductions in both slow potential amplitudes (Jain et al., 2013) and similarly, in higher frequency power modulations during walking (Wagner et al., 2012). Authors have suggested that the reduction in neural activity, observed over the sensorimotor cortex during a volitional movement, could be evidence of centripetal gating. However, in chapter three of this dissertation, we presented evidence that slow potential amplitudes over the sensorimotor cortex during unilateral, active movements are equal or greater than passive movements. Therefore, though there may be a physiological explanation for the reduction of neural activity during active movements, it may also be possible that this phenomenon is created by electrical fields of out-of-phase, symmetric cortical generators within the medial sensorimotor cortex destructively interfere with each other.

In this study, we recorded movement-related slow potentials of the sensorimotor cortex with EEG during unilateral and bilateral rhythmic movements of the ankle. Moreover, passive and active movements were used to examine differences in sensory and motor aspects of movement. During experimental trials, a robotic device constrained the movement trajectory and frequency in order to keep the sensory components of movement constant and allow for better comparisons between conditions. Additionally, we focused on sagittal plane and active dorsiflexion movement to isolate the volitional task to primarily the tibialis anterior muscle. This muscle was chosen as it has been shown to have significant monosynaptic corticospinal drive from the motor cortex (Petersen et al., 2003). We hypothesized that during bilateral movements, the electrical field potentials of independent, symmetric cortical generators constructively or destructively interfere and create accentuated or attenuated potentials at the scalp surface, respectively. If true, we predicted three outcomes of the current study. First, unilateral left and right movements would produce similar slow potentials along the midline. Second, in phase or 0^{o} lag bilateral movements would produce larger slow potential amplitudes compared to unilateral movements due to constructive field interference. Lastly, as the bilateral movements become more out-of-phase with each other, the slow potentials would become misaligned, resulting in destructive interference, with the lowest amplitude observed at 180^{o} out-of-phase.

4.2 METHODS

4.2.1 Study Participants

Ten young, healthy subjects (five male and five female) with an age range of 20 to 32 years old participated in this study. All subjects reported that they were in good health and had no significant medical history that would impede bilateral ankle movement. Before the experiment, subjects reviewed the experimental procedure and provided written, informed consent. The experimental description and procedure were approved by the Institutional Review Board at Marquette University, in accordance with the Declaration of Helsinki (World Medical Association, 2008).

4.2.2 Experimental Protocol

Subjects sat comfortably in an upright position on a therapy table with their backs supported and both feet in a robotic ankle device (Figure 4-1) (For additional details of the ankle robot setup, please see Chapter 3). During the experimental session, the robot controlled the velocity and trajectory of ankle rotation independently for each ankle in the sagittal plane using custom LabVIEW code (National Instruments, Austin, TX). Movements followed a prescribed cyclic trajectory of 0 to 30 degrees of plantar flexion at a frequency of 0.7 Hz consistently throughout all experimental trials. Before the main protocol, subjects performed bilateral, in-phase maximum voluntary contractions (MVC) during only the dorsiflexion phase of four movement cycles. The MVC values for the tibialis anterior (TA), medial gastrocnemius (MG), and soleus (SOL) muscles were

calculated as the maximum value of the root mean squared (RMS) electromyography (EMG) across the cycles.

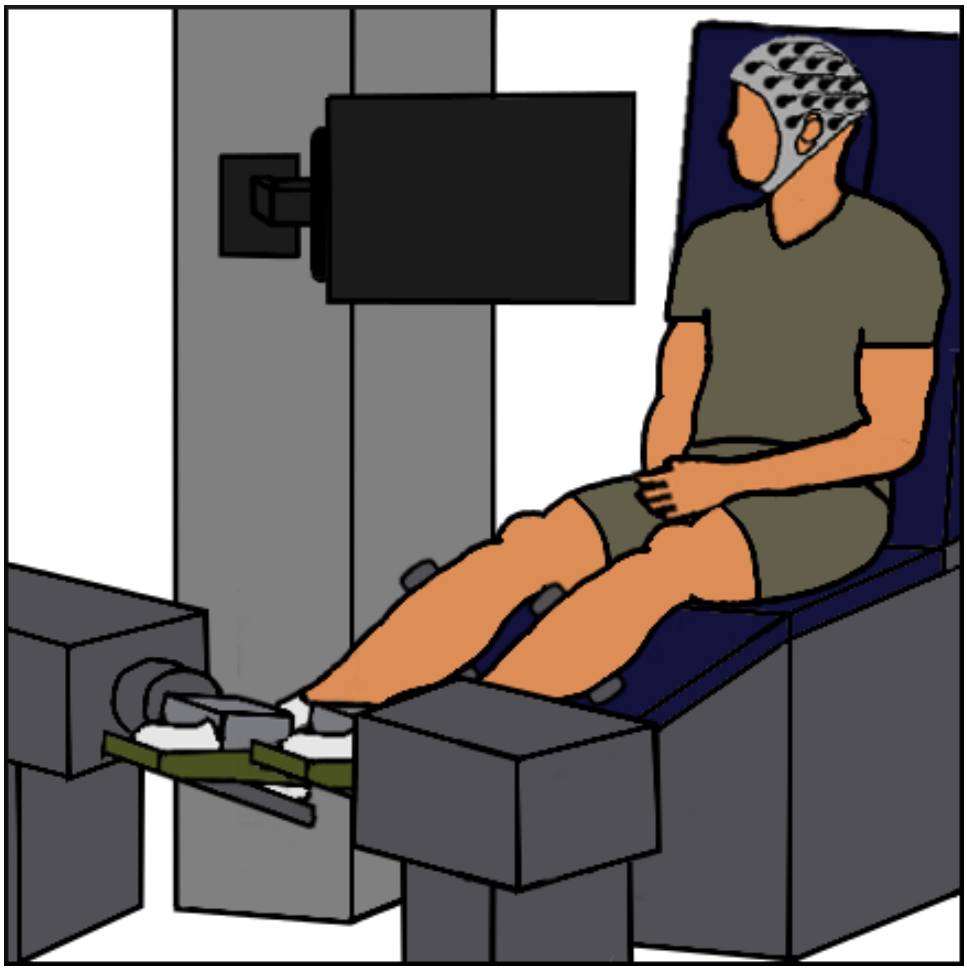

Figure 4-1: Experimental Setup. Subjects sat upright on a therapy table with both feet in the robotic device. During the experimental session, physiological measurements of EEG and EMG were recorded. Additionally, kinematic and force measurements of the ankle were recorded by the robotic device. Finally, subjects were instructed to concentrate on a computer monitor in front of them, and a barrier prevented the subjects from seeing their feet.

The experimental procedure followed the MVC measurements with 12 movement conditions, each 200 cycles in duration that combined an active or passive movement with one of six unique movement patterns. Four of these patterns included bilateral movements, where the left ankle lagged the right ankle by 0^{o}, 90^{o}, 180^{o}, and 270^{o}. The

remaining two patterns were unilateral left and right ankle movements. During all active trials, subjects assisted the robotic device during only the dorsiflexion phase of movement at 10% to 30% of their TA MVC. In contrast, subjects remained relaxed during passive movement trials. An experimenter monitored the muscle activation throughout all trials and provided verbal feedback accordingly.

4.2.3 Physiological Measurements

An active, 64-channel actiCAP (Brain Products, Germany) recorded electroencephalography (EEG) signals during all 12 movement conditions. The EEG cap preparation and all physiological recordings followed the procedure described in chapter three of this dissertation. Briefly, experimenters used SuperVisc gel (Brain Products, Germany) to hydrate and lower the impedance between scalp and each electrode site to below 20 kOhms. During recording, EEG signals were amplified, filtered from 0.3 to 200 Hz, sampled at 1000 Hz using the Synamps^2 system (Neuroscan, El Paso, TX), and recorded using the Neuroscan software, Scan 4.5. Concurrently, analog position, torque, EMG (Delsys, Boston, MA), and trigger signals were anti-alias filtered below 500 Hz using custom analog hardware, sampled at 1000 Hz using a LabVIEW data acquisition system and recording software. Trigger signals were recorded in both EEG and analog systems, and triggers were used offline to synchronize the EEG and analog data.

4.2.4 Data Processing

Many of the data processing steps used for this analysis were similar to those previously explained in this dissertation. Each of the following briefly summarizes these

steps. Please refer to the methods and data processing sections of Chapter 3 for more details.

EEG Artifact Removal

Custom MATLAB code (The MathWorks, Natick, MA) with EEGLAB functions (12.0.0.0b) (Delorme & Makeig, 2004) were written to remove initial EEG signal artifacts. First, EEG data were re-referenced to a common average that also retained the reference (FCz) electrode. Then, low frequency drift was filtered from the data using a 0.5 to 100 Hz, FFT square filter. Additionally, line noise was removed using a fourth-order, zero-phase, Butterworth notch filter from 59 to 61 Hz. EEG signals were decomposed using an Adaptive Mixture Independent Component Analysis (AMICA) (Palmer et al., 2008), and artifact components were identified for removal using the ADJUST plugin (Mognon et al., 2010) for EEGLAB.

Additional Analog Signals Preprocessing

Initial signal processing steps of the analog position, torque, and EMG signals were implemented with custom MATLAB code. Recorded ankle position and torque signals were converted to degrees and newton meters, respectively. Successively, they were low-pass filtered at 5 Hz (Butterworth, zero-phase, 4^{th} order). Then the torque signal was adjusted to remove the inherent torque of the ankle brace (Steldt & Schmit, 2004). Recorded EMG signals were band-pass filtered from 30 to 200 Hz (Butterworth, zero-phase, 4^{th} order). Subsequently, signals were RMS transformed using a 50 ms

sliding window with a 25 ms padding of the first and last points to their respective ends to preserve signal length.

Temporal Processing

Movement-related slow potentials were extracted by temporal averaging across cycles. EEG, EMG, and position data were epoched into single cycles starting at peak dorsiflexion. Cycles were eliminated if they were statistically identified to have excess EEG noise. These cycles were determined by the *pop_autorej* function in EEGLAB with maximum epoch rejection rate of 5% and initial probability threshold of three standard deviations. Cycle data were averaged to produce estimates of mean EEG, EMG, and position signals. Finally, EEG slow potential amplitudes (maximum – minimum values) within each average movement cycle were calculated for each electrode.

Source Localization

Approximate source distributions for each trial were localized to the cortical surface in Brainstorm software (Tadel et al., 2011). Electrode locations were registered to a standard cortical template (MNI/Colin27), which was used for all subjects. The forward model approximation in Brainstorm used the OpenMEEG plugin (Gramfort et al., 2010; Kybic et al., 2005). Sources were calculated for each movement cycle and then the spatial distributions averaged across cycles for inter-subject averages. Intra-subject, grand average plots were calculated by averaging the results from all ten subjects.

Slow Potential Addition and Temporal Correlation

Processed EEG cycles of the right and left unilateral tasks were added together to produce the slow potentials of the bilateral tasks at different phases. The additive process was done for both passive and active movement conditions and at each electrode location. Only half the number of trials was used for each unilateral movement trial so that the total number of averages was similar between the bilateral and added unilateral conditions. In this way, an increased number of averages that would inevitably increase the signal to noise ratio did not bias the slow potential amplitudes. A correlation analysis was run on each electrode independently between the bilateral and added unilateral slow potentials on an individual subject basis. Spatial plots of coefficient of determination values (R^2) at each electrode were constructed for each movement condition. Grand average plots were from the mean of the coefficient of determination values across subjects.

Analysis of Variance for Slow Potential Amplitudes

Conditional and volitional differences in slow potential amplitude were determined independently for the FCz and CPz electrodes using two-way, repeated measures analysis of variances (ANOVA). For each electrode, the conditional factor included the unilateral and bilateral movements and the volitional factor included the active and passive movements. The assumption of sphericity was adjusted for by finding the average of the Greenhouse-Geisser and Huynd-Feldt corrections (Stevens, 2009), and a significance value was set at $\alpha = 0.05$.

Electromyography Amplitude Analysis

Conditional and footedness differences in RMS EMG amplitudes were calculated using a two-way, repeated measure ANOVA. The conditional factor included the unilateral movements together and each of the bilateral conditions. The footedness factor separated the right and left ankle EMG for each condition. Additionally, each subject completed the Waterloo survey (Elias et al., 1998) to determine his or her handedness and footedness, where a score of 2 was completely right handed, 0 was ambidextrous, and -2 was completely left handed.

Beta Power Modulation and Slow Potential Correlation

Cross correlation was used to discern a temporal relationship between the beta power modulations and movement-related slow potentials. Artifact removal, temporal processing, and amplitude calculation were similar to the process described previously for slow potentials. However, before these data were epoched into cycles and averaged, EEG signals were filtered from 13 to 30 Hz (Butterworth, 6^{th} order, zero-phase) and RMS transformed. The maximum cross correlation values between the beta power modulations and movement-related slow potentials were calculated at each electrode location.

4.3 RESULTS

Similar cortical activity was observed during both unilateral right and left ankle movements. Similar to results of chapter two, unique slow potentials were again observed over the motor and sensory cortices during unilateral rhythmic ankle

movements (Figure 4-2) and they were similar across all subjects (Figure 4-3). For both the right and left ankle movements, sensory potentials recorded by the CPz electrode appeared to track the position of the movement with a slight lag. Conversely, the motor potentials had a distinct peak during the dorsiflexion phase of movement that was absent in passive movements. Source localization confirmed that the cortical activity was greatest in the medial sensorimotor cortex.

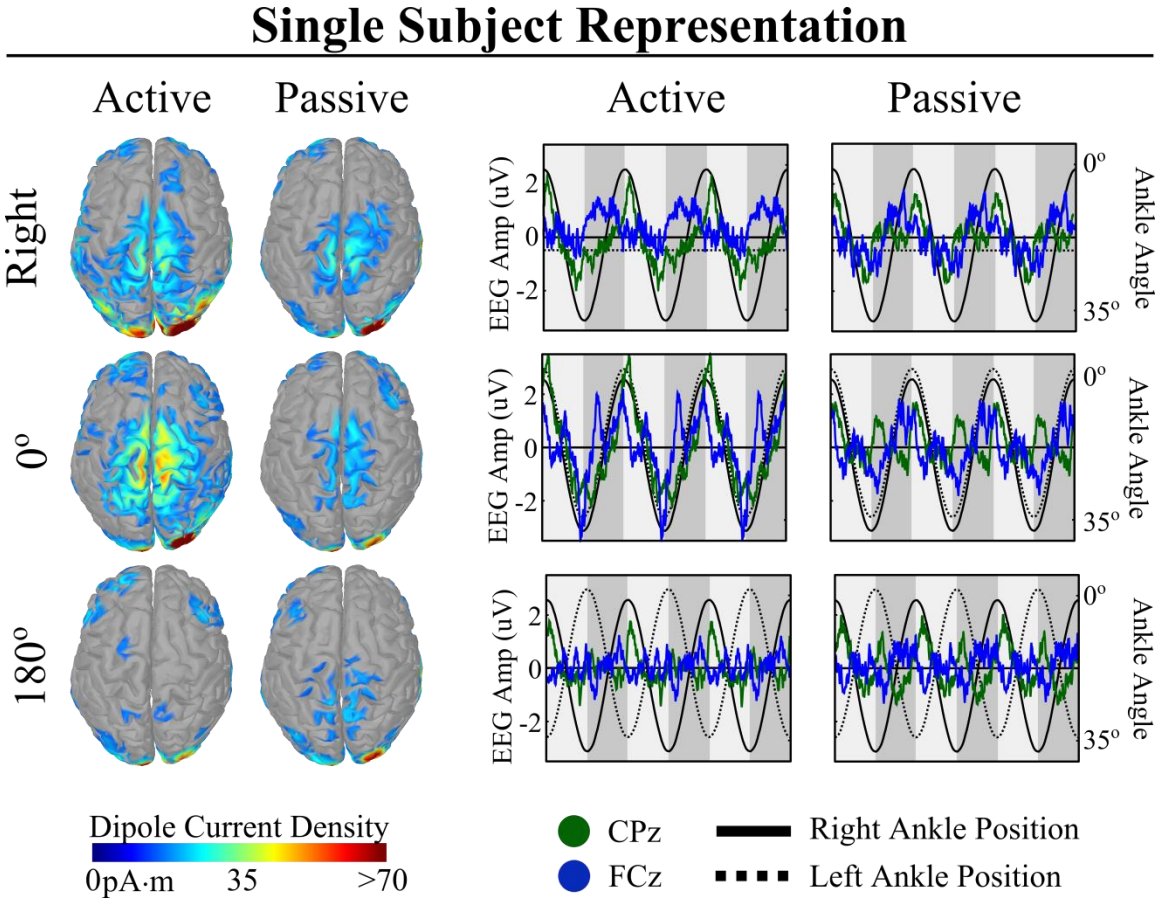

Figure 4-2: Spatiotemporal Profiles of Unilateral and Bilateral Movement (Sub 5). (Left) Time-averaged plots of movement-related cortical activity localized to the area of the medial sensorimotor cortex. A lower bound threshold of 14 pA·m was set for visualization only. (Right) The temporal slow potential profiles recorded by both the FCz (blue) and CPz (green) electrodes. Additionally, both left and right ankle movements produce similar cortical activity. Solid and dashed black lines represent the temporal movement of the right and left ankles, respectively. Additionally, the dark gray backgrounds represent the dorsiflexion phase of movement and light gray backgrounds represent the plantar flexion phase.

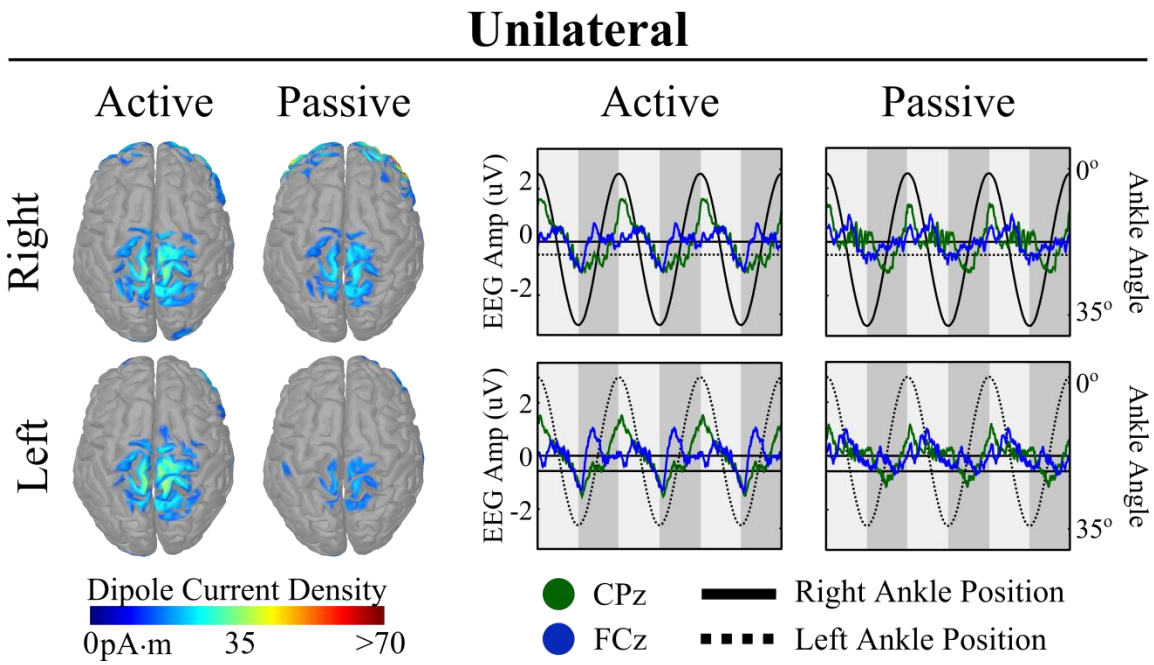

Figure 4-3: Spatiotemporal Properties of Unilateral Active/Passive Movement (Group). (Left) Time-averaged plots of movement-related cortical activity localized to the area of the medial sensorimotor cortex. A lower bound threshold of 14 pA·m was set for visualization only. (Right) The temporal slow potential profiles recorded by both the FCz (blue) and CPz (green) electrodes. Additionally, both left and right ankle movements produce similar cortical activity. Solid and dashed black lines represent the temporal movement of the right and left ankles, respectively. Additionally, the dark gray backgrounds represent the dorsiflexion phase of movement and light gray backgrounds represent the plantar flexion phase.

During bilateral movements, we observed distinct slow potential profiles over the sensory and motor cortices (Figure 4-4) for the different phasing. During in-phase (0^o lag) bilateral movements, the slow potential spatiotemporal characteristics were similar as seen during unilateral movements. However, the bilateral, in-phase, slow potential amplitudes were significantly larger for the FCz and CPz electrodes (Figure 4-5). The other out-of-phase conditions had relatively smaller slow potential amplitudes in both the active and passive conditions compared to the in-phase condition. These amplitudes were similar in the 90^o and 270^o conditions with the largest reduction in amplitude during the 180^o condition. However, the 180^o condition was unique, in that, the slow potential

amplitude during the passive condition was greater than in the active condition over the sensory cortex ($p = 0.005$). Moreover, the sensory and motor slow potentials doubled in fundamental frequency, in the 180^{o} condition, from 0.7 Hz to 1.4 Hz. In general, the slow potential amplitudes recorded over the motor cortex, FCz, were larger during active movements ($p = 0.009$), but not over the sensory cortex, CPz ($p = 0.972$) (Figure 4-5).

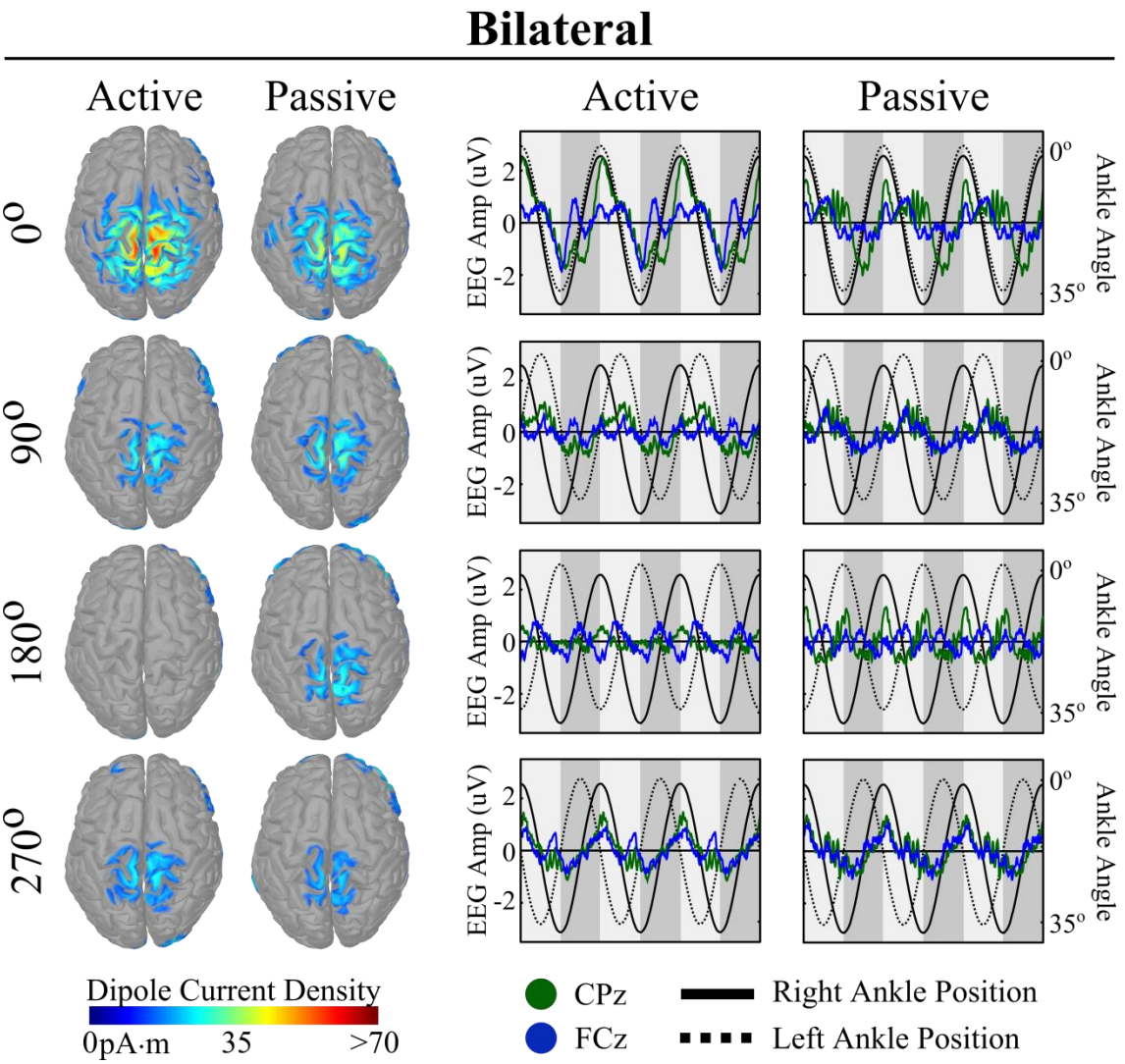

Figure 4-4: Spatiotemporal Profiles of Bilateral, Active/Passive, Out-of-phase (Group). (Left) The localization of cortical sources related to bilateral ankle movement. A lower bound threshold of 14 pA·m was set for visualization purposes. (Right) Movement-related slow potentials recorded by the FCz (blue) and CPz (green) electrodes. Solid gray lines represent the right ankle position for three movement cycles, and the dashed lined similarly represents the left ankle position. The vertical offset in the left ankle position was for visualization purposes only. The dark gray backgrounds indicate the dorsiflexion phase of movement and light gray backgrounds indicate the plantar flexion phase.

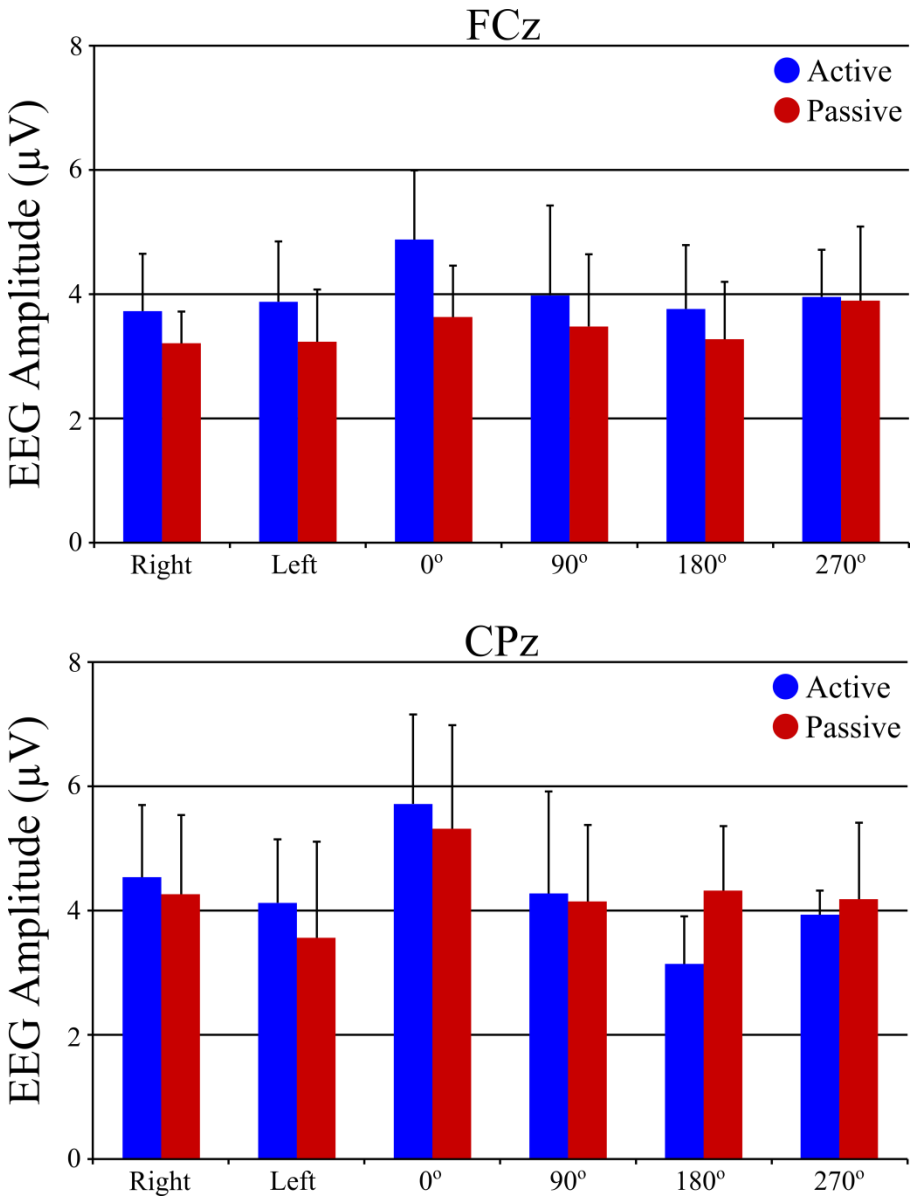

Figure 4-5: Mean Slow Potential Amplitudes of FCz and CPz for Unilteral/Bilateral. These plots represent the mean slow potential amplitudes across subjects for each unilateral or bilateral movement condition for both the FCz (top) and CPz (bottom). Also, these measurements are displayed for both active (blue) and passive (red) movements.

Added unilateral neural activity correlated highly to the bilateral activity over the medial sensorimotor cortex in most conditions (Figure 4-6). The temporal profiles of both the motor and sensory slow potentials are similar to those in the bilateral conditions. The only exception to the localized high correlation in this area was during the active,

180° out-of-phase condition. In this condition, there is a low correlation over the sensory cortex.

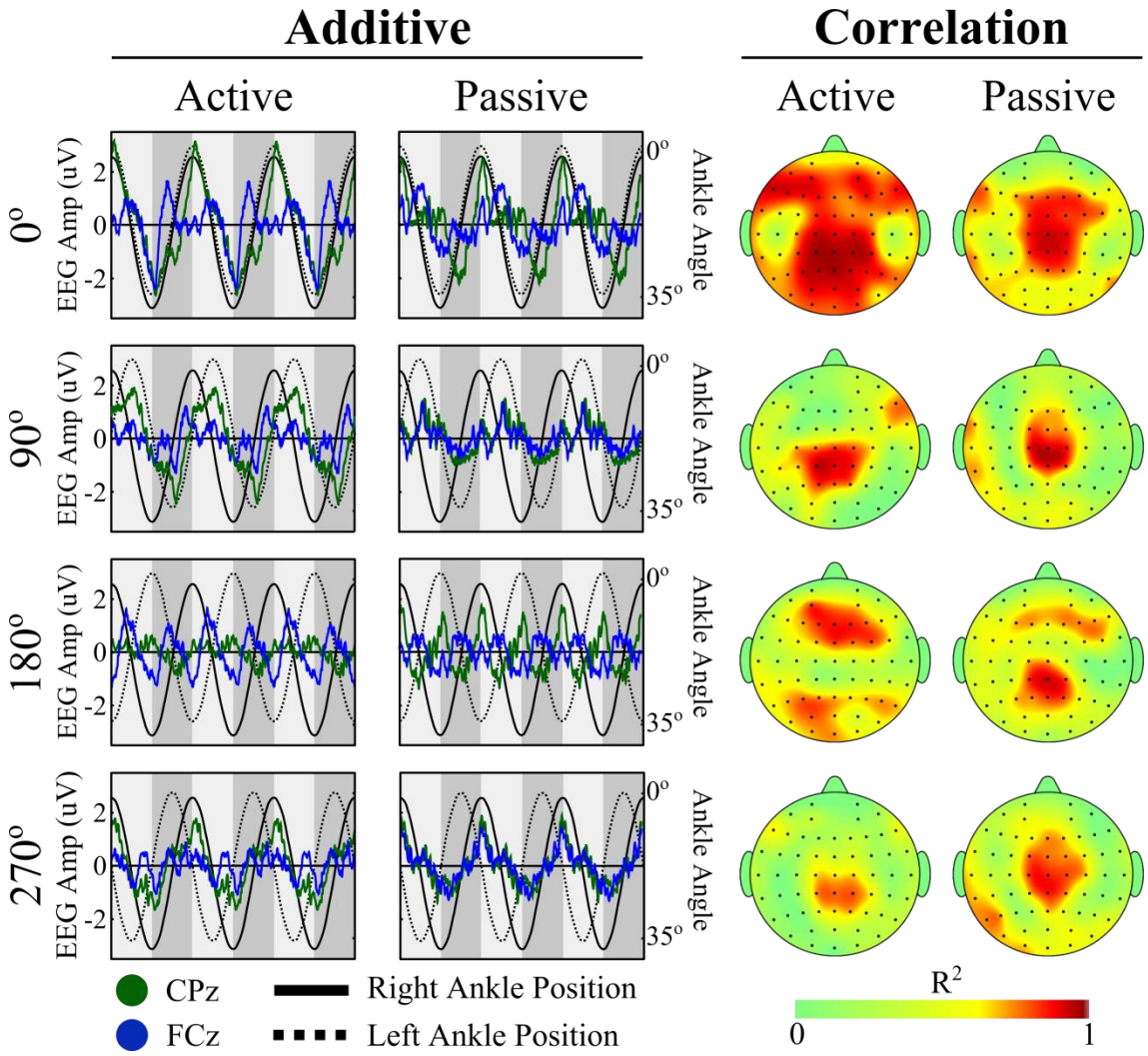

Figure 4-6: Added Temporal Profiles and Correlation with Slow Potentials (Left) Additive temporal responses for the FCz (blue) and CPz (green) electrodes. The solid and dashed lines represent the movement profiles for the right and left ankles, respectively. (Right) Coefficient of determination (R^2) values at each electrode location that represent how well the additive responses reflect the bilateral cortical activations. The backgrounds of the temporal plots indicate the dorsiflexion (dark gray) and plantar flexion (light gray) phases of movement.

The analysis of EMG amplitudes revealed that the amplitude of the Right TA EMG was consistently higher than the Left TA EMG across the conditions (p = 0.001) (Figure 4-7). However, the Right TA EMG was consistent across the conditions (p = 0.719), where the Left TA EMG appears to change amplitude (p = 0.001). Results of the Waterloo handedness and footedness scale indicated that the subjects were on average right handed ($\bar{x}$ = 1.23) and right footed ($\bar{x}$ = 0.91).

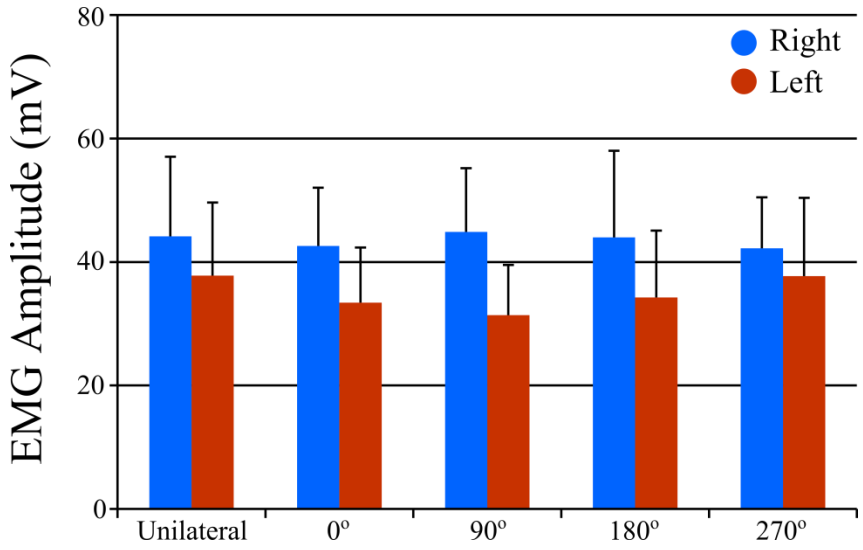

Figure 4-7: Mean EMG of Right and Left Legs for Unilateral/Bilateral. The above plot represents the average EMG amplitude for both the right (blue) and left (red) TA muscles during each of the unilateral and bilateral movement conditions.

Amplitude fluctuations in beta power modulations were similar to the movement-related slow potentials (Figure 4-8). There seems to be no difference in amplitude of beta fluctuations between active and passive conditions or between the different phasing. Interestingly, the frequency of the beta modulations also doubled in the 180^{o} condition.

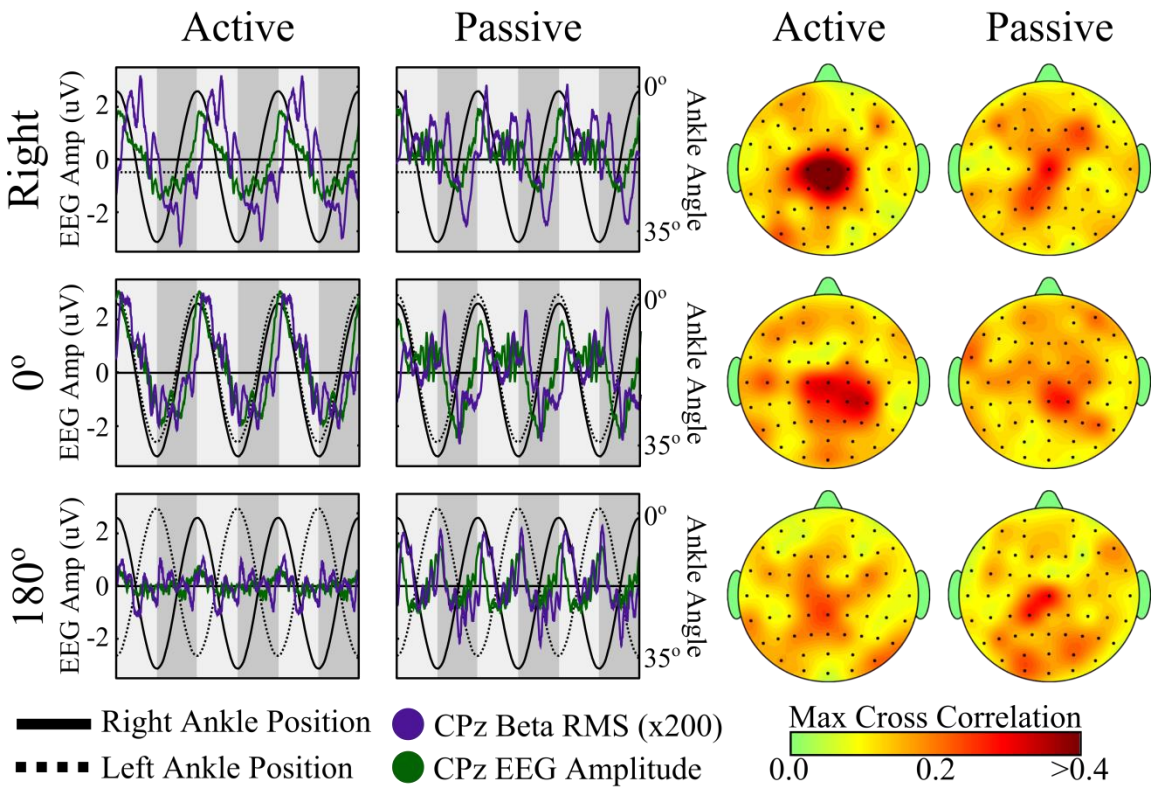

Figure 4-8: Beta Power Modulation and Slow Potential Correlation. (Left) Temporal plots of the modulation of beta power (purple) and movement-related slow potentials (green) recorded over the CPz electrode. The plots are an average of the active and passive responses for the 0^{o}, 180^{o}, and right only conditions. (Right) Max cross correlation of the beta power modulation and movement-related slow potentials plotted at each electrode. This max value is indiscriminate of phase lag.

4.4 DISCUSSION

Results from this study suggest that the sensorimotor cortex is continuously involved in the production of unilateral and bilateral, rhythmic movements of the lower extremities. Spatiotemporal properties of the right ankle movement-related slow potentials were similar to the previous findings from chapter three of this dissertation, in which we observed unique motor and sensory potentials during rhythmic movements. In this study, we have additionally shown that rhythmic movement of the left ankle produces similar movement-related slow potentials (Figure 4-3). The similarities

between the two unilateral movements support the hypothesis that the sensorimotor cortex contains separate cortical generators for each leg. Though slow potentials for both the right and left ankle movements were observed to be most prevalent over the midline, it is most probable that cortical generator for each is located deep to the scalp surface in the respective contralateral hemisphere.

Constructive and destructive interference of symmetric cortical generators produced distinct temporal profiles during bilateral movements. This is evidenced by both the amplitude differences between the phasing conditions and the correlations between the added and bilateral conditions. As would be predicted by this type of interaction, symmetric in-phase signals would be additive and the signal amplitude would grow. This is seen in the bilateral in-phase condition (Figure 4-4). Interestingly, however, theoretically the in phase signal would have an amplitude of exactly the added sum of each, and this is not the case with our data. Therefore, two cases are possible. First, there were slight timing differences or asymmetries between the two generators that caused a reduction in the additive process. Second, part of the slow potential profile and amplitude is due to an underlying process common to both unilateral conditions (Oda & Moritani, 1996).

The out-of-phase bilateral movement conditions demonstrate varying levels of destructive cortical field interference for both active and passive conditions. Within these conditions, we observed that the cortical potentials were further reduced in amplitude from the in phase condition as the movements approached 180^{o} out-of-phase. Moreover, the 90^{o} and 270^{o} out-of-phase conditions had similar slow potential amplitudes with similar temporal patterns. The most curious finding was observed during the 180^{o} out-of-

phase movement pattern and had previously been observed by Jain et al. (2013) during stationary pedaling. In this movement pattern, two distinct features were observed over the medial sensory cortex. First, the fundamental frequency of the slow potential doubled to approximate 1.4 Hz for both the active and passive conditions. Second, the amplitude of the slow potential during the passive condition was greater than the active condition. Jain and colleagues explained the reduction in the slow potential amplitude they observed during the active pedaling as a possible consequence of sensory gating. However, the results from this study suggest that the reduction was due to destructive interference of symmetrical cortical generators that were firing out of phase. This is further supported by the results of the added unilateral and bilateral slow potential cross correlations.

Cross correlation of the additive unilateral and the bilateral slow potentials further supports the theory of cortical field interference. Not only were the added unilateral and bilateral slow potentials highly correlated, these correlations were at their maximum over the medial sensorimotor cortex, except in the 180^{o} active condition. However, just like all the other conditions, we observed the same temporal and amplitude properties from the 180^{o} added unilateral condition as we did in the bilateral condition. The reason the correlation was not localized for the active condition was due to the almost complete attenuation of the sensory signal. Again, the temporal and amplitude similarities between the added and bilateral conditions support the hypothesis that the reduced sensory potential was not sensory gating, but just the destructive nature of two similar signals 180^{o} out-of-phase.

Finally, correlations of the beta power modulations and the movement-related slow potentials were localized to the medial sensory cortex (Figure 4-8). Moreover,

temporal and amplitude changes were similar across both unilateral and bilateral conditions. Of particular interest, we observed that beta frequency modulations doubled their fundamental frequency, and they were reduced in the active 180^{o} out-of-phase condition, similar to the slow potentials. The reasons for the correlations and similar bilateral responses remain unclear. However, it is possible that they are separate biological mechanisms that are just responding to the same ankle movement and therefore are correlated, but may not be causal. On the other hand, perhaps the origin of movement-related slow potentials are the slow frequency modulatory component of the changes in beta frequencies (Mazaheri & Jensen, 2008). However, the latter does not explain the timing difference between the two signals.

In this study, we have provided evidence that unilateral and bilateral ankle movements require similar cortical mechanisms. Moreover, the changes in slow potential and higher frequency modulation amplitudes in out-of-phase movements may be the result of destructive field interference between individual, symmetric cortical generators on either side of the longitudinal fissure. Lastly, beta power modulations of the medial sensory cortex are correlated with movement-related slow potentials in the same location. Whether these two phenomena are causal or only correlated is still unclear. In future studies, we recommend caution when interpreting EEG recordings during bilateral out-of-phase movements for either slow potentials or higher frequency modulations.

CHAPTER 5: MOVEMENT-RELATED SLOW POTENTIALS: ENCODING CORTICAL MOVEMENT CONTROL

5.1 INTRODUCTION

The neural coding of efferent and afferent information between the brain and the spinal cord for the generation muscle contractions and movements is still uncertain. Currently, there exist a number of opposing hypotheses that have been generated by results from intracortical recordings. It has been suggested that the motor cortex in lesser mammals may encode various time-independent movement parameters, such as position, velocity, force, or a combination of these factors (Ashe, 1997; Cheney & Fetz, 1980; Georgopoulos et al., 1992; Hatsopoulos et al., 2007; Moran & Schwartz, 1999; Paninski, et al. 2004). Moreover, less invasive studies of the human sensorimotor cortex have also shown relationships between neural signaling during upper extremity movements and kinematic parameters such as position, velocity, and force (Anderson et al., 2012; Negro & Farina, 2011; Schalk et al., 2007). However, less is known about the neural coding of lower extremity rhythmic movements.

Therefore, in this analysis we used previously collected data from Chapters 2 and 3 of this dissertation to evaluate how the motor and sensory cortices may control rhythmic movements of the ankle. Electroencephalography (EEG) and electromyography (EMG) were used to record cortical and muscle activity during rhythmic ankle movements, respectively. The corticomuscular control and feedback were investigated by observations of the temporal properties, timing, and correlations between movement-related slow potentials and the tibialis anterior (TA) muscle activity. From observations during the experiments, we hypothesized that the movement-related slow potentials

would encode properties of muscle or force production in the motor cortex and positional feedback from the sensory cortex.

5. 2 METHODS

5.2.1 Recording and Signal Processing

Methods for Chapter 5 are similar to those found in Chapters 2 and 3 of this dissertation. Briefly, electroencephalography (EEG) and electromyography (EMG) were recorded during unilateral, volitional ankle movements. The experimental conditions from Chapter 2 included rhythmic, discrete, and cued free movements. Movement conditions from Chapter 3 included rhythmic ankle movements in a robotic device at 0.7 Hz, 1.0 Hz, and 1.3 Hz movement frequencies. After recording, data from all EEG trials were preprocessed to remove physiological and environmental artifacts from the signals. Movement cycles with either additional artifact or were statistically different from the others were removed. Finally, temporal averaging was used to reveal movement-related slow potentials at each electrode location.

The EMG data for each trial were band-pass filtered and root mean square (RMS) transformed. The data were then split into cycles and the average muscle activity per cycle was estimated using temporal averaging. Finally, the derivative of the processed RMS EMG activity was calculated and subsequently filtered below 50 Hz. This reflected the rate of muscle contraction during a movement cycle.

5.2.2 Analysis

For this analysis, we focused on the FCz, Cz, and CPz electrodes, which are located near the vertex on the midline of the scalp. These electrodes were chosen because they are positioned over the medial sensorimotor cortex: the leg area of the homunculus. Specifically, slow potentials recorded over the FCz electrode were hypothesized to be from mostly motor cortical areas. Similarly, the CPz electrode was related to the medial sensory cortex and the Cz considered to be of mixed sensorimotor origin.

Three analyzes were considered in this chapter. First, correlation of the negative movement-related slow potential amplitude was correlated with the maximal amplitude of the rate of muscle activation, during dorsiflexion of uninhibited ankle movements. A coefficient of determination (R^2) was calculated to approximate the linear relationship between the two variables. Second, the delay in timing of the motor (FCz) and sensory (CPz) movement-related slow potentials were compared to the rate of muscle activation profile. Relative timing was determined by calculating the differences in peak potentials during the dorsiflexion phase of movement. Finally, we examined whether the motor and sensory movement-related slow potentials were independent of the movement frequency by calculating and comparing the total duration of each potential at each frequency.

5.3 RESULTS

Temporal profiles of the movement-related slow potentials over the medial sensory motor cortex demonstrate a relationship with the rate of TA muscle contraction or derivative of RMS EMG activity. The similarity between the two temporal profiles

was consistent for continuous, discrete, and cued movements for a single representative subject and the group average (Figure 5-1). Moreover, there were two specific components of the movement-related slow potential associated with the rate of EMG contraction. First, there was a temporal component related to the kinematics profile of the movement. This similarity was seen when the movement frequency component (MFC_1) was filtered out in Chapter 2 (Figure 2-5). This was also observed when the slower potential, MFC_1, was removed from the EEG, even when the EMG pattern was not sinusoidal (Figure 5-2). Second, the amplitude of the rate of EMG was correlated with the amplitude of the movement-related slow potential negativity during dorsiflexion (Figure 5-3). The correlation between the rate of EMG and negative EEG potentials was $R^2 = 0.785$, after removing three trials. These three movement trials were removed from analysis because their movement patterns were not similar, and therefore could not be equally compared.

There exist unique timings of the movement related slow potentials over the individual sensory and motor cortices. During the dorsiflexion phase of movement, the local maximum of the movement-related slow potential over the motor cortex preceded the rate of EMG contraction by increasing amounts for each movement frequency (Figure 5-4). Moreover, the sensory potential lagged the rate of EMG contraction profile by decreasing amounts for each movement frequency. The duration of the motor potentials was consistent across the movement frequencies at approximately 235 ms. However, the duration of the sensory potential appeared dependent on the frequency of movement.

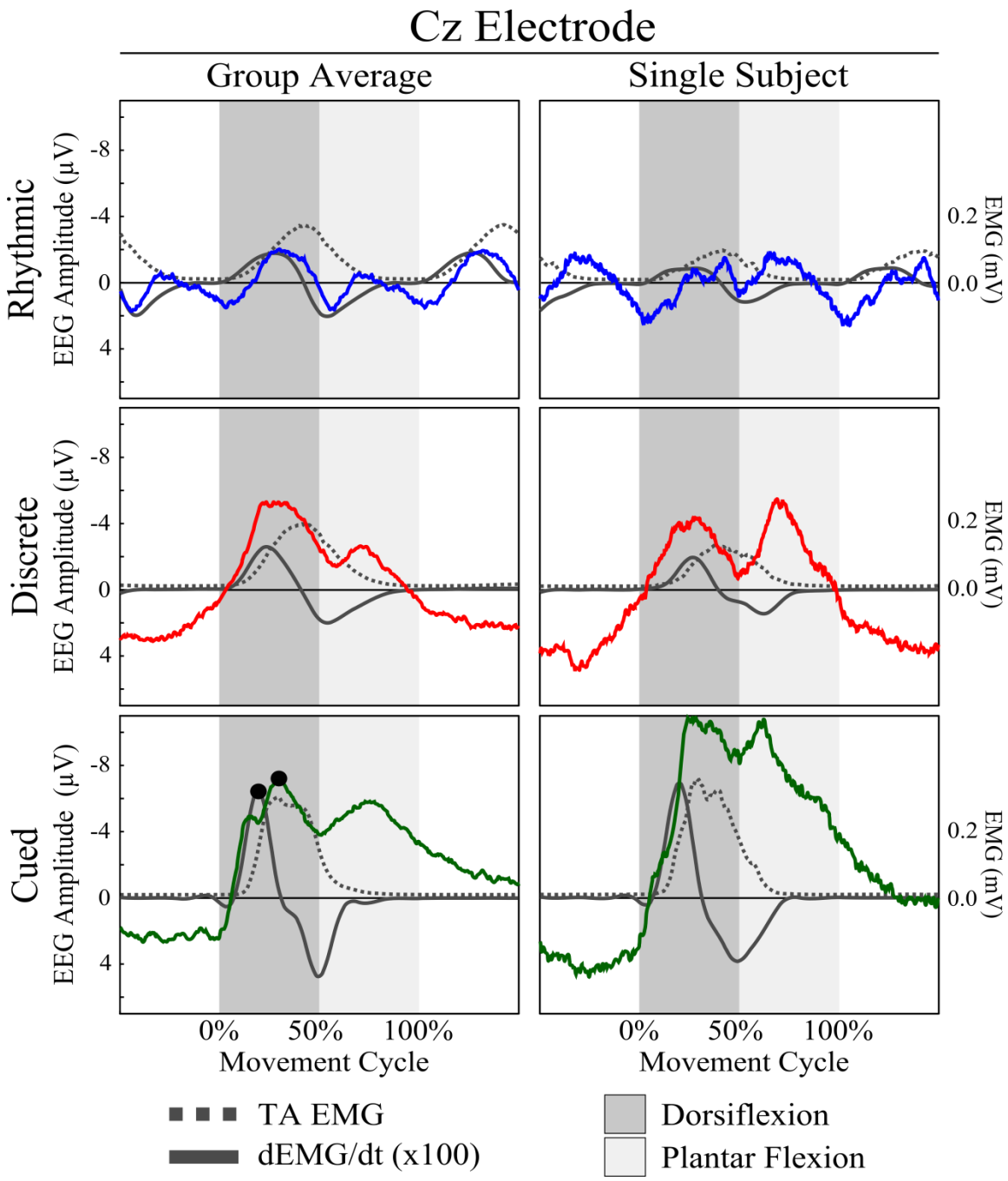

Figure 5-1: Temporal Relationship between EEG and Derivative of EMG. Temporal relationship between the movement-related slow potentials during continuous (blue), discrete (red), and cued (green) trial recorded over the Cz electrode and the TA EMG (dotted black), and the derivative of EMG (gray). Signals are represented as a percentage of the movement cycle with both dorsiflexion (dark gray background) and relaxation (light gray background) phases and half a cycle before and after the movement (white background). Results are presented as group averages (left) and as a representative single subject (Sub 1, right). Black circles represent the amplitude values used for correlation analysis (Figure 5-3).

5.4 DISCUSSION

Results of this analysis support the previous studies presented in this dissertation by providing further insight into the cortical mechanisms that control rhythmic lower extremity movements. First, we demonstrated that the movement-related slow potentials might be related to the derivative of the TA EMG activity. Second, a temporal sequence of the motor potential, EMG derivative, and sensory potential reflects a causal relationship between them. Lastly, there is evidence that the motor potential has a constant timing for all movement frequency. This is in contrast to the sensory potential, which has a temporal profile that is reliant on the movement-frequency.

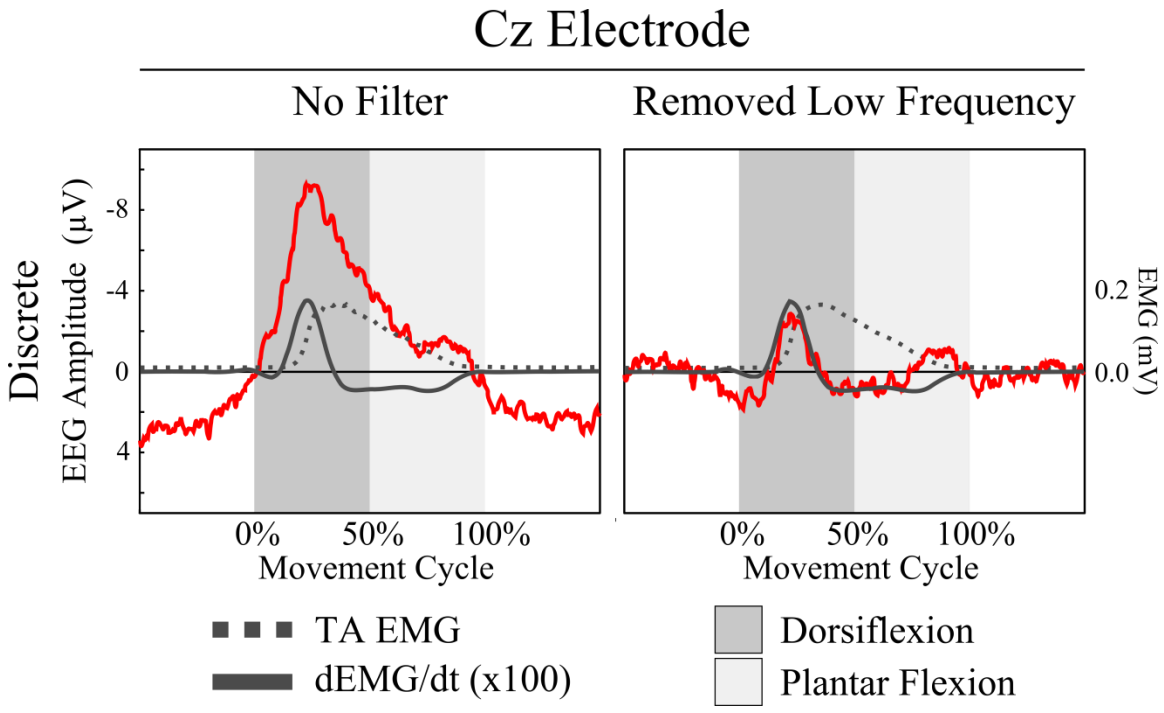

Figure 5-2: High-pass Filtered Slow Potential and EMG Derivative. Similar to Figure 5-1, discrete movement-related slow potential (red), EMG (dotted black), and the derivative of EMG (gray) are shown before filtering (left) and after elimination of low frequencies, such as MFC_1 (right).

The movement-related slow potentials appear to be comprised of two components that relate to the concurrent muscle activity. The first component modulated at the movement frequency, MFC_1, and the amplitude of this component is correlated to the max amplitude of the derivative of the EMG signal, which is the rate of muscle contraction (Figure 5-3). This was similar to the correlation observed between the amplitude of the movement-related cortical potentials and the rate of rising force produced during elbow flexion (Siemionow et al., 2000).

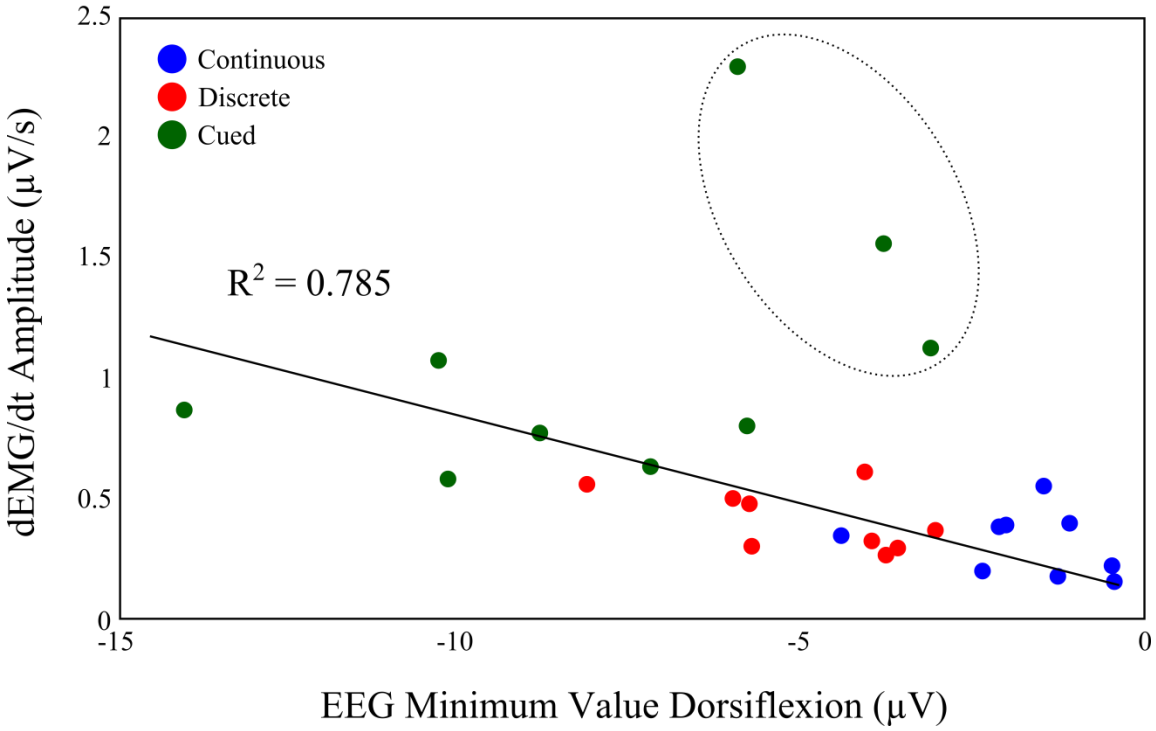

Figure 5-3: Correlation of EEG and Derivative of TA EMG. Correlation between the negative EEG amplitude of the movement-related slow potential recorded over the Cz electrode and the amplitude of derivative of the TA EMG during the dorsiflexion phase of movement. The correlation included continuous (blue), discrete (red), and cued (green) movement types. Three cued trials were excluded from the analysis (dotted circle).

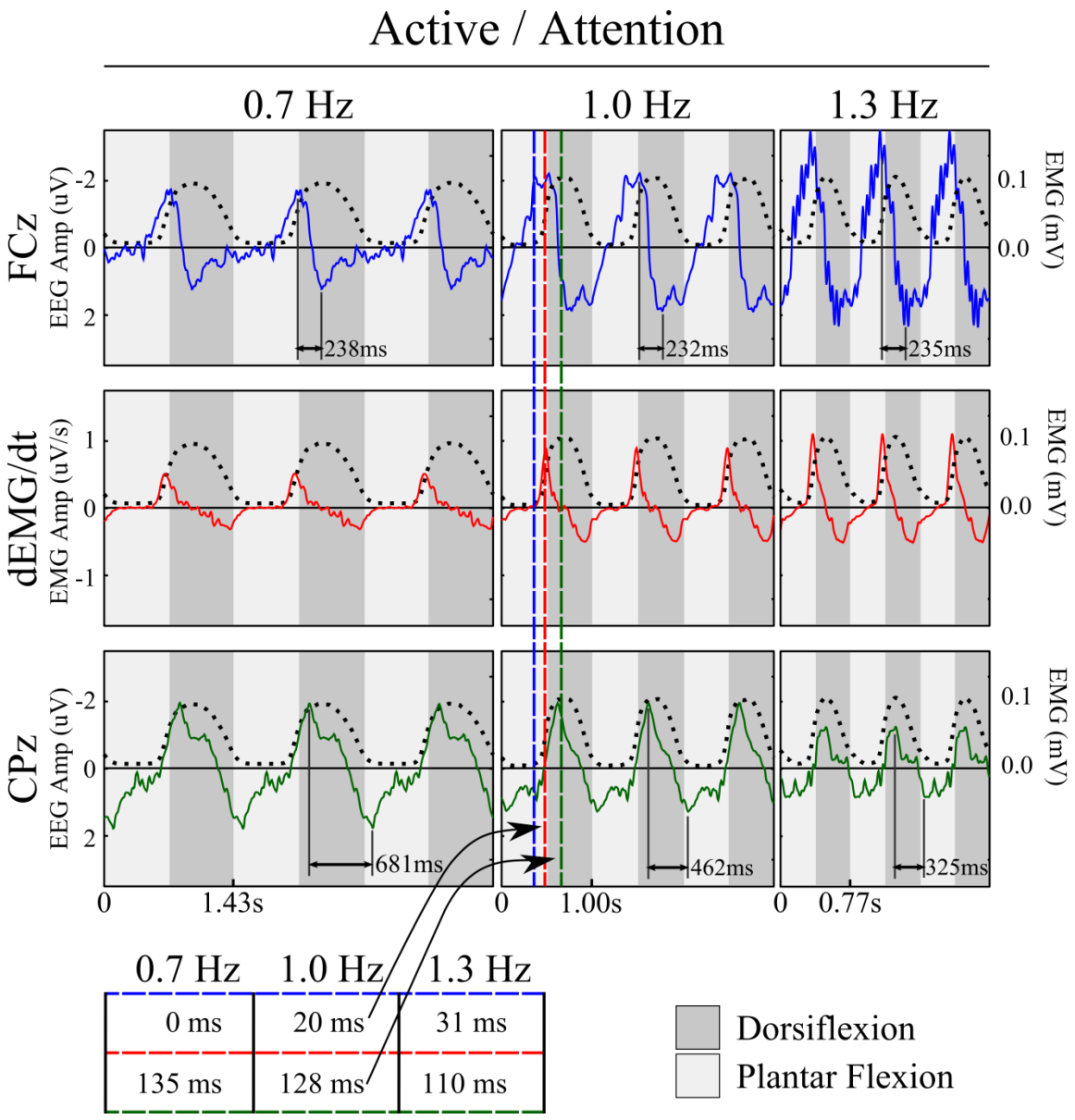

Figure 5-4: Sensory and Motor Movement-Related Slow Potential Timing. Average temporal profiles of movement-related slow potentials recorded during volitional ankle movements in a robotic device with focused attention. Timing values in milliseconds between peak FCz (top), derivative of EMG (middle), and CPz (bottom) are reported in the table at the bottom for the 0.7 Hz (left), 1.0 Hz (middle), and 1.3 Hz (right) movement frequencies. Temporal signals are plotted with the time of one cycle duration indicated at the bottom of each column. Background represents the dorsiflexion (dark gray) and planter flexion (light gray) phases of movement.

The second component is revealed when the lower frequency component is removed and this component has a similar temporal pattern to the derivative of the associated EMG signal (Figure 5-2). These results are supported by previous studies that have also concluded that the sensorimotor cortex may be encoding the force derivative of muscle contractions (Soto & Cros, 2011). Interestingly, the temporal changes in spiking rates of motor units have been shown to be correlated to the derivative of muscle activation and force produced (Evarts, 1968; Yoshitake & Shinohara, 2013).

The temporal organization of movement-related slow potentials of the sensorimotor cortex suggests a causal relationship. The temporal profiles of movement-related slow potentials over both the sensory and motor cortices were similar to the derivative of the associated EMG activity at all movement frequencies (Figure 5-4). Moreover, during dorsiflexion, the progression of motor, EMG derivative, then sensory potential with the observed timings suggests that the motor potential is causing a muscle contraction and that an afferent sensory signal is observed over the medial somatosensory cortex. However, the measured values are highly variable between subjects and so it is difficult to determine the precise timing of each slow potential.

Motor and sensory movement-related slow potentials demonstrate different effects of movement frequency. Over the medial motor cortex, the recorded movement-related slow potentials appear to have similar temporal duration, approximately 235 ms, irrespective of the frequency of movement (Figure 5-4). However, the amplitude of the slow potential did increase with increased frequency. This is similar to a theory of motor control known as pulse-step (Ghez, 1979), in which the motor command is given in as a pulse of a constant duration and the amplitude is modulated to change the output.

Conversely, the duration of the movement-related slow potential over the medial sensory cortex did vary with increasing movement frequency, and we believe this is related to afferent sensory feedback related to the position of the movement.

In this analysis, we have shown that there exist amplitude and temporal relationships of the movement-related slow potentials of the sensorimotor cortex and the derivative or rate of EMG activity during rhythmic movements of the ankle. Moreover, the motor cortex appears to always send a similar duration potential previous to the muscle contraction, irrespective of the movement frequency. Furthermore, the movement-related slow potential recorded over the sensory cortex lags the muscle activity and appears to relay positional information about the ankle movement.

CHAPTER 6: SUMMARY OF RESULTS AND FUTURE DIRECTIONS

The following chapter summarizes the experimental results and conclusions presented in this dissertation. Furthermore, we explain the significance of this work and its impact within the broader scientific community. Finally, future research directions will be discussed, which address questions that have emerged while preparing this dissertation.

6.1 SUMMARY OF RESULTS AND CONCLUSIONS

Throughout this dissertation, we have demonstrated that the sensorimotor cortex is continuously involved in the propagation of rhythmic movements of the ankle. We support this conclusion with the evidence that temporal profiles of movement-related slow potentials are continuous throughout the movement cycle and have modulation patterns related to kinematic or kinetic properties of the movement. Additionally, this is supported by the spatial localization of the movement-related slow potentials over the medial sensorimotor cortex: the ankle area of the sensorimotor homunculus. The following are results and conclusions for each individual aim of this dissertation.

6.1.1 Aim 1: Identify the sensorimotor cortical contribution of rhythmic and discrete movements of the ankle.

Results from this study suggest that rhythmic lower extremity movements may require a subset of neural mechanisms required for discrete movements. We believe that discrete movements require these additional cortical mechanisms for the initiation and termination of movement. Retention of similar spatiotemporal properties as discrete movements supports the conclusion that rhythmic movements require similar neural

mechanisms to propagate movement. Moreover, the differences in low delta power and amplitude of pre- and post-movement potentials are mostly likely the neural component required to initiate and terminate a discrete movement.

6.1.2 Aim 2: Differentiate the sensory and motor cortical contributions to rhythmic movements of the ankle.

The identification of separate movement-related slow potentials suggests that the sensory and motor cortices are uniquely involved in the propagation of rhythmic movements of the ankle. The temporal profile of the slow potential over the medial sensory cortex tracked the position of the movement with a slight lag. This suggests that the sensory cortex may receive proprioceptive information of the ankle joint position. However, the temporal slow potential profile over the motor cortex was only active during contraction of the TA muscle. Furthermore, the slow potential amplitude increased proportionally with the frequency of movement or continuity of the EMG, during both active and passive movements. Together, these results suggest that the motor cortex may encode kinetic efferent profiles to the muscles, possibly the rate (derivative) of EMG contraction. Lastly, temporal modulations in beta power were most highly correlated over the medial sensorimotor cortex. It is still unclear whether the observed correlation between the two signals is also causal.

6.1.3 Aim 3: Determine the sensory and motor cortical contributions to bilateral, rhythmic movements of the ankle.

Unilateral and bilateral, rhythmic movements of the ankle appear to be propagated by similar cortical generators. Spatiotemporal profiles of unilateral right and left ankle movement-related slow potentials suggest that both are produced through similar,

symmetric cortical mechanisms. The symmetry and temporal similarities of the two generators caused constructive and destructive interference of their respective electric fields during bilateral, active and passive movements. This was confirmed by high correlations between added unilateral trials with bilateral movement trials. Similar consequences of field interference were observed for the temporal modulations of beta power recorded over the sensorimotor cortex. We caution that EEG recordings of bilateral, lower extremity rhythmic movements may produce results that do not reflect the true underlying physiology.

6.2 BROADER SCIENTIFIC IMPACT AND FUTURE DIRECTIONS

There is still a significant amount of research required to understand the basic physiology of movement-related slow potentials. The following sections highlight possible studies that explore further the basic physiology of movement-related slow potential. In addition, we address two scientific areas in which movement-related slow potentials may have a broader scientific impact: cortical physiology of movement disorders and brain machine interfacing.

6.2.1 Movement-related Slow Potential Physiology

From results of this dissertation, we have only begun to understand the physiology of movement-related slow potentials. This research has opened the door to an overabundant number of new experimental possibilities. One example of a future experiment would be to examine the differences in cortical control between dorsiflexion and plantar flexion of the ankle. Others could include, but are not limited to, single and

multi-joint movements, distal vs. proximal muscle control, multimodal imaging (EEG & fMRI or MEG), robotically controlled rhythmic and discrete movement patterns, and pseudorandom active and passive movements used to develop a neural model of movement control. Furthermore, a firm understanding of the relationship between the motor cortex and muscle activation through a noninvasive technology would be very advantageous for studying the neural control of movement in humans.

6.2.2 Cortical Physiology of Movement Disorders

We demonstrated in this dissertation that there are distinct relationships between movement-related slow potentials and the kinematic and kinetic properties of movement. As this line of research continues, we believe these slow potentials will be specifically useful in understanding the sensory and motor cortical changes in people with a neural injury or disease. For example, experiments could include unilateral active and passive ankle or hip movements in the robotic device used compare physiological differences between neurologically intact people and people who have a spinal cord injury or have had a stroke. In spinal cord injury (SCI), the localization or temporal properties of the sensory and motor potentials could be compared to infer changes in cortical structure or plasticity after injury. Also, It could be questioned whether people who have a chronic, complete spinal cord injury still retain the similar motor drive, or how cortical motor drive is different in people with partial SCI. In stroke, specifically subcortical strokes, it could be tested whether there are changes to the sensory and motor cortices, and if this has any effect on movement dysfunction. Moreover, the information gained from

specific subject populations may prove beneficial in developing new rehabilitation strategies.

6.2.3 Brain Machine Interfacing

Another field related to neural rehabilitation that movement-related slow potential may impact is brain-machine interfacing (BMI). BMI uses naturally occurring neural signals to interface with robotic devices, such as a prosthetic arm for an amputee or exoskeleton robotic legs for a person with a spinal cord injury. Knowledge from both the basic physiological and movement disorder studies previously mentioned could aid in new decoding algorithms for these devices. With the knowledge of movement-related slow potential physiology from this dissertation, it may advantageous to combine advanced mathematical techniques from other, such Hidden Markov Model from the field of Speech Recognition fields, to develop improved neural decoding methods. Finally, similar ideas are already being in practice. For example, delta band (0.5 to 5 Hz) signals have been decoded during walking to reconstruct full lower leg kinematics (Presacco et al., 2011), and further research using EEG signals from this frequency band are underway.

BIBLIOGRAPHY

Altenmüller, E., Berger, W., Prokop, T., Trippel, M., & Dietz, V. (1995). Modulation of sural nerve somatosensory evoked potentials during stance and different phases of the step-cycle. *Electroencephalography and clinical neurophysiology*, *96*, 516–25.

Anderson, N. R., Blakely, T., Schalk, G., Leuthardt, E. C., & Moran, D. W. (2012). Electrocorticographic (ECoG) correlates of human arm movements. *Experimental brain research. Experimentelle Hirnforschung. Expérimentation cérébrale*, *223*, 1–10.

Ashe, J. (1997). Force and the motor cortex. *Behavioural brain research*, *87*, 255–69.

Ball, T., Kern, M., Mutschler, I., Aertsen, A., & Schulze-Bonhage, A. (2009). Signal quality of simultaneously recorded invasive and non-invasive EEG. *NeuroImage*, *46*, 708–16.

Benjamini, Y., & Hochberg, Y. (1995). Controlling the False Discovery Rate: A Practical and Powerful Approach to Multiple Testing. *Journal of the Royal Statistical Society. Series B (Methodolical)*, *57*, 289–300.

Berger, H. (1929). Über das elektrenkephalogramm des menschen. *European Archives of Psychiatry and Clinical Neuroscience*, *87*, 527–570.

Bertrand, O., Perrin, F., & Pernier, J. (1985). A theoretical justification of the average reference in topographic evoked potential studies. *Electroencephalography and clinical neurophysiology*, *62*, 462–4.

Birbaumer, N., Elbert, T., Canavan, A. G., & Rockstroh, B. (1990). Slow potentials of the cerebral cortex and behavior. *Physiological reviews*, *70*, 1–41.

Brown, T. G. (1911). The Intrinsic Factors in the Act of Progression in the Mammal. *Proceedings of the Royal Society B: Biological Sciences*, *84*, 308–319.

Bushberg, J., Seibert, J., Leidholdt, E., & Boone, J. (2002). *The Essential Physics of Medical Imaging*. *Medical Physics* (Vol. 30, p. 933). Lippencott Williams & Wilkins.

Buurke, J. H., Nene, A. V, Kwakkel, G., Erren-Wolters, V., Ijzerman, M. J., & Hermens, H. J. (2008). Recovery of gait after stroke: what changes? *Neurorehabilitation and neural repair*, *22*, 676–83.

Buzsáki, G., Anastassiou, C. a, & Koch, C. (2012). The origin of extracellular fields and currents--EEG, ECoG, LFP and spikes. *Nature reviews. Neuroscience*, *13*, 407–20.

Cheney, P. D., & Fetz, E. E. (1980). Functional classes of primate corticomotoneuronal cells and their relation to active force. *Journal of neurophysiology*, *44*, 773–91.

Christensen, L. O. D., Johannsen, P., Sinkjaer, T., Petersen, N., Pyndt, H. S., & Nielsen, J. B. (2000). Cerebral activation during bicycle movements in man. *Experimental Brain Research*, *135*, 66–72.

Ciccarelli, O., Toosy, A. T., Marsden, J. F., Wheeler-Kingshott, C. M., Sahyoun, C., Matthews, P. M., Miller, D. H., & Thompson, A. J. (2005). Identifying brain regions for integrative sensorimotor processing with ankle movements. *Experimental brain research. Experimentelle Hirnforschung. Expérimentation cérébrale*, *166*, 31–42.

Clausen, J. (2011). Conceptual and ethical issues with brain-hardware interfaces. *Current opinion in psychiatry*, *24*, 495–501.

Colebatch, J. G. (2007). Bereitschaftspotential and movement-related potentials: origin, significance, and application in disorders of human movement. *Movement disorders : official journal of the Movement Disorder Society*, *22*, 601–10.

Contreras-Vidal, J., Presacco, A., Agashe, H., & Paek, A. (2012). Restoration of whole body movement: toward a noninvasive brain-machine interface system. *IEEE pulse*, *3*, 34–7.

Cooper, R., Winter, A., Crow, H., & Walter, W. (1965). Comparison of subcortical, cortical and scalp activity using chronically indwelling electrodes in man. *Electroencephalography and clinical neurophysiology*, *18*, 217–228.

Deecke, L., Bashore, T., Brunia, C. H. M., Grünewald-Zuberbier, E., Grünewald, G., & Kristeva, R. (1984). Movement-Associated Potentials and Motor Control Report of the EPIC VI Motor Panel. *Annals of the New York Academy of Sciences*, *425*, 398–428.

Delorme, A., & Makeig, S. (2004). EEGLAB: an open source toolbox for analysis of single-trial EEG dynamics including independent component analysis. *Journal of neuroscience methods*, *134*, 9–21.

Desmedt, J. E., Tomberg, C., Noël, P., & Ozaki, I. (1990). Beware of the average reference in brain mapping. *Electroencephalography and clinical neurophysiology. Supplement*, *41*, 22–7.

Dien, J. (1998). Issues in the application of the average reference: Review, critiques, and recommendations. *Behavior Research Methods, Instruments, & Computers*, *30*, 34–43.

Dietz, V., Colombo, G., Jensen, L., & Baumgartner, L. (1995). Locomotor capacity of spinal cord in paraplegic patients. *Annals of neurology*, *37*, 574–82.

Dobkin, B., Barbeau, H., Deforge, D., Ditunno, J., Elashoff, R., Apple, D., Basso, M., Behrman, A., Harkema, S., Saulino, M., & Scott, M. (2007). The evolution of walking-related outcomes over the first 12 weeks of rehabilitation for incomplete traumatic spinal cord injury: the multicenter randomized Spinal Cord Injury Locomotor Trial. *Neurorehabilitation and neural repair*, *21*, 25–35.

Duysens, J., Tax, A. A., Nawijn, S., Berger, W., Prokop, T., & Altenmüller, E. (1995). Gating of sensation and evoked potentials following foot stimulation during human gait. *Experimental brain research. Experimentelle Hirnforschung. Expérimentation cérébrale*, *105*, 423–31.

Elias, L. J., Bryden, M. P., & Bulman-Fleming, M. B. (1998). Footedness is a better predictor than is handedness of emotional lateralization. *Neuropsychologia*, *36*, 37–43.

Evarts, E. V. (1968). Relation of pyramidal tract activity to force exerted during voluntary movement. *Journal of neurophysiology*, *31*, 14–27.

Ferree, T. C., Luu, P., Russell, G. S., & Tucker, D. M. (2001). Scalp electrode impedance, infection risk, and EEG data quality. *Clinical neurophysiology : official journal of the International Federation of Clinical Neurophysiology*, *112*, 536–44.

Ferree, T., Clay, M., & Tucker, D. (2001). The spatial resolution of scalp EEG. *Neurocomputing*, *38-40*, 1209–1216.

Formaggio, E., Storti, S. F., Boscolo Galazzo, I., Gandolfi, M., Geroin, C., Smania, N., Spezia, L., Waldner, A., Fiaschi, A., & Manganotti, P. (2013). Modulation of event-related desynchronization in robot-assisted hand performance: brain oscillatory changes in active, passive and imagined movements. *Journal of neuroengineering and rehabilitation*, *10*, 24.

Frigon, A. (2012). Central pattern generators of the mammalian spinal cord. *The Neuroscientist : a review journal bringing neurobiology, neurology and psychiatry*, *18*, 56–69.

Georgopoulos, a P., Ashe, J., Smyrnis, N., & Taira, M. (1992). The motor cortex and the coding of force. *Science (New York, N.Y.)*, *256*, 1692–5.

Ghez, C. (1979). Contributions of central programs to rapid limb movement in the cat. In Asanuma, H. & Wilson, V. (Eds.), *Integration in the nervous system* (pp. 305–320). Tokyo: Isaku-Shoin.

Goldman, D. (1950). The clinical use of the "average" reference electrode in monopolar recording. *Electroencephalography and clinical neurophysiology*, *2*, 209–12.

Gourab, K., & Schmit, B. D. (2010). Changes in movement-related β-band EEG signals in human spinal cord injury. *Clinical neurophysiology : official journal of the International Federation of Clinical Neurophysiology*, *121*, 2017–23.

Gramfort, A., Papadopoulo, T., Olivi, E., & Clerc, M. (2010). OpenMEEG: opensource software for quasistatic bioelectromagnetics. *Biomedical engineering online*, *9*, 45.

Grillner, S. (1975). Locomotion in vertebrates: central mechanisms and reflex interaction. *Physiological reviews*, *55*, 247–304.

Grünewald-Zuberbier, E., & Grünewald, G. (1978). Goal-directed movement potentials of human cerebral cortex. *Experimental brain research. Experimentelle Hirnforschung. Expérimentation cérébrale*, *33*, 135–8.

Grünewald-Zuberbier, E., Grünewald, G., Schuhmacher, H., & Wehler, A. (1980). Scalp recorded slow potential shifts during isometric ramp and hold contractions in human subjects. *Pflügers Archiv : European journal of physiology*, *389*, 55–60.

Guerrero-Mosquera, C., Trigueros, A., & Navia-Vazquez, A. (2012). EEG Signal Processing for Epilepsy. In Stevanovic, D. (Ed.), *Epilepsy - Histological, Electroencephalographic and Psychological*.

Guzzetta, A., Staudt, M., Petacchi, E., Ehlers, J., Erb, M., Wilke, M., Krägeloh-Mann, I., & Cioni, G. (2007). Brain representation of active and passive hand movements in children. *Pediatric research*, *61*, 485–90.

Gwin, J. T., Gramann, K., Makeig, S., & Ferris, D. P. (2011). Electrocortical activity is coupled to gait cycle phase during treadmill walking. *NeuroImage*, *54*, 1289–96.

Hämäläinen, M. S., & Ilmoniemi, R. J. (1994). Interpreting magnetic fields of the brain: minimum norm estimates. *Medical & biological engineering & computing*, *32*, 35–42.

Hatsopoulos, N. G., Xu, Q., & Amit, Y. (2007). Encoding of movement fragments in the motor cortex. *The Journal of neuroscience : the official journal of the Society for Neuroscience*, *27*, 5105–14.

Hogan, N., & Sternad, D. (2007). On rhythmic and discrete movements: reflections, definitions and implications for motor control. *Experimental brain research. Experimentelle Hirnforschung. Expérimentation cérébrale*, *181*, 13–30.

Holtmann, M., Steiner, S., Hohmann, S., Poustka, L., Banaschewski, T., & Bölte, S. (2011). Neurofeedback in autism spectrum disorders. *Developmental medicine and child neurology*, *53*, 986–93.

Hultborn, H., & Nielsen, J. B. (2007). Spinal control of locomotion--from cat to man. *Acta physiologica (Oxford, England)*, *189*, 111–21.

Ivanenko, Y. P., Poppele, R. E., & Lacquaniti, F. (2009). Distributed neural networks for controlling human locomotion: lessons from normal and SCI subjects. *Brain research bulletin*, *78*, 13–21.

Jackson, A., Moritz, C. T., Mavoori, J., Lucas, T. H., & Fetz, E. E. (2006). The Neurochip BCI: towards a neural prosthesis for upper limb function. *IEEE transactions on neural systems and rehabilitation engineering : a publication of the IEEE Engineering in Medicine and Biology Society*, *14*, 187–90.

Jain, S., Gourab, K., Schindler-Ivens, S., & Schmit, B. D. (2013). EEG during pedaling: evidence for cortical control of locomotor tasks. *Clinical neurophysiology : official journal of the International Federation of Clinical Neurophysiology*, *124*, 379–90.

Jankowska, E., Jukes, M. G., Lund, S., & Lundberg, A. (1967). The effect of DOPA on the spinal cord. 5. Reciprocal organization of pathways transmitting excitatory action to alpha motoneurones of flexors and extensors. *Acta physiologica Scandinavica*, *70*, 369–88.

Jasper, Herbert, & Penfield, W. (1949). Electrocorticograms in man: Effect of voluntary movement upon the electrical activity of the precentral gyrus. *Archiv für Psychiatrie und Nervenkrankheiten*, *183*, 163–174.

Jasper, HH. (1958). The 10/20 international electrode system. *EEG and Clinical Neurophysiology*, *10*, 371–375.

Jones, S. J., Halonen, J. P., & Shawkat, F. (1989). Centrifugal and centripetal mechanisms involved in the "gating" of cortical SEPs during movement. *Electroencephalography and clinical neurophysiology*, *74*, 36–45.

Joundi, R. a, Brittain, J.-S., Green, A. L., Aziz, T. Z., Brown, P., & Jenkinson, N. (2013). Persistent suppression of subthalamic beta-band activity during rhythmic finger tapping in Parkinson's disease. *Clinical neurophysiology : official journal of the International Federation of Clinical Neurophysiology*, *124*, 565–73.

Kalaska, J. F. (2009). From intention to action: motor cortex and the control of reaching movements. *Advances in experimental medicine and biology*, *629*, 139–78.

Kapreli, E., Athanasopoulos, S., Papathanasiou, M., Van Hecke, P., Strimpakos, N., Gouliamos, A., Peeters, R., & Sunaert, S. (2006). Lateralization of brain activity during lower limb joints movement. An fMRI study. *NeuroImage*, *32*, 1709–21.

Kilavik, B. E., Zaepffel, M., Brovelli, A., Mackay, W. a, & Riehle, A. (2013). The ups and downs of beta oscillations in sensorimotor cortex. *Experimental neurology*, *245*, 15–26.

Kybic, J., Clerc, M., Abboud, T., Faugeras, O., Keriven, R., & Papadopoulo, T. (2005). A common formalism for the integral formulations of the forward EEG problem. *IEEE transactions on medical imaging*, *24*, 12–28.

Leiser, S. C., Dunlop, J., Bowlby, M. R., & Devilbiss, D. M. (2011). Aligning strategies for using EEG as a surrogate biomarker: a review of preclinical and clinical research. *Biochemical pharmacology*, *81*, 1408–21.

Libit, B. (1999). Do we have free will? *Journal of Consciousness Studies*, *6*, 47–57.

Liddell, E., & Sherrington, C. (1924). Reflexes in response to stretch (myotatic reflexes). *Proceedings of the Royal Society of London. Series B, Containing Papers of a Biological Charater*, *96*, 212–242.

Lin, C.-T., Chen, S.-A., Chiu, T.-T., Lin, H.-Z., & Ko, L.-W. (2011). Spatial and temporal EEG dynamics of dual-task driving performance. *Journal of neuroengineering and rehabilitation*, *8*, 11.

Lin, C.-T., Liao, L.-D., Liu, Y.-H., Wang, I.-J., Lin, B.-S., & Chang, J.-Y. (2011). Novel dry polymer foam electrodes for long-term EEG measurement. *IEEE transactions on bio-medical engineering*, *58*, 1200–7.

Lofthouse, N., Arnold, L. E., & Hurt, E. (2012). Current status of neurofeedback for attention-deficit/hyperactivity disorder. *Current psychiatry reports*, *14*, 536–42.

Lopes, F. (2010). EEG: Origin and Measurement. In Mulert, C. & Lemieux, L. (Eds.), *EEG - fMRI: Physiological Basis, Technique, and Applications* (pp. 19–39). Berlin, Heidelberg: Springer Berlin Heidelberg.

MacKay-Lyons, M. (2002). Central pattern generation of locomotion: a review of the evidence. *Physical therapy*, *82*, 69–83.

Maynard, E. M., Nordhausen, C. T., & Normann, R. a. (1997). The Utah intracortical Electrode Array: a recording structure for potential brain-computer interfaces. *Electroencephalography and clinical neurophysiology*, *102*, 228–39.

Mayville, J. M., Fuchs, A., & Kelso, J. A. S. (2005). Neuromagnetic motor fields accompanying self-paced rhythmic finger movement at different rates. *Experimental brain research. Experimentelle Hirnforschung. Expérimentation cérébrale*, *166*, 190–9.

Mazaheri, A., & Jensen, O. (2008). Asymmetric amplitude modulations of brain oscillations generate slow evoked responses. *The Journal of neuroscience : the official journal of the Society for Neuroscience*, *28*, 7781–7.

Mehta, J. P., Verber, M. D., Wieser, J. a, Schmit, B. D., & Schindler-Ivens, S. M. (2009). A novel technique for examining human brain activity associated with pedaling using fMRI. *Journal of neuroscience methods*, *179*, 230–9.

Mehta, J. P., Verber, M. D., Wieser, J. a, Schmit, B. D., & Schindler-Ivens, S. M. (2012). The effect of movement rate and complexity on functional magnetic resonance signal change during pedaling. *Motor control*, *16*, 158–75.

Mima, T., Sadato, N., Yazawa, S., Hanakawa, T., Fukuyama, H., Yonekura, Y., & Shibasaki, H. (1999). Brain structures related to active and passive finger movements in man. *Brain : a journal of neurology*, *122 (Pt 1*, 1989–97.

Miyai, I., Tanabe, H. C., Sase, I., Eda, H., Oda, I., Konishi, I., Tsunazawa, Y., Suzuki, T., Yanagida, T., & Kubota, K. (2001). Cortical mapping of gait in humans: a near-infrared spectroscopic topography study. *NeuroImage*, *14*, 1186–92.

Mognon, A., Jovicich, J., Bruzzone, L., & Buiatti, M. (2010). ADJUST: An automatic EEG artifact detector based on the joint use of spatial and temporal features. *Psychophysiology*, *48*, 229–240.

Moran, D. W., & Schwartz, a B. (1999). Motor cortical representation of speed and direction during reaching. *Journal of neurophysiology*, *82*, 2676–92.

Müller-Putz, G. R., Zimmermann, D., Graimann, B., Nestinger, K., Korisek, G., & Pfurtscheller, G. (2007). Event-related beta EEG-changes during passive and attempted foot movements in paraplegic patients. *Brain research*, *1137*, 84–91.

Negro, F., & Farina, D. (2011). Linear transmission of cortical oscillations to the neural drive to muscles is mediated by common projections to populations of motoneurons in humans. *The Journal of physiology*, *589*, 629–37.

Nicolas-Alonso, L. F., & Gomez-Gil, J. (2012). Brain computer interfaces, a review. *Sensors (Basel, Switzerland)*, *12*, 1211–79.

Niedermeyer, E. (1999). The Normal EEG of the Waking Adult. In *Electroencephalography: Basic Principles, clinical Applications and Related Fields.* (pp. 149–173). Baltimore, MD: Lippincott Williams & Wilkins.

Nielsen, J. B. (2003). How we walk: central control of muscle activity during human walking. *The Neuroscientist : a review journal bringing neurobiology, neurology and psychiatry*, *9*, 195–204.

Oda, S., & Moritani, T. (1996). Cross-correlation studies of movement-related cortical potentials during unilateral and bilateral muscle contractions in humans. *European journal of applied physiology and occupational physiology*, *74*, 29–35.

Onishi, H., Sugawara, K., Yamashiro, K., Sato, D., Suzuki, M., Kirimoto, H., Tamaki, H., Murakami, H., & Kameyama, S. (2013). Neuromagnetic activation following active and passive finger movements. *Brain and behavior*, *3*, 178–92.

Palmer, J. A., Makeig, S., Kreutz-Delgado, K., & Rao, B. D. (2008). Newton method for the ICA mixture model. In *2008 IEEE International Conference on Acoustics, Speech and Signal Processing* (pp. 1805–1808). IEEE.

Paninski, L., Fellows, M. R., Hatsopoulos, N. G., & Donoghue, J. P. (2004). Spatiotemporal tuning of motor cortical neurons for hand position and velocity. *Journal of neurophysiology*, *91*, 515–32.

Petersen, N. T., Pyndt, H. S., & Nielsen, J. B. (2003). Investigating human motor control by transcranial magnetic stimulation. *Experimental brain research. Experimentelle Hirnforschung. Expérimentation cérébrale*, *152*, 1–16.

Petersen, T. H., Willerslev-Olsen, M., Conway, B. a, & Nielsen, J. B. (2012). The motor cortex drives the muscles during walking in human subjects. *The Journal of physiology*, *590*, 2443–52.

Pfurtscheller, G., Neuper, C., Müller, G. R., Obermaier, B., Krausz, G., Schlögl, a, Scherer, R., Graimann, B., Keinrath, C., Skliris, D., Wörtz, M., Supp, G., & Schrank, C. (2003). Graz-BCI: state of the art and clinical applications. *IEEE transactions on neural systems and rehabilitation engineering : a publication of the IEEE Engineering in Medicine and Biology Society*, *11*, 177–80.

Presacco, A., Goodman, R., Forrester, L., & Contreras-Vidal, J. L. (2011). Neural decoding of treadmill walking from noninvasive electroencephalographic signals. *Journal of neurophysiology*, *106*, 1875–87.

Raethjen, J., Govindan, R. B., Binder, S., Zeuner, K. E., Deuschl, G., & Stolze, H. (2008). Cortical representation of rhythmic foot movements. *Brain research*, *1236*, 79–84.

Sabes, P. N. (2000). The planning and control of reaching movements. *Current opinion in neurobiology*, *10*, 740–6.

Salmelin, R., & Baillet, S. (2009). Electromagnetic brain imaging. *Human brain mapping*, *30*, 1753–7.

Schaal, S., Sternad, D., Osu, R., & Kawato, M. (2004). Rhythmic arm movement is not discrete. *Nature neuroscience*, *7*, 1136–43.

Schalk, G., Kubánek, J., Miller, K. J., Anderson, N. R., Leuthardt, E. C., Ojemann, J. G., Limbrick, D., Moran, D., Gerhardt, L. A., & Wolpaw, J. R. (2007). Decoding two-dimensional movement trajectories using electrocorticographic signals in humans. *Journal of neural engineering*, *4*, 264–75.

Schneider, S., Rouffet, D. M., Billaut, F., & Strüder, H. K. (2013). Cortical current density oscillations in the motor cortex are correlated with muscular activity during pedaling exercise. *Neuroscience*, *228*, 309–14.

Schubert, M., Curt, A., Jensen, L., & Dietz, V. (1997). Corticospinal input in human gait: modulation of magnetically evoked motor responses. *Experimental brain research. Experimentelle Hirnforschung. Expérimentation cérébrale*, *115*, 234–46.

Sherrington, C. S. (1908). *The integrative action of the nervous system*.

Shibasaki, H., & Hallett, M. (2006). What is the Bereitschaftspotential? *Clinical neurophysiology : official journal of the International Federation of Clinical Neurophysiology*, *117*, 2341–56.

Siemionow, V., Yue, G. H., Ranganathan, V. K., Liu, J. Z., & Sahgal, V. (2000). Relationship between motor activity-related cortical potential and voluntary muscle activation. *Experimental brain research. Experimentelle Hirnforschung. Expérimentation cérébrale*, *133*, 303–11.

Soto, O., & Cros, D. (2011). Direct corticospinal control of force derivative. *The Journal of neuroscience : the official journal of the Society for Neuroscience*, *31*, 1944–8.

Steldt, R. E., & Schmit, B. D. (2004). Modulation of coordinated muscle activity during imposed sinusoidal hip movements in human spinal cord injury. *Journal of neurophysiology*, *92*, 673–85.

Stevens, J. P. (2009). *Applied Multivariate Statistics for the Social Sciences* (Fifth.). New York: Routledge.

Stone, J. (2004). *Independent component analysis: a tutorial introduction* (p. 193). Cambridge, MA: MIT Press.

Student. (1908). The Probable Error of a Mean. *Biometrika*, *6*, 1–25.

Swedler, R. M. (2012). *Examining Lower Extremity Motor Activity Using Magnetoencephalography*. Marquette University. Retrieved from http://epublications.marquette.edu/theses_open/159/

Tadel, F., Baillet, S., Mosher, J. C., Pantazis, D., & Leahy, R. M. (2011). Brainstorm: a user-friendly application for MEG/EEG analysis. *Computational intelligence and neuroscience*, *2011*.

Teplan, M. (2002). Fundamentals of EEG Measurement. In *Measurement Science Review* (Vol. 2, pp. 1–11).

Van Hecke, A. V., Stevens, S., Carson, A. M., Karst, J. S., Dolan, B., Schohl, K., McKindles, R. J., Remmel, R., & Brockman, S. (2013). Measuring the Plasticity of Social Approach: A Randomized Controlled Trial of the Effects of the PEERS Intervention on EEG Asymmetry in Adolescents with Autism Spectrum Disorders. *Journal of autism and developmental disorders*. Retrieved from http://www.ncbi.nlm.nih.gov/pubmed/23812665

Wagner, J., Solis-Escalante, T., Grieshofer, P., Neuper, C., Müller-Putz, G., & Scherer, R. (2012). Level of participation in robotic-assisted treadmill walking modulates midline sensorimotor EEG rhythms in able-bodied subjects. *NeuroImage*, *63*, 1203–11.

Wieser, M., Haefeli, J., Bütler, L., Jäncke, L., Riener, R., & Koeneke, S. (2010). Temporal and spatial patterns of cortical activation during assisted lower limb movement. *Experimental brain research. Experimentelle Hirnforschung. Expérimentation cérébrale*, *203*, 181–91.

Windhorst, U. (1996). On the role of recurrent inhibitory feedback in motor control. *Progress in neurobiology*, *49*, 517–587.

Windhorst, U. (2007). Muscle proprioceptive feedback and spinal networks. *Brain research bulletin*, *73*, 155–202.

World Medical Association. (2008). Declaration of Helsinki: ethical principles for medical research involving human subjects. World Medical Association.

Yao, D. (2001). A method to standardize a reference of scalp EEG recordings to a point at infinity. *Physiological measurement*, *22*, 693–711.

Yoshitake, Y., & Shinohara, M. (2013). Oscillations in motor unit discharge are reflected in the low-frequency component of rectified surface EMG and the rate of change in force. *Experimental brain research. Experimentelle Hirnforschung. Expérimentation cérébrale*, *231*, 267–76.

APPENDIX A: ACTICAP ELECTRODE POSITIONS (10-20 SYSTEM)

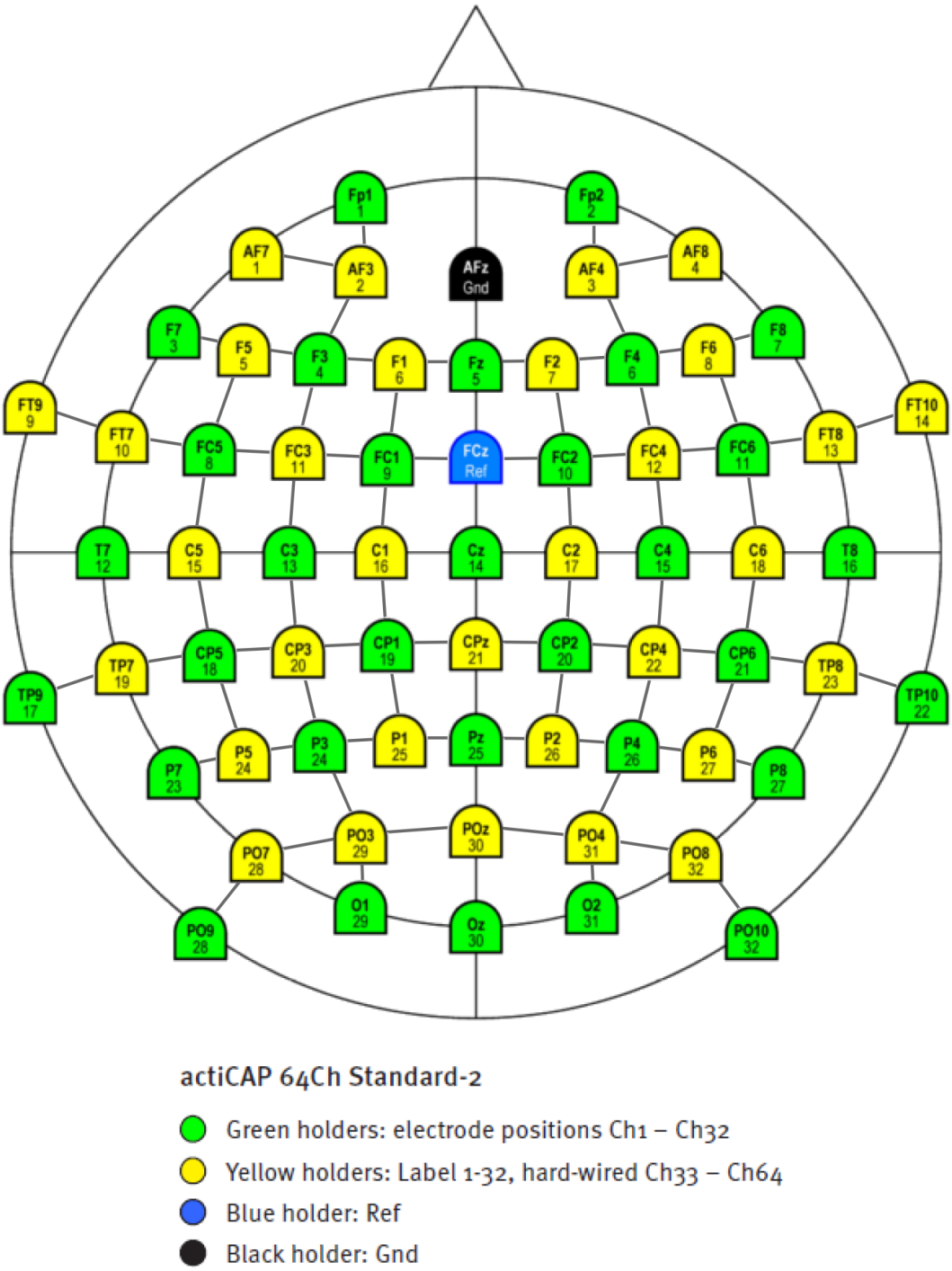

Figure A-1: Electrode locations of the 64-channel actiCAP. As indicated by the legend, there are two, 32-electrode sets (green and yellow), a reference electrode (blue), and a ground electrode (black). [Reference *actiCAP-64-channel-Standard-2_1201.pdf*, Version .002, Written 1 September 2012]

APPENDIX B: ANKLE ANGLE CALCULATION

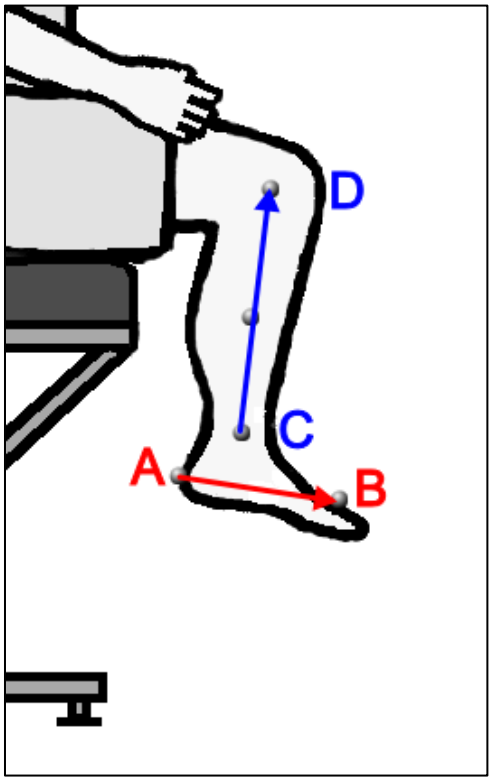

Figure B-1: Ankle Angle Calculation. Foot and tibial vectors define from the 3-dimensional coordinates of the Vicon markers places on the lower right leg. A denotes the heel, B the toe, C the medial ankle, and D the medial knee markers.

Equation B-1: $angle = -\tan^{-1}\left\|\left[\left(\overrightarrow{CD} \times \overrightarrow{AB}\right), \left(\overrightarrow{CD} \cdot \overrightarrow{AB}\right)\right]\right\| * \frac{180^o}{\pi} + 90^o$

Equation B-2: angle(i) = atan2(norm(cross(tibia(i,:),foot(i,:))),dot(tibia(i,:),foot(i,:)));
angle = -angle*180/pi+90;
where foot = $\overrightarrow{AB}$ & tibia = $\overrightarrow{CD}$

Calculation of the angle between the two vectors $\overrightarrow{AB}$ and $\overrightarrow{CD}$ (Figure B-1) and the MATLAB equivalent formula (Equation B-2) was modified from a suggestion by Roger Stafford [http://www.mathworks.com/matlabcentral/newsreader/view_thread/276582]. The variable *angle* is calculated using the three Cartesian coordinates for each vector at each time point of the ankle movement path. The signal is inverted and 90 degrees is added in order to define the reference (0 degrees) when the ankle is at a right angle.

APPENDIX C: DISCRETE MOVEMENT START AND STOP POINTS

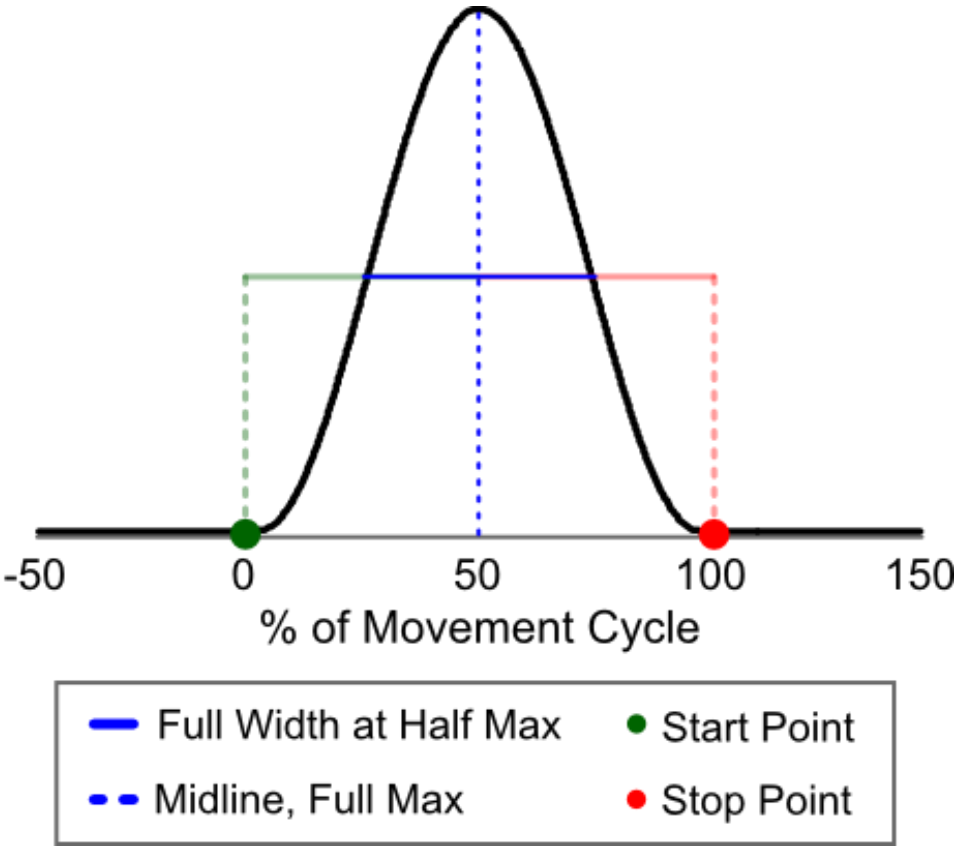

Figure C-1: Discrete Movement Start and Stop Points. Discrete and cued movements used the Full Width at Half Max (FWHM) measure to define the start and stop points. The profile of a discrete sinusoidal movement (black) is displayed with the location of max amplitude (blue dashed) and the FWHM line (blue solid). One FWHM distance from the midline is displayed and projected down to the movement profile for the start (green) and stop (red) points. [Suggested by Benjamin Kalinowsky]

During discrete and cued movements, there are no specific signal features (i.e. local maxima or minima) to define the start and stop of the movement. Therefore, one FWHM distance before and after the midline (define at peak dorsiflexion) was used to indicate initiation (green) and termination (red) of movement, respectively. Additionally, the half a cycle before and after the movement points that were used to epoch each discrete and cued movement were defined as two FWHM values on either side of the midline. These are shown in Figure C-1 as -50% and 150% of the movement cycle.

APPENDIX D: RESAMPLE AND TIME WARP EXPLANATION

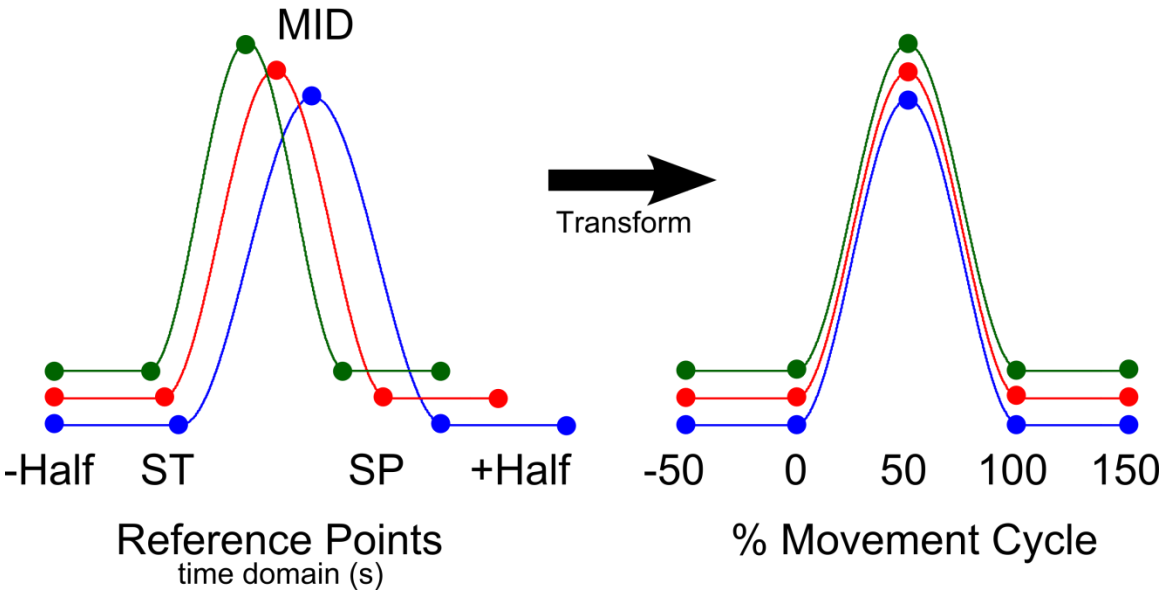

Figure D-1: Resample and Time Warp Explanation. (Left) Three movement profiles (epoched cycles) starting at the top with the fastest (green) to the slowest at the bottom (blue). The baseline value for each movement is offset for visual differentiation in this figure only. (Right) The same three movement profiles displayed after resampling and time warping.

Equation D-1: $\frac{\text{Average Samples per Cycle}}{\textit{Original Sampling Rate}} = \frac{\textit{Number of Resampled Points per Cycle}}{\textbf{\textit{New Average Sampling Rate}}} \rightarrow \frac{5714}{2000} = \frac{2000}{\textbf{700Hz}}$

Due to the variability in the movement profile, resampling and time warping of the position, EMG, and EEG data was necessary to allow for temporal averaging. Five distinct points were used to time warp the signals and all signals were resampled to have 2000 equally sampled points for each epoched cycle (Figure D-1). The EEGLAB function *timewarp* was used to perform this transformation. It should be observed that the average epoch time series length before the transformation is approximately 5714 points (sampled at 2000 Hz), which was resampled to 2000. Therefore, the new approximate average sampling rate per cycle was 700 Hz (Equation D-1). Since the data was low-pass filtered at 100 Hz previous to this transformation, the Nyquist sampling

theorem was not violated. As noted in the main text, both of these nonlinear processes will affect the frequency content of the signal; therefore, this transformation was not performed before any frequency (spectral) analysis of the data.

APPENDIX E: SIGNAL PROCESSING PSEUDO CODE

This appendix contains the signal processing pseudo code for MATLAB scripts written for this the analysis in this dissertation. Specific functions are denoted in *italics*, when necessary. These include native MATLAB functions and functions from the EEGLAB, Biomechanics Toolkit, and Brainstorm toolboxes.

Preprocessing EEG Data (Aims 1-3)

1. Load EEG data (64 channels) – *pop_loadcnt*
2. Add channel locations (actiCAP.xyz) – *pop_chanedit*
3. Average reference and retain FCz refence – *pop_reref*
4. Notch Filter (59 to 61 Hz) – butter 4^{th} order, *filtfilt* (zero-phase)
5. Filter band-pass (0.2 or 0.5 to 100) – *pop_eegfilt*
6. AMICA analysis – *runamica12* (Palmer et al., 2008)
7. Split into 1 second epochs – *pop_importevent*, *pop_epoch*
8. Determine artifact components with ADJUST (Mognon, 2010)

Analog Processing (only Aim 1)

1. Load .c3d files (Vicon) with BTK toolbox
    a. Markers – *btkGetMarkers*
    b. Analog Data – *btkGetAnlogs*

2. Root mean square of EMG data (for each muscle individually)
    a. Band-pass filter (30 to 200 Hz) – Butter, 4th order, *filtfilt* (zero-phase)
    b. Square each point
    c. Sliding filter – 50 ms window
    d. Square root of each point
3. Calculate ankle angle from Vicon makers
    a. Define tibia as Knee – Ankle marker
    b. Define foot as Toe – Heel marker
    c. Calculate angle for each time point (see Appendix B for equation)
    d. Convert to degrees (*180/pi)
    e. Add 90^{o} so that zero degrees is equal to 90^{o} between the tibia and foot
4. Cycle Definition
    a. Upsample ankle angle signal from 100 to 2000 Hz – interp1 (linear)
    b. Filter ankle angle signal (0.1 to 1.5 Hz), butter, 4th order, *filtfilt* (zero-phase)
    c. Rhythmic movements
        i. Find peaks of filtered signal (findpeaks, minpeakheight,0)
        ii. Find actual max point of unfiltered signal using previous points
        iii. Find local minima (start points) between each max point
        iv. Determine end points as the point before each start point
        v. Remove start and stop point pairs that overlap times of visual feedback
        vi. Calculate half a cycle before and after each cycle

d. Discrete movements

i. Find peaks of filtered signal (findpeaks, minpeakheight,15)

ii. Find mid points between each max point

iii. Calculate half the amplitude of each max point and previous midpoint

iv. Calculate Full Width at Half Max (FWHM) (See Appendix C)

v. Start and Stop points are calculated as 2 FWHM before and after each midpoint

vi. Half a cycle before and after are defined at 4 FWHM from each midpoint

Analog Processing (Aims 2-3)

1. This procedure is performed for each experimental movement trial recorded and individual for each ankle brace and robot. Coefficients were between for each robotic device and ankle braces were slightly different. For further details see, (Steldt & Schmit, 2004).

2. Load data files (recorded in LabVIEW)

3. Root mean square of EMG data (for each muscle individually)

    a. Band-pass filter (30 to 200 Hz) – Butter, 4^{th} order, *filtfilt* (zero-phase)

    b. Square each point

    c. Sliding filter – 50 ms window

    d. Square root of each point

4. Position calibration

    a. Load position calibration coefficients, passive movement trial, and inertial trial

    b. Convert all recorded values of volts to degrees (linear transform using coefficients)

5. Torque calibration

    a. Load torque calibration coefficients, passive movement trial, and inertial trial

    b. Convert all recorded values of volts to Nm (linear transform using coefficients)

6. Torque correction

    a. Passive torque

        i. Find the mean torque at each step of the passive trials. This trial was run with the subject in the robotic system and ankle position stepped down from peak dorsiflexion to plantar flexion in a staircase fashion.

        ii. Determine 3rd order polynomial to fit those points – *polyfit*

        iii. Calculate the torque due to passive movement at each point in the movement cycle for each trial – *polyval*

    b. Inertial torque

        i. The inertial trial rotated the ankle in the robotic system quickly (1.5 Hz) for 10 cycles.

        ii. Velocity and acceleration of the position data for this trial were calculated (filtered after each step, Butter, low-pass, *filtfilt*, 5 Hz)

        iii. Calculate the passive torque values for the inertial trial, similar to above – *polyval*

        iv. Remove passive component from the inertial trial to get the final torque due to inertia.

        v. Calculate the moment of inertia for the trial, which is the inertial torque multiplied by the acceleration.

    c. Correction

        i. Calculate the velocity and acceleration for the movement trial (filtered after each step, Butter, low-pass, *filtfilt*, 5 Hz)

ii. The final corrected torque is as follows:

$$T_c = T_o - T_p - I_m\alpha$$

Where,

T_c = Torque corrected

T_o = Torque from the original movement trial

T_p = Torque passive component

I_m = Moment of Inertia

α = Acceleration of the original movement trial

7. Cycle definition: Analog pulses recorded with the data marked each cycle. Start points were determined by the maximum value (maximum dorsiflexion) between pairs of pulses.

Processing (Aims 1-3)

1. Remove EEG artifact components – *pop_subcomp*

2. Epoch EEG and Analog data into cycles *(different lengths for Aim 1)*

3. *(Aim 1 only)* Remove cycles with statistically different data

    a. Eliminate cycles with EEG amplitudes that have values more or less than 3 SD of the mean

    b. Eliminate cycles with lengths that have lengths more or less than 3 SD of the mean

4. *(Aim 1 only)* Resample and timewarp the EEG and Analog cycles (timewarp function) (See Appendix D)

5. Identify and remove cycles that have EEG content that are statistically different from the other cycles (pop_autorej, maxrej = 5, startprob = 3)

Temporal Processing

1. After the previous processing steps, movement-related slow potentials were extracted by temporally averaging the signals.

2. *(Aim 1)* Signals were averaged from half a cycle before to half a cycle after each movement.

3. *(Aim 2 and 3)* Data was epoched into three consecutive cycles and averaged.

Spatial Localization

1. The following was performed in Brainstorm Software (Tadel et al., 2011).

2. The coordinates for the actiCAP were uploaded (65 channels, includes the reference channel, FCz)

3. Individual cycles were loaded in Brainstorm. *(Aim 1, the time warped signals were loaded with their individual new sampling rate)*

4. Spatial localization of the cortical signals were calculated for each movement cycle individually – Compute Sources

5. Computed sources for the cycles were averaged together within each trial/subject combination.

6. Grand average plots were created by averaging across subjects with each trial type.

Spectral Analysis

1. After artifact and cycle rejection, remaining EEG cycles are concatenated in time

2. Power spectral density was estimated using Welch's method. – *pwelch*

3. Section sizes

    a. Aim 1: 8192 points (signal sampled at 2000 Hz)

    b. Aim 2 and 3: 2948 points (signal sampled at 1000 Hz)

4. Each section was windowed with a Hamming window

5. Each analysis used 50% overlap

6. Power spectral densities were split into the EEG bands
    a. Delta (0 – 4 Hz)
    b. Theta (4 – 8 Hz)
    c. Alpha (8 – 12 Hz)
    d. Beta (12 – 30 Hz)
    e. Gamma (30 – 50 Hz)
7. Power for each band was calculated by using discrete integration – *trapz*

Repeated Measure Analysis of Variance

The repeated measures Analysis of Variance (ANOVA) was run in MATLAB with an m-file from the MathWorks file exchange by Thomas Gladwin. This code was tested against the statistical software SPSS and found the same results. The code can be downloaded from http://www.mathworks.com/matlabcentral/fileexchange/30737-n-way-repeated-measures-anova. The function used was *teg_repeated_measures_ANOVA*.